AFGL-TR-86-0012

Intercomparison of DMSP OLS, NOAA AVHRR, GOES
VISSR, and Landsat MSS Imagery for Cloud Property
Determination: Recommendations for Digital Data Analysis

R. G. Isaacs
J. C. Barnes
L. D. Petro
R. D. Worsham

Atmospheric & Environmental Research, Inc
840 Memorial Drive
Cambridge, MA 02139

18 January 1986

Final Report
18 June - 18 December 1985

AIR FORCE GEOPHYSICS LABORATORY
AIR FORCE SYSTEMS COMMAND
UNITED STATES AIR FORCE
HANSCOM AIR FORCE BASE, MASSACHUSETTS 01731

AD-A169 285

DTIC
ELECTE
JUL 0 3 1986
S
D

86   7   1   073

REPORT DOCUMENTATION PAGE	READ INSTRUCTIONS BEFORE COMPLETING FORM

1. REPORT NUMBER	2. GOVT ACCESSION NO.	3. RECIPIENT'S CATALOG NUMBER
AFGL-TR-86-0012	*A197 285*	

4. TITLE *(and Subtitle)*	5. TYPE OF REPORT & PERIOD COVERED
Intercomparison of DMSP OLS, NOAA AVHRR, GOES VISSR, and Landsat MSS Imagery for Cloud Property Determination: Recommendations for Digital Data Analysis	Final Report 18 June – 18 December 1985
	6. PERFORMING ORG. REPORT NUMBER P142F

7. AUTHOR(s)	8. CONTRACT OR GRANT NUMBER(s)
R. G. Isaacs L. D. Petro J. C. Barnes R. D. Worsham	F19628-85-C-0102

9. PERFORMING ORGANIZATION NAME AND ADDRESS	10. PROGRAM ELEMENT, PROJECT, TASK AREA & WORK UNIT NUMBERS
Atmospheric and Environmental Research, Inc. (AER) 840 Memorial Drive Cambridge, MA 02139	65502F 550202AD

11. CONTROLLING OFFICE NAME AND ADDRESS	12. REPORT DATE
Air Force Geophysics Laboratory Hanscom Air Force Base, MA 01731 LYS/Rupert Hawkins (Contract Manager)	18 January 1986
	13. NUMBER OF PAGES 138

14. MONITORING AGENCY NAME & ADDRESS*(if different from Controlling Office)*	15. SECURITY CLASS. *(of this report)*
	Unclassified
	15a. DECLASSIFICATION/DOWNGRADING SCHEDULE

16. DISTRIBUTION STATEMENT *(of this Report)*

APPROVED FOR PUBLIC RELEASE; DISTRIBUTION UNLIMITED

17. DISTRIBUTION STATEMENT *(of the abstract entered in Block 20, if different from Report)*

18. SUPPLEMENTARY NOTES

SBIR Phase I Final Report

19. KEY WORDS *(Continue on reverse side if necessary and identify by block number)*

DMSP OLS   Landsat MSS Imagery
NOAA AVHRR
GOES VISSR

20. ABSTRACT *(Continue on reverse side if necessary and identify by block number)*

Concurrent visible and infrared cloud imagery from four satellite sensors (DMSP OLS, NOAA AVHRR, GOES VISSR, Landsat MSS) have been intercompared. Inherent differences in cloud field analyses are noted due to sensor characteristics such as spatial and spectral resolution and scene/sensor geometry. Digital data were manipulated to simulate one sensor's data from that of another. Recommendations for further analysis of the collected data set are provided.

DD FORM 1473 1 JAN 73   EDITION OF 1 NOV 65 IS OBSOLETE

TABLE OF CONTENTS

Distribution/

Availability Codes

Dist	Avail and/or Special
A-1	

iii

LIST OF TABLES

LIST OF FIGURES

LIST OF FIGURES (cont.)

1. INTRODUCTION

1.1 Background

Since the first images were collected from space on a routine basis from
the TIROS series of meteorological satellites some 25 years ago, satellite
technology has evolved to the point where several satellite systems now pro-
vide imagery for meteorological and other geophysical purposes. The two that
have most directly evolved from TIROS are the polar orbiting (LEO - Low Earth
Orbit) Air Force DMSP (Defense Meteorological Satellite Program) and Civilian
NOAA systems. The GOES satellites, in geosynchronous (GEO) orbit, also pro-
vide imagery on a regular basis, covering the earth's disk every half-hour.
The GOES IR sensor resolution is not as good as that of DMSP or NOAA and ob-
servations are not useful at high latitudes; however, with the introduction of
improved processing techniques to display cloud motion in sequential GOES
images, these data are gaining increasing use by forecasters. In the early
1970s the first of the Landsat series of earth-resources satellites was or-
bited. Although not designed for meteorological purposes, Landsat has never-
theless provided imagery useful for cloud studies. Landsat data are not use-
ful for operational analysis because of limited spatial coverage and repeat
frequency, but the very high resolution of the images enables cloud features
not seen by other satellites to be detected.

Each of these satellite systems, all of which provide visible and thermal
infrared cloud imagery, has differing orbital and sensor characteristics, such
as platform altitude, time of passage, repeat cycle, spatial coverage, sensor
resolution, wavelength sensitivity, and physical calibration. Because of
these differences it is difficult to compare quantitatively the imagery from
the different systems even though analysts often use data from more than one
satellite. For example, DMSP and GOES, or NOAA and GOES, are often used in
combination for operational cloud analysis. With the increasing use of data
from more than one satellite, improved methods are needed for direct quantita-
tive comparison of the different satellite imagery. With the continued devel-
opment of automated, interactive processing systems, improved inter-satellite
image comparison methods will lead to improved cloud analysis and more reli-
able forecasts.

The primary goal of this study was to develop techniques to aid in the
correct interpretation of satellite cloud imagery data sets from various sen-

1

sor systems. By quantifying the differences in cloud signatures observed from various sensors, it will eventually be possible to circumvent some of the problems associated with utilizing multiple sensor data sets in the analysis of clouds. In this initial effort, the focus was on direct comparison of actual image samples selected to provide as closely as possible, near simultaneous and collocated data from the satellites of interest (i.e., DMSP, NOAA, GOES, Landsat). Based on this approach, identical cloud features could be observed from different sensor platforms and the characteristic differences in their appearance due to instrumental factors qualitatively noted. The desired data comparisons are GOES to DMSP, NOAA to DMSP, Landsat to DMSP, and Landsat to GOES.

Experience gained from the intersatellite image comparison can eventually be employed in the development of analogous numerical schemes. These schemes can be applied to digital sensor data sets to make data from one satellite system comparable to that of another for the purpose of effectively applying cloud analysis algorithms developed for a particular sensor. For example, it would be desirable for some purposes (such as operational nephanalysis) to transform GOES and NOAA data to provide synthetic DMSP formats so that visible and infrared cloud data processors developed and tuned for DMSP data can be applied. To investigate the feasibility of these numerical approaches, digital data sets corresponding to selected imagery data samples were obtained and basic preprocessors were developed to simulate numerically the effects of spatial resolution, sensor response, and dynamic range compression.

1.2 Previous Studies Comparing Satellite Imagery

Few studies have been carried out for the specific purpose of directly comparing one type of satellite imagery with another. An example of an early effort in this area is a study of the effects of sensor resolution on estimates of cloud cover (Shenk and Salomonson, 1972). Recently, a comparative study of image data produced by satellites with differing characteristics has been completed in France (ESA, 1983). In most instances, however, comparisons of imagery have been carried out as part of a study of satellite observation of some particular geophysical parameter rather than in a study specifically designed to compare one satellite with another.

In one such effort, a study was performed for the Navy to compare DMSP and Landsat imagery in which anomalous gray-shade patterns associated with low visibility in light fog or haze can be detected (Barnes et al., 1979a; Fett and Isaacs, 1979). The purpose of the investigation was to use the Landsat MSS data (four spectral bands) to determine which wavelengths within the overall DMSP range (0.4-1.1 μm) are responsible for the anomalous gray-shade patterns. This study provided valuable experience with the difficulties in acquiring a suitable comparative data sample from two different satellite systems. Because of these difficulties, only a limited sample of imagery could be analyzed. Nevertheless, useful qualitative results were obtained from the imagery analysis and a theoretical simulation of radiances provided a basis for quantitative interpretation. The simulations indicated that the relative contributions of energy from the different spectral intervals comprising the total DMSP response must be considered rather than the response function alone. It was also concluded that the differing spatial resolutions of the sensors are an important factor when viewing atmospheric features with continuously varying intensity response, such as haze or a developing cloud.

Data from different satellite sensors have also been compared in an evaluation of the capabilities of satellite imagery for monitoring regional air pollution episodes (Barnes et al., 1979b). In this study, samples of visible imagery from NOAA/VHRR (the sensor flown prior to the AVHRR), GOES, and Landsat were compared for a day on which a haze episode occurred. All of the differing satellite/sensor characteristics, such as spectral sensitivity, viewing angle in relation to the sun angle, and spatial resolution were taken into account in the comparative analysis. The results demonstrated that for monitoring pollution episodes, GOES was the most useful because of its frequent observations, thus enabling a region to be viewed at varying sun angles.

Two geophysical parameters that have been mapped extensively using imagery from various satellites are the earth's snow and ice cover. Handbooks for snow mapping provide guidelines on the interpretation, and discuss the advantages and disadvantages, of imagery from all available satellites (Bowley et al., 1979). In a related investigation of Heat Capacity Mapping Mission (HCMM) thermal data for snow hydrology (Barnes et al., 1981), comparative snow maps were prepared from HCMM, NOAA/ AVHRR, and Landsat imagery and digitized data; the relative resolutions and other characteristics of the different sen-

sors were evaluated. In this study, as well as in all of the above cited studies, the effects of sensor characteristics such as spectral and spatial resolution, viewing geometry, and sensitivity were found to impact significantly the accuracy of the analyses.

In addition to work such as the above related to analysis of meteorological and other geophysical parameters, extensive research is ongoing related to the development of improved cloud climatologies. The compilation of global cloud climatologies can only be accomplished using satellite data, usually from several space platforms. The three-dimensional (3-D) nephanalysis developed by the Air Force has been used operationally for several years, as well as having been used extensively in comparative studies. The 3-D nephanalysis model (now referred to by the Air Force as the Real-Time (RT) nephanalysis), which is described in reports such as Bunting et al. (1983) and Hughes and Henderson-Sellers (1985), provides the only current global cloud archive.

The requirement for an accurate global cloud climatology has now been internationally recognized by the establishment of the International Satellite Cloud Climatology Project (ISCCP), a five-year project undertaken in 1983 (Schiffer and Rossow, 1983, 1985). It is important for the success of the ISCCP to develop algorithms for the accurate retrieval of cloud information from satellites and, thus, to understand the inherent differences in the various satellite systems. Related research work includes studies to develop improved methods to retrieve cloud cover parameters from satellites (Arking and Childs, 1985) and studies of the problems in working with satellite data (Snow et al., 1985).

1.3 Phase I Technical Objectives

The purpose of this Phase I effort was to develop methods to aid in the interpretation of cloud from essentially different imaging sensors based on experience gained from the analysis of actual image data sets. In particular, it was proposed to develop ways to compare data samples from a variety of imaging sensor systems (i.e., DMSP OLS, NOAA AVHRR, GOES VISSR, Landsat TM/MSS) in order to abet cloud analysis and interpretation. It was also proposed to investigate techniques to transform from one data source to another taking into account sensor specific considerations such as: resolution, bandpass, scan characteristics, orbital geometry, and physical calibration. In order to accomplish this goal, the specific Phase I technical objectives were:

4

(1) To provide a thorough description of the salient characteristics of each satellite sensor system and identify which of these may be used as parameters in the development of quantitative data intercomparison transformations.

(2) To select and acquire concurrent imagery sample sets (both visible and thermal infrared) from each of the candidate sensor systems cited above.

(3) To compare directly the imagery sample sets acquired for each sensor and quantitatively analyze characteristics of cloud and other features observed in each. Specific image sample comparisons are GOES to DMSP, NOAA to DMSP, Landsat to DMSP, and Landsat to GOES.

(4) To develop techniques based on the results of the above data intercomparison to aid in correctly interpreting images from various systems. These techniques will provide guidelines for implementation in image analysis and when appropriate, algorithms for machine processing.

1.4 Overview of Report

This report consists of six sections and four appendices. In the following section (Section 2), the salient characteristics of the four sensor systems under consideration -- the DMSP OLS, NOAA AVHRR, GOES VISSR, and Landsat MSS -- are summarized. Section 3 discusses the approach and criteria used for the selection of both imagery and digital data used in this study. Those with experience in the acquisition of satellite data sets will appreciate that this is not a trivial task, particularly in a six-month study. Section 3 also provides a catalog of the data sets acquired and available for future analysis.

Section 4 describes the actual intercomparison of imagery from the various satellite sensors. This includes complete descriptions of the selected test cases including meteorological data consisting of surface and upper air observations. For clarity, the data intercomparisons are divided into two categories: those consisting of DMSP, NOAA, and GOES data alone, and those including Landsat imagery.

The experience gained in the imagery analysis is applied to the development of numerical techniques in Section 5. This section discusses the necessary preprocessing of digital data, methods used to provide McIDAS renditions of the data, and a demonstration of digital imagery transformatino from one sensor characteristics to another, simulating some of the quantitative cloud analysis effects noted in Section 4. Based on this analysis, a functional

5

block diagram is presented which provides a roadmap for future data transformation algorithm development. Conclusions and recommendations are presented in Section 6.

Appendices are provided to illustrate a simple digital data spatial averaging program (A), a spectral averaging program (B), and the approach to evaluating scene/sensor geometry factors (C). Finally, addresses and telephone numbers for satellite data archives used in this study are provided in Appendix D.

2. CHARACTERISTICS OF IMAGING SENSORS

2.1 DMSP OLS

The DMSP (Defense Meteorological Satellite Program) has provided polar-orbiting satellite data to the military services for some 20 years. The program was declassified in the later 1960s, and archived DMSP imagery have been made available to nonmilitary users since that time. In recent years, the DMSP and civilian polar-orbiting satellite systems have become more similar in many respects as the result of an attempt to attain some uniformity between the two systems and thus reduce the costs of developing and launching complex satellite systems. The DMSP system is described in several references including Nichols (1975), Rivers and Arnold (1982), Kaehn (1982), and Haig (1982). The current DMSP system is the Block 5D spacecraft, which transmits direct readout data to transportable terminals deployed worldwide. The platform and sensor characteristics for the DMSP and the other imaging systems are summarized in Table 2-1 and 2-2, respectively.

The OLS (Operational Linescan System), first flown in 1976 on the Block 5D spacecraft, is the primary meteorological sensor of the DMSP (Spangler, 1974). Current plans call for the OLS to continue to be included in the sensor package at least until the 1990 timeframe. The OLS is a two-channel radiometer, but its operation is somewhat different from that of other radiometers (such as the TIROS/AVHRR) in that the mirror oscillates rather than rotates. This back-and-forth sinusoidal motion of the optical telescope system moves the instantaneous field of view of the detectors across the satellite subtrac, with maximum scanning velocity at nadir and reversals at the ends of the scans. The detector size of the optics is dynamically changed to reduce the field of view near the end of each scan, thus maintaining an essentially unchanged footprint size on the Earth's surface. The gain of the sensor is also adjusted along the scan line to compensate for larger variations in the reflected light level as the satellite crosses the terminator. Furthermore, through use of a photomultiplier tube, it is possible for the OLS to collect reflected visible radiation at night, with illumination as low as that corresponding to a quarter moon.

The OLS visible sensor ("L" data) covers a relatively broad spectral band (0.4-1.1 μm). The IR ("T" data) bandwidth is 10.4-12.5 μm (before June 1979,

Table 2-1

Operational Platform Characteristics

	DMSP	NOAA	GOES	LANDSAT
Orbit	LEO	LEO	GEO	LEO
Altitude (km)	833	854	36000	705
Approximate time of Equator Crossing (LST)	0000/1200* 0700/1900	0300/1500 0730/1930	n/a	0945
Period (m)	101	102	n/a	98.9
Inclination (deg)	98.7	98.9	n/a	98.2
Latitude Range (deg)	n/a	n/a	60N/ 60S	n/a
Data Swath (Km)	2560	2240	earth disk	185
Repeat Cycle	12 hours	12 hours	1/2 hour	16 days

*May vary, but usually in dawn/dusk and noon/midnight orbits.

Table 2-2

Characteristics of Current Meteorological Imagers

Sensor	OLS	AVHRR	VISSR	TM	MSS
Spacecraft	DMSP	NOAA	GOES	Landsat	Landsat
Orbit	Polar (LEO)	Polar (LEO)	GEO	Polar (LEO)	Polar (LEO)
Wavelength (μm)					
Channel 1	0.4–1.10	0.58–0.68	0.55–0.70	0.45–0.52	0.50–0.60
2	10.4–12.5[a]	0.725–1.1	10.5–12.5	0.52–0.60	0.60–0.70
3		3.55–3.93		0.63–0.69	0.70–0.80
4		10.5–11.3		0.76–0.90	0.80–1.10
5		11.5–12.5		1.55–1.75	
6				2.08–2.35	
7				10.40–12.50	
Resolution at Nadir (meters)					
Visible	600,2800[b]	1100	800	30	80
IR	600,2800	1100	7000	120	

[a]OLS IR wavelength was 8.0–13.0 μm before June 1979

[b]600m at fine resolution, 2800m at smoothed resolution.

this bandwidth was 8.0-13.0 μm). Direct readout data at "fine" (F) resolution (0.6 km) and "smoothed (S) resolution (2.8 km) can be received at the transportable terminals; data can also be recorded onboard the spacecraft at the smoothed resolution for transission to the central receiving stations (low light level nighttime visible data are at 2.8 km resolution). The main features of the OLS are listed in Table 2.2, and the instrument is described in more detail in Spangler (1974), Nichols (1975), Cornillon (1982), and Haig (1982). The meteorological interpretation of the Block 5D OLS and earlier DMSP imagery is discussed in reports by Brandli (1976) and Fett and Mitchell (1977). The archive for DMSP imagery is listed in Appendix D (no digital DMSP archive exists).

2.2 NOAA AVHRR

The current civilian polar-orbiting satellites (the TIROS-N/NOAA A-G Series) have been operational since late 1978 and carry an instrument package consisting of the AVHRR (Advanced Very High Resolution Radiometer) and the TOVS (TIROS Operational Vertical Sounder). The characteristics of these instruments are described below; a more detailed description of the instruments can be found in references such as Schwalb (1978), NOAA (1981), Barnes and Smallwood (1982), and Cornillon (1982).

The AVHRR is a 5-channel radiometer with two channels in the visible and three in the thermal infrared. The two visible channels fall within the broader wavelength band of the DMSP/OLS (see Table 2.1 for orbital characteristics of the spacecraft and Table 2.2 for characteristics of the AVHRR). The ground resolution of the AVHRR at nadir is 1.1 km; at a satellite altitude of 850 km, the data swath is 2240 km. Data from the AVHRR instrument are available from the satellite in four operational modes (the archive for NOAA and GOES data is given in Appendix D):

- APT (Automatic Picture Transmission): direct readout to worldwide ground stations of the APT visible and infrared data degraded to 4 km resolution.
- HRPT (High Resolution Picture Transmission): direct readout (S-band) to worldwide ground stations of the HRPT data for all spectral channels (1.1 km resolution).

- GAC (Global Area Coverage): global on-board recording of 4 km resolution data from all spectral channels for commanded readout for processing in the NOAA central computer facility at Suitland, Maryland.

- LAC (Local Area Coverage): on-board recording of data from selected portions of each orbit at 1.1 km resolution and all spectral channels for central processing.

2.3 GOES VISSR

The existing civilian geosynchronous satellites (SMS/GOES Series) carry the VAS (VISSR Atmospheric Sounder) which is an improved version of the VISSR (Visible Infrared Spin-Scan Radiometer) carried on the earlier SMS and GOES satellites. GOES-4, launched in September 1980, was the first to carry the VAS and thus is considered to be the first of the second generation of operational, geosynchronous meteorological satellites. The VAS is described below; for a more complete description, see Santa Barbara Research Center (1978) and Cornillon (1982).

The improvements in the instrument consist of the addition of several infrared detectors, the addition of an infrared filter wheel in the optical train, and the capability of operating the instrument in several different modes. The filter wheel consists of 12 filters, any one of which may be placed in the optical path; the filtered radiation is then directed to one of three pairs of infrared detectors. Scanning is achieved by rotation of the satellite; the filter wheel is not rotated while the Earth is being scanned. The VAS may be operated in three modes: the VISSR mode, the MSI (Multispectral Imaging) mode, and the DS (Dwell) or Sounding mode.

According to Cornillon (1982), the VAS has been operated primarily in the VISSR mode; the MSI mode has not been used extensively because of limited ground-station capability to receive these data (i.e., the down-link for MSI is different than that for VISSR). The instrument has been operated in the DS mode to collect data for comparative studies with other atmospheric sounders and radiosonde data.

In the VISSR mode, the data collected are similar to that of the earlier GOES VISSR instruments. The visible channel (0.55-0.70 μm) has a resolution of 0.8 km by 0.8 km at nadir, whereas the thermal infrared channel (10.5-

11

12.6 μm) has a resolution of 7 km, somewhat improved over that of the earlier GOES. The GOES imagery is routinely processed to cover the full Earth disk or certain sectors. The effective resolutions of the resulting images varies; the North America sector (WB1) has a resolution (visible data) of 2 km whereas the Eastern U.S. sector (DB5) is at 1 km (Dismachek et al., 1980). Data for the complete Earth disk can be collected and transmitted every 30 minutes; data for selected portions of the disk can be collected more frequently.

2.4 Landsat MSS

The Landsat series of satellites, the first of which was launched in 1972, has been designed primarily to view the Earth's surface rather than the Earth's clouds. This is in contrast to meteorological operational satellite systems, such as the polar-orbiting NOAA and DMSP satellites and the geosynchronous GOES satellites, which are described in the above sections. Nevertheless, as Landsat data were accumulated, it became obvious that the images also displayed a considerable amount of information relevant to meteorology. One of the first investigations directed toward detection of cloud features by Landsat was reported by Feteris et al. (1976). In that study, some 50 Landsat Multispectral Scanner (MSS) scenes were analyzed in photographic format to identify the structure and characteristics of mesoscale cloud features; the types of clouds examined in the Landsat images included cumulus bands, low-level offshore cloud streets, terrain-induced wave clouds, and severe storm clouds. These detailed cloud features cannot be observed in the lower resolution meteorological satellites imagery; thus, Landsat can be considered as a source of "ground truth" cloud information, which can be useful for interpreting cloud features seen in the other types of satellite data.

All Landsat spacecraft have carried the MSS, which has a resolution an order of magnitude higher than that of the best meteorological satellite sensor (80 m vs. 0.6 km for the DMSP fine-resolution data). The MSS, however, views a very narrow swath (185 km) and provides repeat coverage of the same area only once every 16 days. The MSS has four spectral bands (see Table 2-2) covering the interval from 0.5 to 1.1 μm. Thus, the MSS data can be used to simulate narrower band sensors, such as the GOES VSSR (0.55-0.7 μm) as well as the broader band (0.4-1.1 μm) of the DMSP OLS; the relative response curves of the MSS and DMSP OLS are shown in Figure 2-1. As cited in an earlier section,

Landsat MSS data were used in a study to determine which wavelengths within
the overall DMSP band were responsible for anomalous gray-shade patterns
detected in DMSP images in areas of light fog or haze over ocean (Barnes et
al., 1979; Fett and Isaacs, 1979). The Landsat MSS is described in detail in
many documents available through EOSAT, the private sector company granted
exclusive rights to the distribution of Landsat data under the Landsat
Commercialization Act of 1984 (see Appendix D).

Landsat 4, launched in July 1982, and Landsat 5 carry both the
Multispectral Scanner (MSS) and the Thematic Mapper (TM). The TM is designed
to achieve finer spatial resolution, sharper spectral separation, improved
geometric fidelity, and greater radiometric accuracy and resolution than
previous sensors. The instrument and the orbital characteristics of Landsat 4
are described in the Landsat Data Users Notes (NASA, 1982) and in a paper by
Engel and Weinstein (1983). A comparison of the MSS and TM and the other
current imagers is shown in Table 2-2.
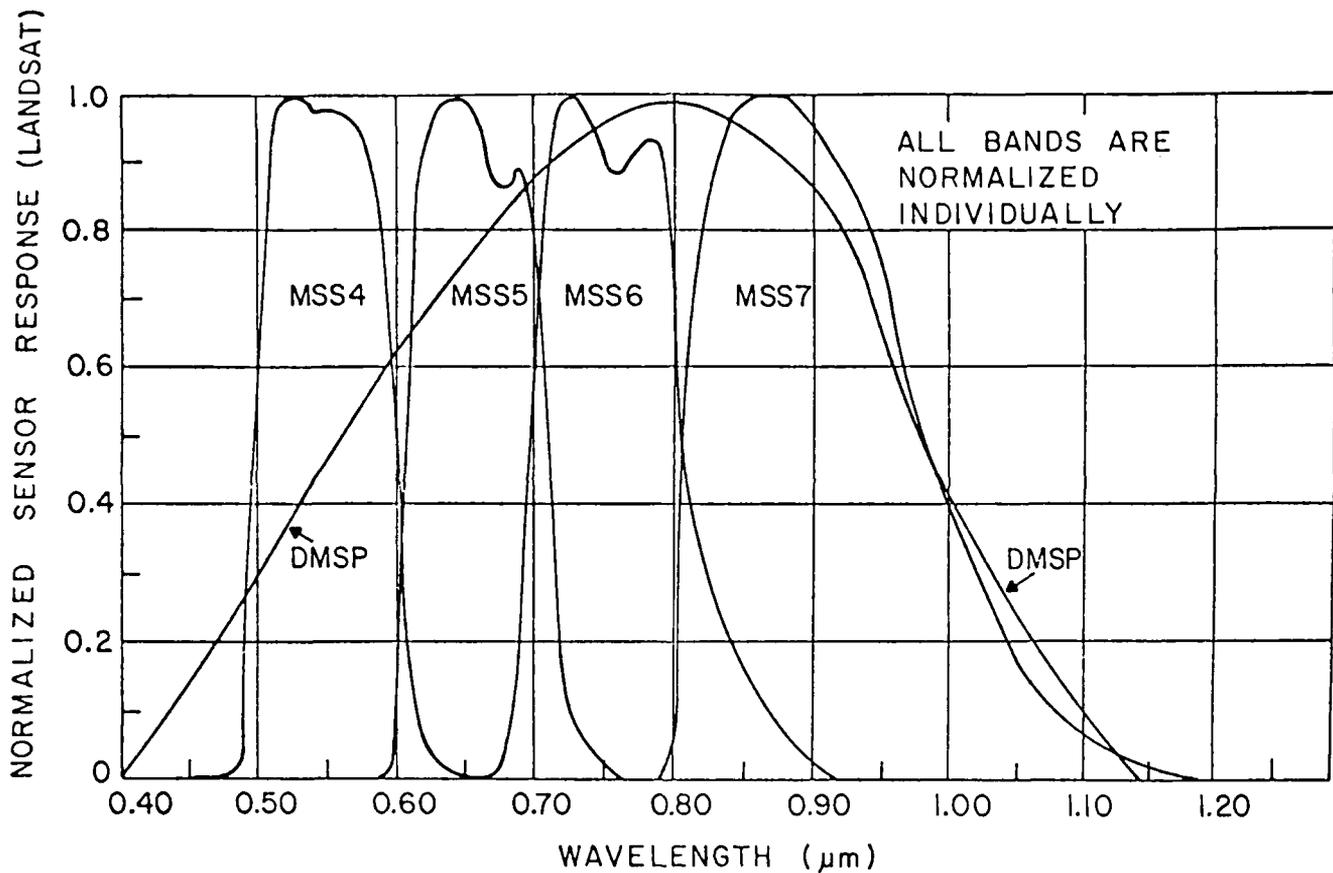
Figure 2-1.   Landsat and DMSP relative spectral response (Barnes et al., 1979; Norwood et al., 1972)

3. DATA SAMPLE

3.1 Selection and Acquisition of Data Sample

The acquisition of a concurrent sample of each type of pertinent satellite data was not an easy task. As described in the previous section, each satellite has differing orbital and sensor characteristics, which may change from time to time as systems are upgraded. Also, data from one of the satellite systems may be missing for a period of time because of satellite failure or may be missing for a particular observation time because of a readout or archival problem. The Air Force and civilian satellite data are not available from the same source; moreover, because DMSP imagery is designed to be used as an operational analysis product, the Air Force does not maintain a data archive.

In light of the inherent difficulties in acquiring a suitable data sample, especially the lack of an official Air Force DMSP archive, the initial task of the data selection procedure was to review previous studies to determine whether a sample of DMSP imagery suitable for the current study might already be on hand (a considerable amount of DMSP imagery had been acquired previously from the civilian archive oeprated by the Cooperative Institute for Research in Environmental Sciences at the University of Colorado). A suitable sample for a period in early May 1979, covering the central and eastern U.S., was located. In fact, May of 1979 was an opportune time to acquire DMSP data, because thee spacecraft were in operation during that period (Block 5D F1, F2, and F3); thus, on some days, images were available for three or more different observation times, increasing the chances for an observation concurrent with an observation from another type of satellite. The DMSP data sample on hand was reviewed to select days with good quality images and distinctive cloud features.

The second step in the data acquisition procedure was to acquire GOES and NOAA imagery for the days for which DMSP imagery had been selected. Both types of data are archived at the NOAA Satellite Data Services Division in Washington, DC. Acquisition of GOES images concurrent with the DMSP observations was not a problem since GOES data are archived at half-hourly or, at worst, hourly intervals. NOAA AVHRR images covering the same portions of the U.S. were also acquired for each day of the sample period. Because of the orbital characteristics of the two systems, however, it was not possible to ac-

15

quire concurrent NOAA and DMSP data; the NOAA observation time was at best three to four hours later than the DMSP observation.

The final step in the acquisition of a usable sample for imagery inter-comparison was to initiate a search for Landsat data. Although Landsat has a repeat cycle over the same area of only once every 16 days, an orbit covering some portion of the eastern U.S. (185 km wide swath) should exist every day. In May 1979, the chances of Landsat coverage were increased, because both Landsat 2 and Landsat 3 were in operation. A data search for the sample period was initiated through EOSAT (the private sector company now operating the nation's Earth Resources Satellite Program), and a listing was received of the orbits for each day. These orbits were in turn plotted on the GOES and DMSP images, and scenes were selected for areas with distinctive cloud features on the orbits most nearly concurrent with GOES and DMSP observation times (with observations from more than one DMSP spacecraft available, it was possible to find some cases where the DMSP pass was within one hour or less of the Landsat midmorning overpass time.) Because of cost considerations, images were ordered for only one spectral band (MSS Band 5) for a limited number of Landsat scenes; after reviewing the images, all four MSS bands were ordered for two scenes.

Correlative meteorological data were also acquired for the sample period. In addition to surface and upper air charts, additional data were obtained for the cases with Landsat imagery. These data included hourly surface observations for reporting stations within the areas of Landsat coverage.

3.2 Imagery Data Sample

The imagery data sample used in the study is listed in Table 3-1. This table gives the types of satellite imagery, times of observations, and areas covered for each day of the sample period. The specific images used for the intercomparative imagery analysis were selected from this overall sample based on the time interval between comparative observations, colocation of the areas covered, quality of the images, and availability of Landsat coverage. The imagery analysis is presented in Section 4.

16

Table 3-1

Imagery Data Sample (May 1979)

Satellite and Sensor	2 May Time (GMT)	2 May Type of Data	2 May Area	3 May Time (GMT)	3 May Type of Data	3 May Area	4 May Time (GMT)	4 May Type of Data	4 May Area	6 May Time (GMT)	6 May Type of Data	6 May Area
DMSP OLS (see Code)	1309	LF(F3)	Western U.S.	1442	LF(F2)	Central U.S.	1229	LF(F3)	Central U.S.	1149	LF(F3)	Eastern U.S.
	1218	LF(F2)	Eastern U.S.	1709	LS,TS(F1)	Central U.S.	1651	LF,TS(F1)	Central U.S.	1348	LF(F2)	Eastern U.S.
	1728	LS(F1)	Central U.S.							1600	LS(F1)	Eastern U.S.
GOES VISSR See Code	1300	FIS(WB1)	N. America	1500	VIS(WB1)	N. America	1230	VIS(DB5)	Eastern U.S.	1200	VIS(WB1)	N. America
	1330	VIS(DB5)	Eastern U.S.	1700	VIS,IR (WB1)	N. America	1700	VIS(WB1)	N. America	1400	VIS(WB1)	N. America
				1700	VIS (Enlarged)	Southeast U.S.	1700	IR(DB5)	Eastern U.S.	1600	VIS(WB1)	N. America
										1600	VIS,IR (Enlarged)	N. Centra. U.S.
NOAA AVHRR (TIROS N)	2012	VIS (2 scenes)	Eastern U.S.	2002	VIS	Eastern U.S.	1951	VIS,IR (2 Scenes)	Eastern U.S.	2112	VIS,IR	Southeast U.S.
	2154	VIS (2 scenes)	Western U.S.	2144	VIS,IR	Western U.S.						
Landsat MSS	1550	Band 5(2) (4 scenes)	N. Central U.S.	1516	Band 5(3) (2 scenes)	N. Central U.S.	1600	Band 5(2) (4 scenes; 1 with all 4 bands)	N. Central U.S.	1614	Band 5(2) (4 scenes; 1 with all 4 bands)	N. Central U.S.

DMSP Code:
LF – Fine Resolution VIS
TF – Fine Resolution IR
LS – Smoothed Resolution VIS
TS – Smoothed Resolution IR
F1, F2, and F3 are numbers of the block 5D spacecraft

GOES Code: WB1 – North america
DB5 – Eastern U.S. Sector

Landsat Code: Number in ( ) indicates either either Landsat 2 or Landsat 3

17

3.3 Digital Data Sample

No digital DMSP archive exists. However, a sample of Landsat and GOES digital data were acquired for use in the study. NOAA AVHRR digital data are also archived, but none were acquired because of the time difference between the NOAA and other satellite observations. The Landsat scenes for which digital data were acquired (May 6 case) were selected because of distinctive cloud features within the scene and because the Landsat pass on that day was at almost exactly the same time as the corresponding DMSP and GOES observations; the digital tapes contain all four spectral bands of the MSS. The GOES digital data (VIS and IR) are for a portion of the overall GOES scene covering the same area as the Landsat scene. The digital data were used in the technique development phase of the study, as presented in Section 5. Because of the time constraints of the initial Phase I effort, it was only possible, however, to work with one of the Landsat scenes. The digital data sample is listed in Table 3-2.

Table 3-2

Digital Data Sample

Landsat

6 May 1979	1614 GMT	North Central U.S.
Landsat 2 MSS Scenes No. 82156516115		
(4 spectral bands)	82156516122	
	82156516124	

GOES

6 May 1979	1600 GMT	North Central U.S.
(VIS and IR)		

4. DATA INTERCOMPARISON — ANALYSIS OF IMAGERY

Satellite data are most familiar to users in the form of imagery. In fact, DMSP OLS data received at transportable terminals are used operationally only in imagery format as are most NOAA AVHRR and GOES data at National Weather Service forecast centers. Moreover, because DMSP OLS data are treated as an operational analysis product, digital tapes are not archived as they are for other types of satellite data.

Satellite data intercomparison carried out in this study was devoted primarily to the analysis of imagery. Results of the analysis provide guidelines for interpretation of the data products most familiar to field personnel. Because of several factors, however, analysis of imagery provides only a qualitative intercomparison of satellite sensors; these factors are discussed in the following section. Data in a digital format are necessary to intercompare sensors quantitatively and to develop techniques that will lead toward future, more automated, analysis methods; digital data technique development is discussed in Section 5.

The analysis of imagery was undertaken in two phases. Under the first phase, the results of which are presented in Section 4.2, overall cloud features in DMSP, GOES, and NOAA imagery are intercompared. This analysis is primarily a comparison between GOES and DMSP because of the availability of several excellent nearly concurrent data sets. This phase of the imagery analysis also provides an opportunity for a NOAA to DMSP intercomparison, as best possible considering the inherent time interval between the observations. Several types of cloud features are examined over the broad areas covered by the DMSP, GOES, and NOAA images.

In the second phase of the imagery analysis, presented in Section 4.3, a more detailed analysis of specific cloud features over limited areas was undertaken for cases in which Landsat coverage was available. These data sets provide the opportunity for intercomparison of Landsat to DMSP and Landsat to GOES, as well as GOES to DMSP, for the limited areas. In these cases, Landsat can be considered as a source of "ground truth" as it provides information on cloud structure far more detailed than possible from the other sensors. Supporting meteorological data were also collected for these cases.

The results of the imagery intercomparisons -- NOAA to DMSP, GOES to DMSP, Landsat to DMSP, and Landsat to GOES -- are summarized in Section 4.4.

4.1 Considerations for Imagery Intercomparison

Several factors, which make quantitative intercomparison difficult, must be taken into consideration when comparing imagery from different satellite systems. The first consideration when working with DMSP data is that the archived imagery may not be a consistent set of data, because DMSP is treated as an operational analysis product and is not designed for use as a research tool.

The DMSP satellites and characteristics of the OLS system are described in Section 2.1. At the receiving sites, various enhancement curves can be used to produce images from the original data tapes. In the interpretive handbook by Fett and Mitchell (1977), the various mapping curves are shown and are discussed in detail (see Figure 4-1). For example, an enhancement curve may be applied to enhance cloud features (more gray-levels at high reflectances) or to enhance subtle cloud or terrain features (more gray levels at the lower reflectances). Since the original data tapes are not saved, and there may not be documentation on which enhancement curve was used to produce a certain image, the images in the DMSP archives do not comprise a consistent data set. Enhancement curves are also used to produce imagery from other sensor systems, such as the GOES IR data; however, documentation on the enhancement is usually available with the imagery.

Another important consideration is that satellite images are photographic products and, thus, are subject to the variations inherent in photographic processing. An example of the impact of processing differences on a DMSP image is shown in Figures 4-2(a) and 4-2(b). The two images shown in this figure are two photographic copies made from the same archival print (ordered at different times with no processing instructions given). The two prints are obviously quite different, with the image shown in Figure 4-2(a) being overall significantly brighter than that shown in 4-2(b). The second image (b) contains considerably more detail in the larger cloud masses, such as those to the west of Florida, as some of these features are saturated in the first image (a); on the other hand, terrain features and some thin clouds are more difficult to detect in (b) than in (a). These two prints could be considered
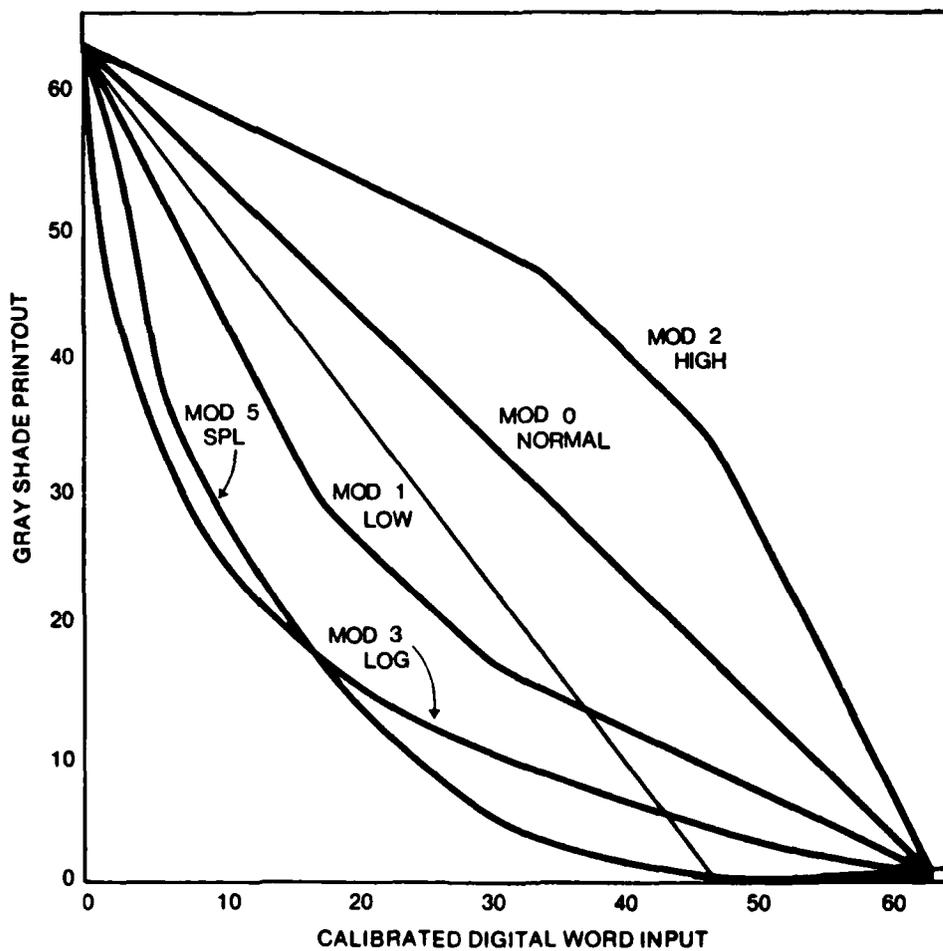
Figure 4-1. DMSP OLS Enhancement Curves (Fett and Mitchell, 1979)

Figure 4-2(a): DMSP (LS) 6 May 161436 - Brighter image
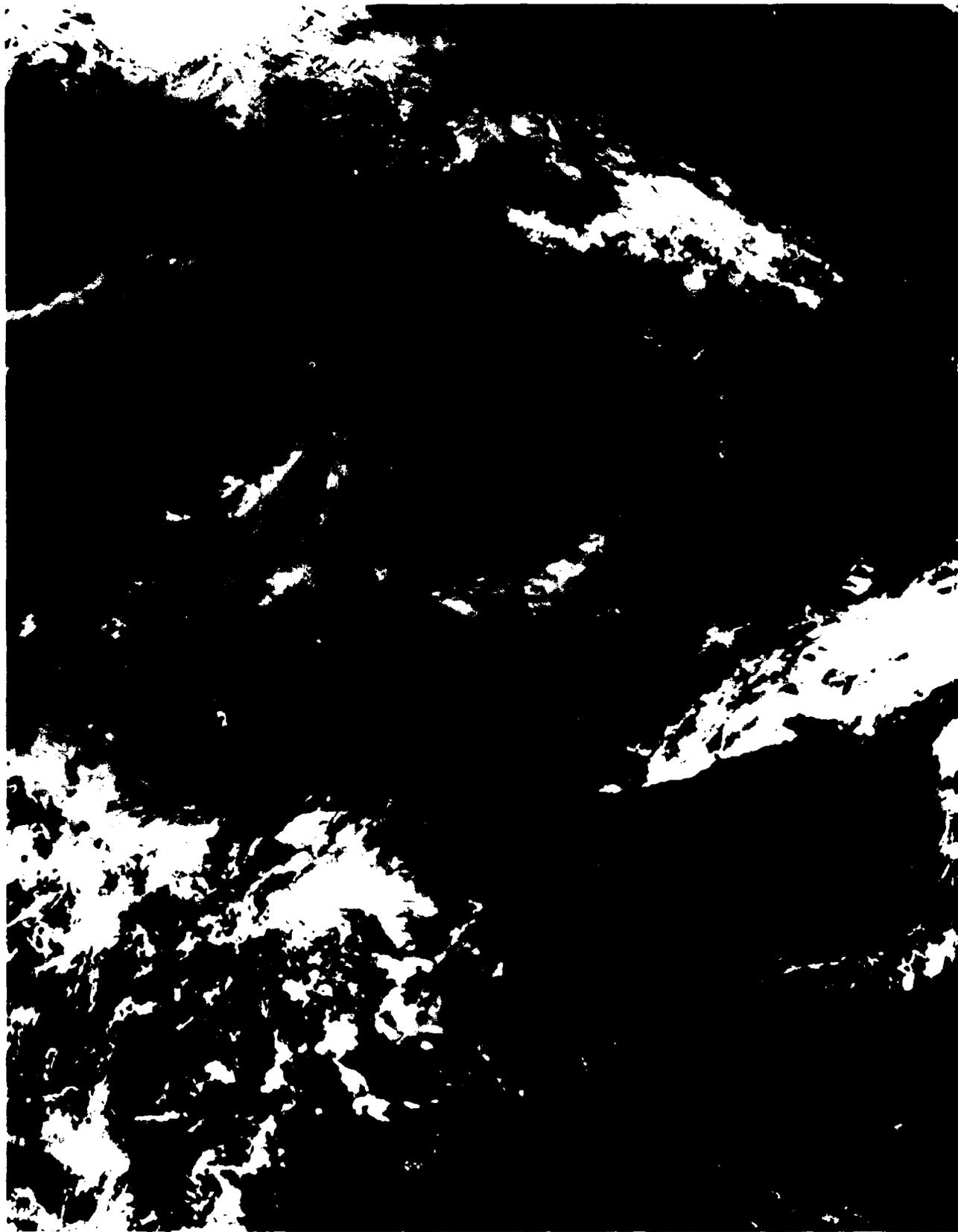
Figure 4-2(b): DMSP (LS) 6 May 1614G - Darker image

23

as simulations of different enhancement curves, with one being a product to enhance terrain and subtle cloud features and the other to enhance brighter clouds.

Other considerations when analyzing imagery include variation in imagery format and image distortion. The DMSP OLS can be presented as fine (LF, TF) or smoothed (LS, TS) resolution data. Similarly, GOES data can be presented in various formats ranging from full disk, to North America (WB1), to a sectorized image such as the eastern United States (DB5); each of these formats have different resolution. The GOES images have increasing distortion with latitude, and the NOAA AVHRR images are displayed without edge distortion removed (edge distortion is removed in DMSP images). Also, since Landsat has a gain level set for viewing terrain, clouds tend to saturate quickly in Landsat images.

Even when all influencing factors are taken into consideration, identifying and locating the same cloud feature in two different images may be difficult. Although large cloud masses may be easy to identify, specific cloud elements, such as along the edge of a larger cloud mass, may be more difficult. The lack of a superimposed geographic grid on DMSP and NOAA may make colocating difficult, especially in areas with no terrain features. Cloud elements may also undergo considerable change over relatively short time intervals between observations; these changes present a particular problem when comparing Landsat with meteorological satellite data because of the fine scale of the cloud features viewed at Landsat resolution.

4.2 Image Intercomparison of Overall Cloud Features in DMSP, GOES, and NOAA Imagery

4.2.1 2 May 1979 (GOES to DMSP)

A DMSP image (LF) at 1318 GMT on 2 May is shown in Figure 4-3(a); GOES visible images for 1300 GMT (WB1) and 1330 GMT (DB5) are shown in Figures 4-3(b) and 4-3(c). These images present a good intercomparison of DMSP with two GOES formats (North America and eastern U.S. sectorized).

Overall, DMSP has considerably higher contrast than GOES; many terrain features that cannot be detected in the GOES images can be readily identified in DMSP (it should be noted that the cloud and terrain features discussed were interpreted from the photographic prints; some of these features may not be

24

Figure 4-3(a): DMSP (LF) 2 May 1318G

Figure 4-3(b):   GOES (WB1 VIS) 2 May 1300G

26
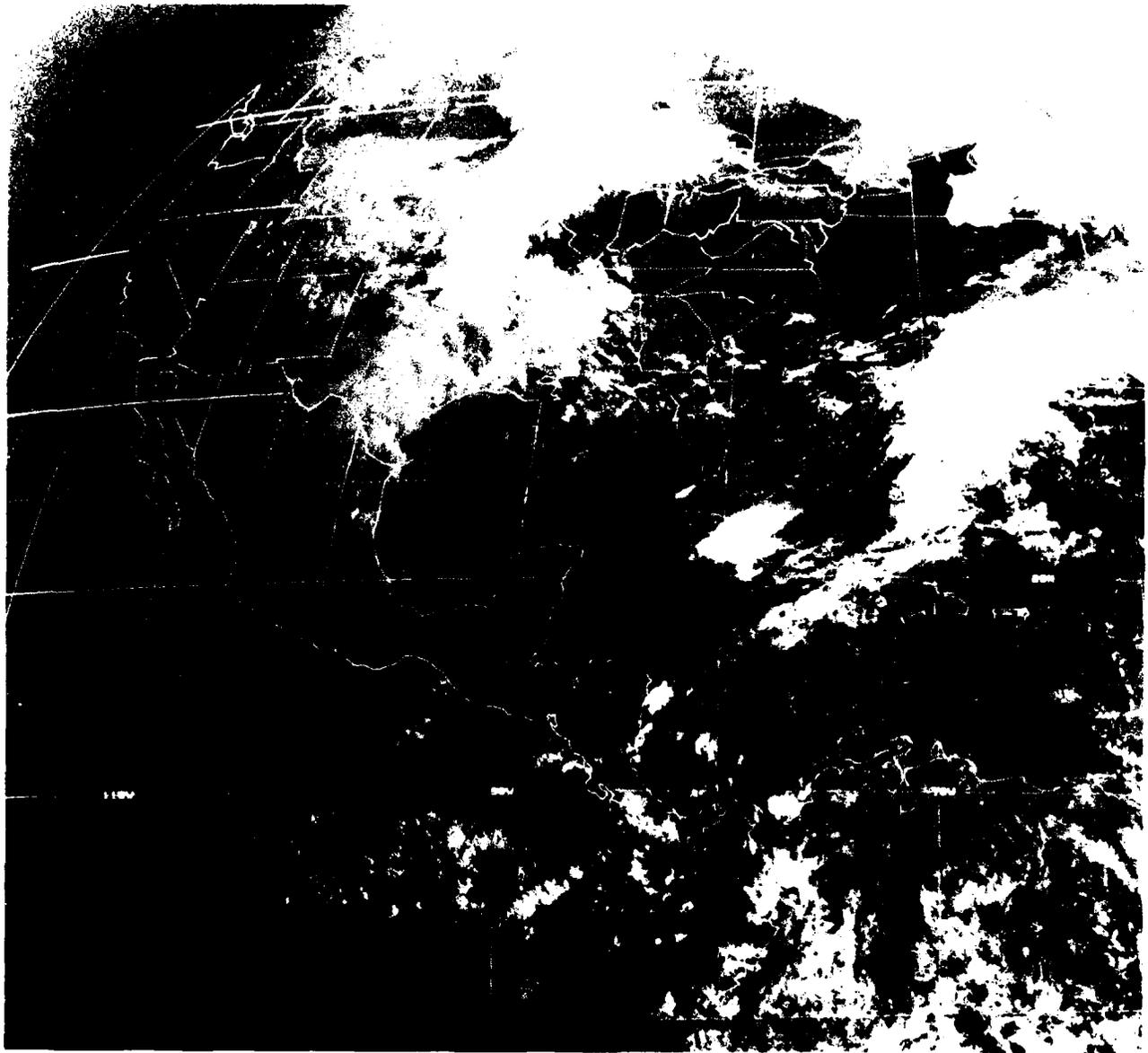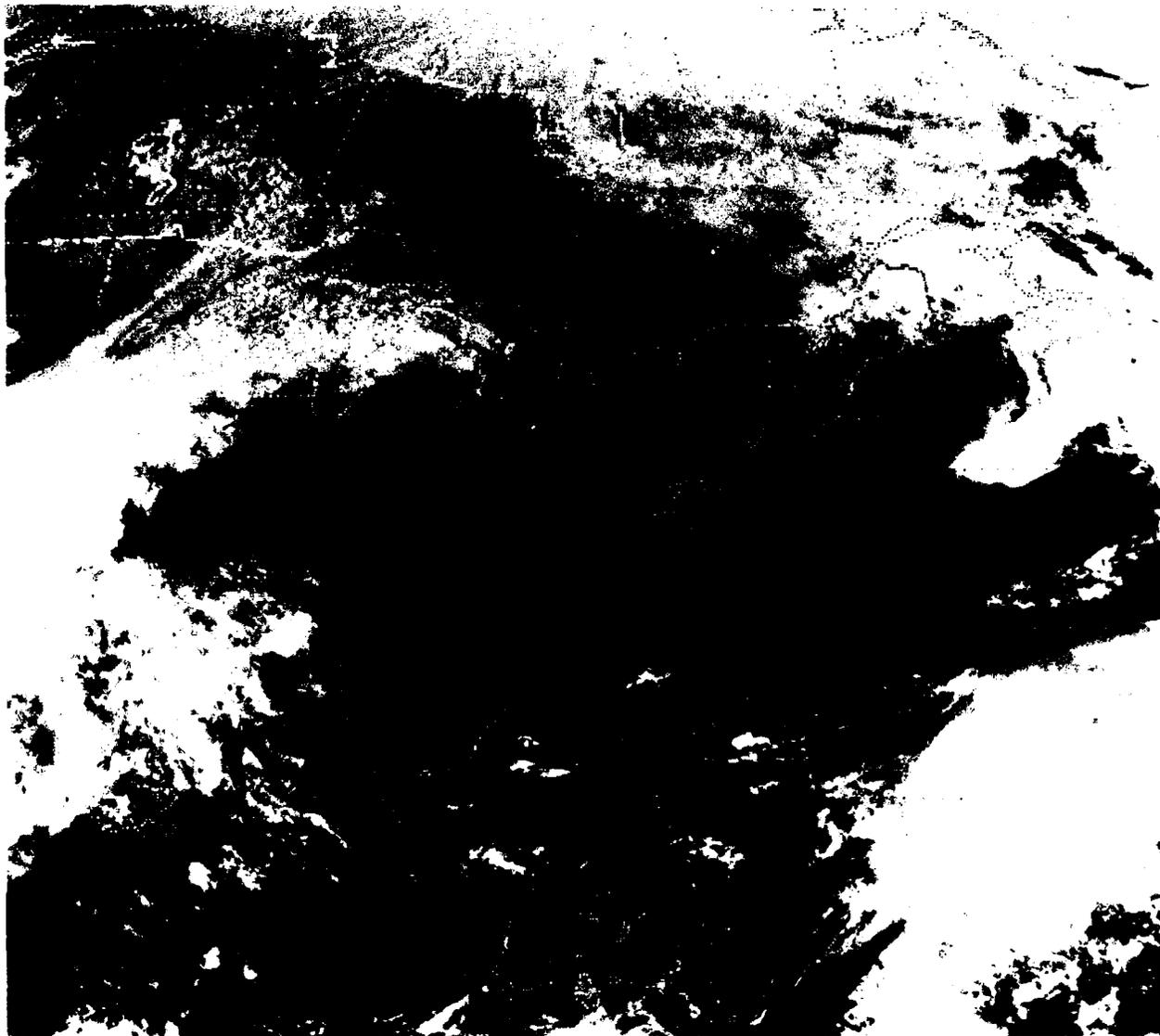
Figure 4-3(c): GOES (DB5 VIS) 2 May 1330G

detectable in the report figures because of degradation through the printing process). Coastal features, lakes, and rivers, as well as the freeze-line in Canada northeast of the Great Lakes, can be seen in the DMSP image (Fig. 4-3(a)); these features are much less distinct in the GOES DB5 image (Fig. 4-3(c)) and are difficult to detect at all in the WB1 image (Fig. 4-3(b)).

Since these images are nearly concurrent, little change in cloud cover occurs between the times of the GOES and DMSP observations. Cloud features that can be seen in the corresponding images include the following:

a) A major cloud system associated with a low in central Canada covers a large portion of the central United States. The eastern portion of this cloud system can be seen in the DMSP and GOES sectorized images, whereas the entire system can be seen in the GOES North America image. The major elements of this cloud system can be identified in all three images, although the structure within the cloud, such as in the Great Lakes area, is not as well defined in the GOES WB1 image (Fig. 4-3(a)). The definition of the cloud edge appears similar in the DMSP and GOES DB5 images.

b) The cloud mass over the Atlantic east of Florida in the GOES images -- especially the DB5 image -- appears to consist of a substantial amount of cirriform cloud; much of this cloud area is saturated in the DMSP image making the cirriform cloud difficult to distinguish.

c) A thunderstorm complex over Cuba shows more definition even in the GOES WB1 image than in the DMSP image because of the saturation problem. However, thin cirrus just north of this complex near Florida and extending eastward over the Atlantic is very sharply defined in DMSP; this cirrus can be seen in the GOES DB5 but is difficult to detect in the GOES WB1 image. Many small cloud elements in this area are much more sharply defined in DMSP than in GOES.

d) An area of wave clouds over New England provides an excellent opportunity for comparing the corresponding resolutions of the sensors. These wave clouds are very distinct in DMSP because of the higher resolution and picture contrast. The clouds are less sharp in the GOES DB5 and are difficult to detect in the GOES WB1 image. Similarly, the cloud band across Pennsylvania, which appears to be jet stream induced cirrus, has much greater definition in the DMSP image.

28

4.2.2 3 May 1979 (GOES to DMSP; NOAA to DMSP)

Excellent DMSP and GOES images on 3 May enable image intercomparisons at two observation times. Moreover, both visible and IR images were available for one of the observation times. Also, although the time interval is substantial, it is possible on this date to intercompare NOAA and DMSP data.

4.2.2.1 GOES (1500 GMT) to DMSP (1442 GMT)

A DMSP fine resolution visible image is shown in Figure 4-4(a); a GOES visible image about 40 minutes later is shown in Figure 4-4(b). These images view a good portion of the United States, which is covered by extensive cloudiness. Only the western part of the country is cloud-free, where many terrain features, including mountain snow, can be readily identified in the DMSP image. These images enable a comparison of a large and very complex cloud system; some of the main features of the cloud system are the following:

a) Large cells are embedded in the overall cloud mass in the Texas-Oklahoma area. These cells can be detected in both images because of their shadows at the low sun angle, but they are much more distinct in DMSP.

b) Cirrus bands extending from Mexico northeastward over the U.S. are visible in both DMSP and GOES; these bands originate over the central Mexican mountains. The fine detail of these bands, such as transverse waves, can be identified in the DMSP image.

c) The cloud area over the southeastern U.S. to the east of the large cells has considerable detail that is distinct in DMSP but tends to be smoothed out in GOES.

4.2.2.2 GOES (1700 GMT) to DMSP (1709 GMT)

DMSP smoothed resolution visible and IR images (Figs. 4-5(a) and 4-5(b)) were also available on 3 May, approximateley two hours after the image discussed in the previous section. These data sets can be compared with GOES visible and IR images at nearly the same time (Figs. 4-6(a) and 4-6(b)). Because the DMSP images view essentially the same area as the earlier observation, many of the same cloud features can be recognized, including those described below.

Figure 4-4(d):   DMSP (LF) X-Ray Image

Figure 4-4(b): GOES (WB1 VIS) 3 May 1500G

31
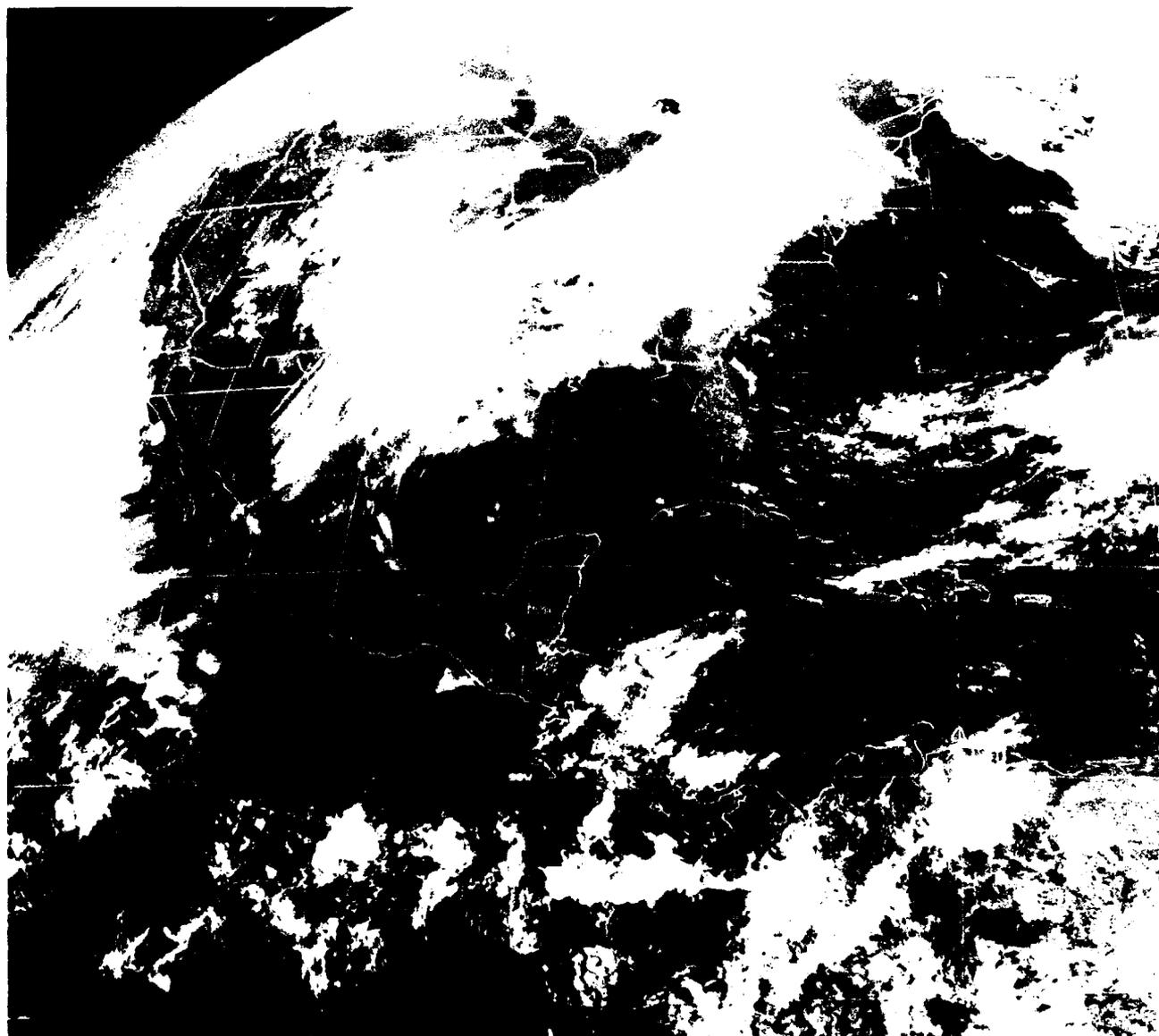
Figure 4-5(a): DMSP (LS) 3 May 1709G
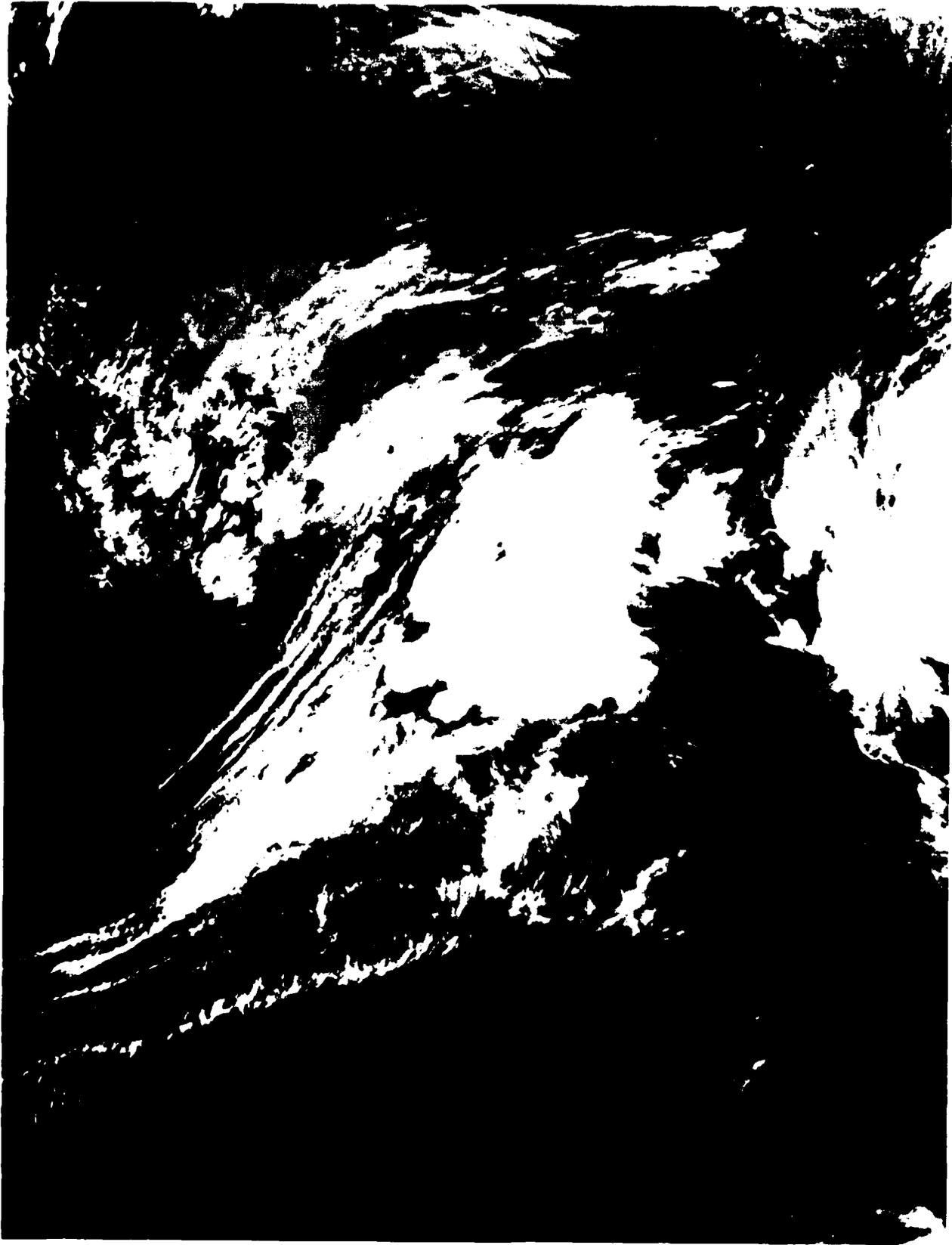
Figure 4-5(b):   DMSP (TS) 3 May 1709G

33
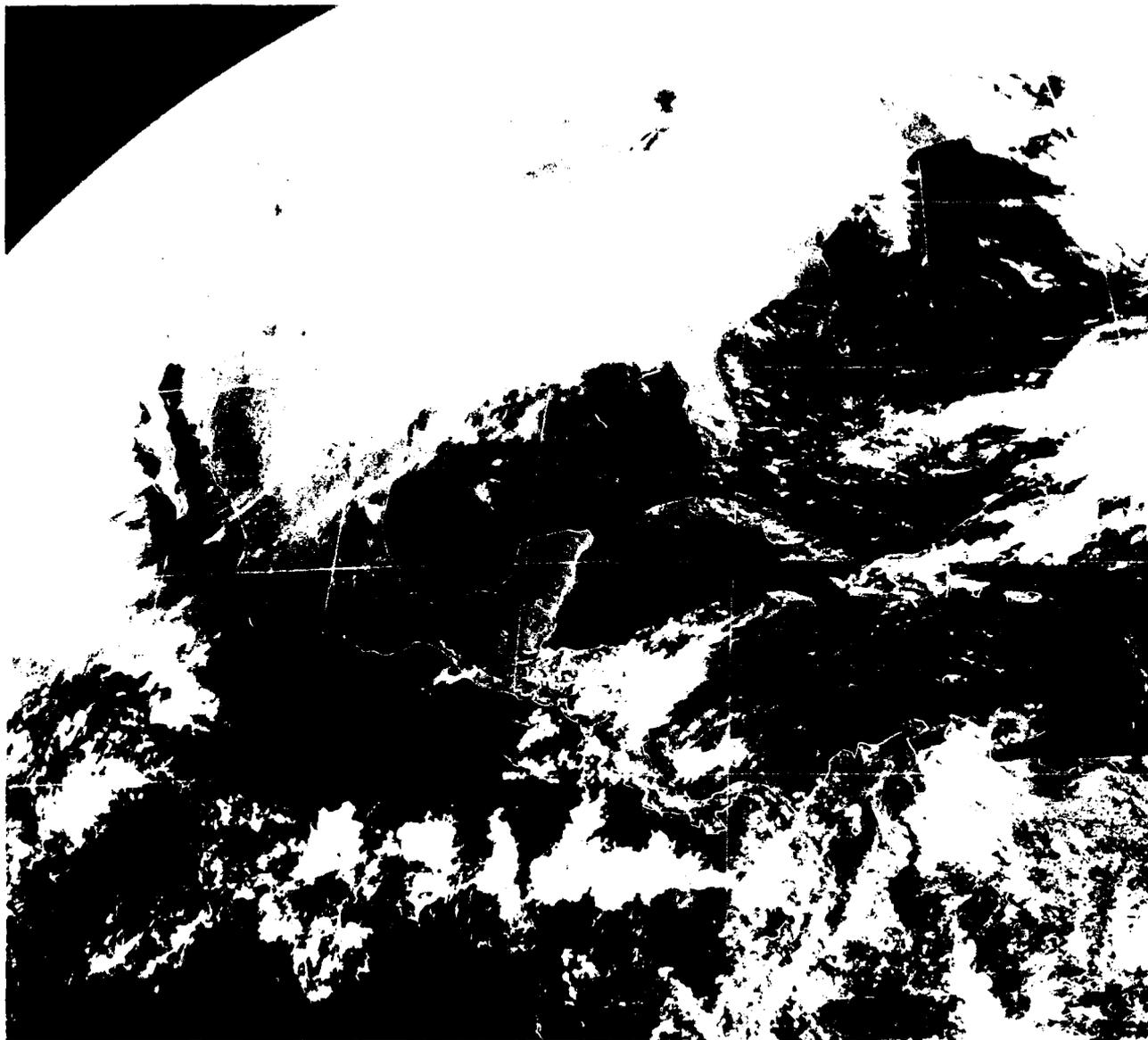
Figure 4-6(a): GOES (WBl VIS) 3 May 1700G
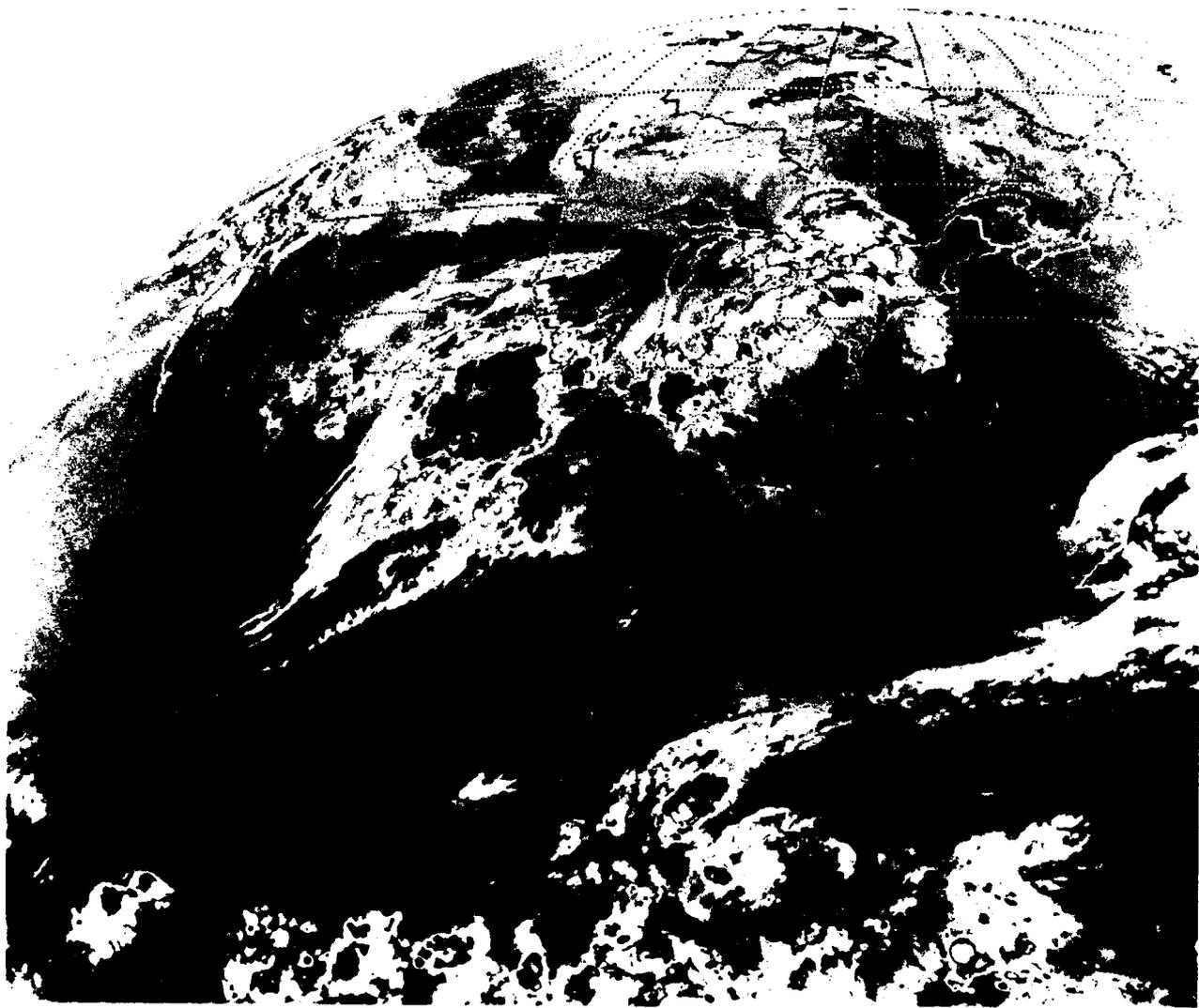
Figure 4-6(b): GOES (WB1 IR) 3 May 1700G

35

a)   Large cells still exist in the Texas-Oklahoma area and are still considerably more distinct in the DMSP visible image because of more pronounced shadowing. The area of the cells is very distinct from other clouds in the DMSP IR, but definition of individual cells is not possible, because the entire area appears saturated (Fig. 4-5(b)). The GOES IR data (Fig. 4-6(b)) are presented with an enhancement curve that brings out better definition in the area of the large cells.

b)   The cirrus bands that were seen earlier are still very evident. Both of the IR images give excellent definition of these bands over the lower (warmer) cloud.

c)   Terrain features in the northern Rocky Mountain area can be identified in both the DMSP visible and IR images; these features are more difficult to detect in the GOES images because of the poor viewing angle.

4.2.2.3   NOAA (2144 GMT) to DMSP (1709 GMT)

NOAA AVHRR images covering the western U.S. about four hours later than the DMSP images (Figs. 4-5(a) and 4-5(b)) are shown in Figures 4-7(a) and 4-7(b) (visible) and 4-8(a) and 4-8(b) (IR); since the NOAA prints are produced at a larger scale, two frames cover approximately the same area as one DMSP image. Because of the time interval, the overall cloud patterns can be recognized, but individual features have undergone considerable change. Terrain features, such as the Great Salt Lake and mountain snow patterns, of course, remain stable and can be identified in both types of data. These features provide an indication of the comparative resolution and contrast of the NOAA and DMSP images. Since these DMSP images are the smoothed resolution data, the NOAA AVHRR resolution is better; the difference in resolution is evident when the images are compared. The NOAA images, however, are not corrected for edge distortion as are the DMSP images.

Although mountain areas to the north of the Great Salt Lake remain clear over the four-hour period (stable snow patterns), cloudiness covering the mountains to the east of the lake in the DMSP images appears to have dissipated by the time of the NOAA observation; conversely, areas of small cellular cloud not evident in DMSP appear to have developed four hours later. Some of the cirrus bands over the southweatern U.S. appear to remain remarkably stable. The stability of these clouds is particularly evident in the

36

Figure 4-7(a):   NOAA AVHRR (VIS) 3 May 2148G - Northern frame

Figure 4-7(b): NOAA AVHRR (VIS) 3 May 2144G - Southern frame

Figure 4-8(a): NOAA AVHRR (IR) 3 May 2148G – Northern frame

Figure 4-8(b): NOAA AVHRR (IR) 3 May 2144G – Southern frame

corresponding IR images (Figs. 4-5(b) and 4-8(b)), both of which depict excellent definition of the high cirrus bands over the lower cloud.

4.2.3. 4 May 1979 (GOES to DMSP, NOAA to DMSP)

4.2.3.1 GOES (1230 GMT) to DMSP (1229 GMT)

On 4 May, two DMSP observations about four hours apart were available. The earlier of these observations, taken in the morning at a very low sun angle, is shown in Fig. 4-9(a); the concurrent GOES image is shown in Fig. 4-9(b). Because of the low sun angle, the GOES image has considerable cloud shadowing but is rather low contrast overall. The high resolution DMSP image has pronounced shadowing, which serves to enhance many of the cloud features (in this image, terrain shadowing can even be detected along the western edge of the image). Considerable information on the vertical structure within the large cloud mass over the central United States can be deduced from the cloud shadows.

Another effect of the low sun angle in the DMSP image (Fig. 4-9(a)) is the pronounced sun glint along the eastern edge of the image, especially in the Florida area. The sunglint in combination with the shadowing appears to enhance small cloud elements over the ocean in that area. The analyst must also be aware of the reversal in reflectance caused by sunglint; water bodies in Florida appear bright against a darker background whereas some of the clouds over the water near Florida appear dark against a brighter background. Because the GOES satellite is at geosynchronous altitude, sunglint is not an effect in that image (a slight error in the geogrphic grid of the GOES image is evident in Fig. 4-9(b).)

4.2.3.2 GOES (1700 GMT) to DMSP (1651 GMT)

DMSP high resolution visible and smoothed resolution IR images about four hours later are shown in Figures 4-10(a) and 4-10(b). These images are very high contrast with the major cloud features saturated in both; on the other hand, considerable terrain detail is evident. Corresponding GOES images are shown in Figures 4-11(a) and 4-11(b); in this instance, the GOES IR is the eastern U.S. sectorized, whereas the visible is the North American image.

In the major cloud mass covering the south central U.S., the higher cloud tops are distinct from the lower clouds, but little detail is evident within

Figure 4-9(a): DMSP (LF) 4 May 1229G

42
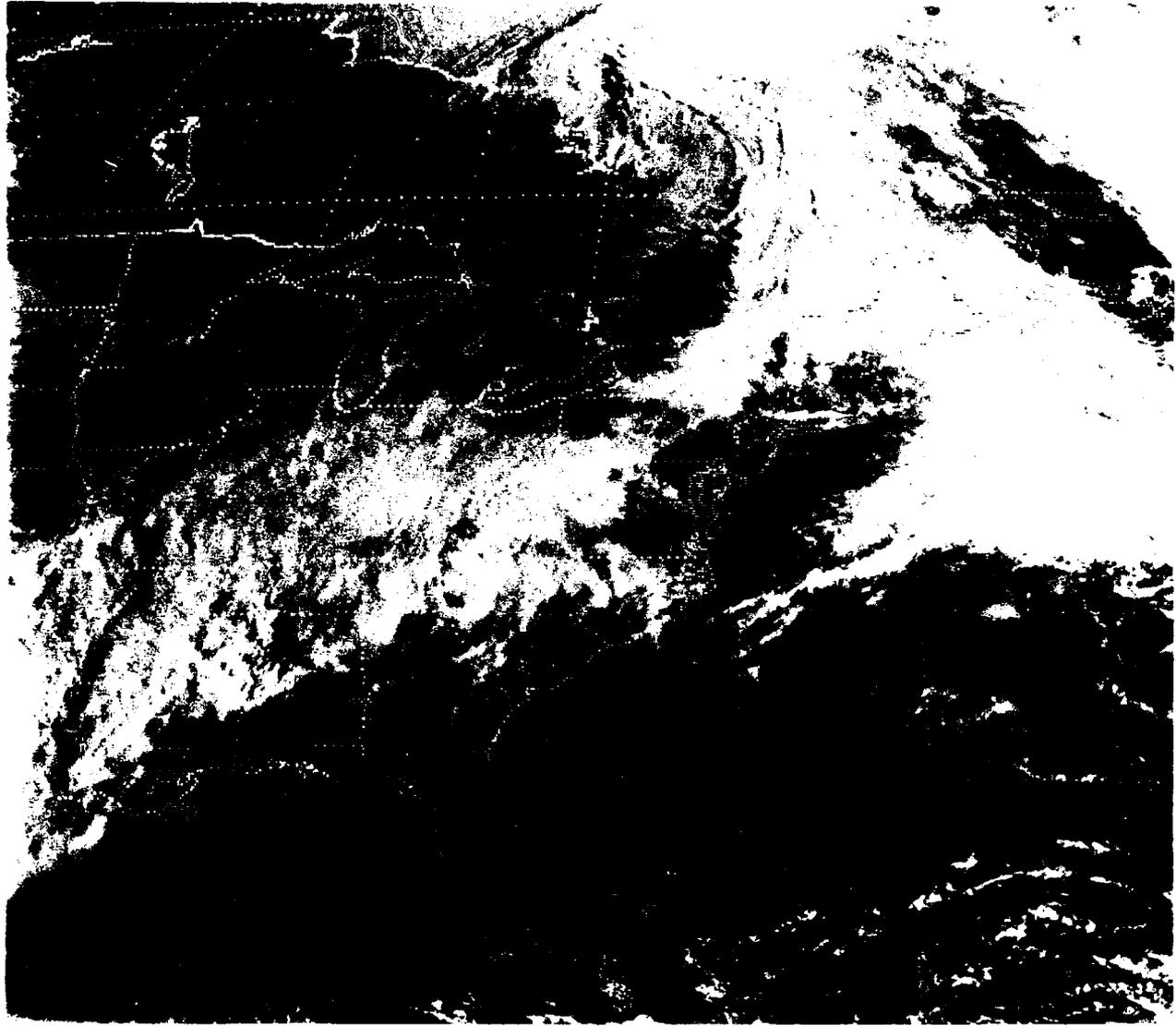
Figure 4-9(b): GOES (DB5 VIS) 4 May 1230G

43

Figure 4-10(a): DMSP (LF) 4 May 1651G

Figure 4-10(b): DMSP (TS) 4 May 1651G

45
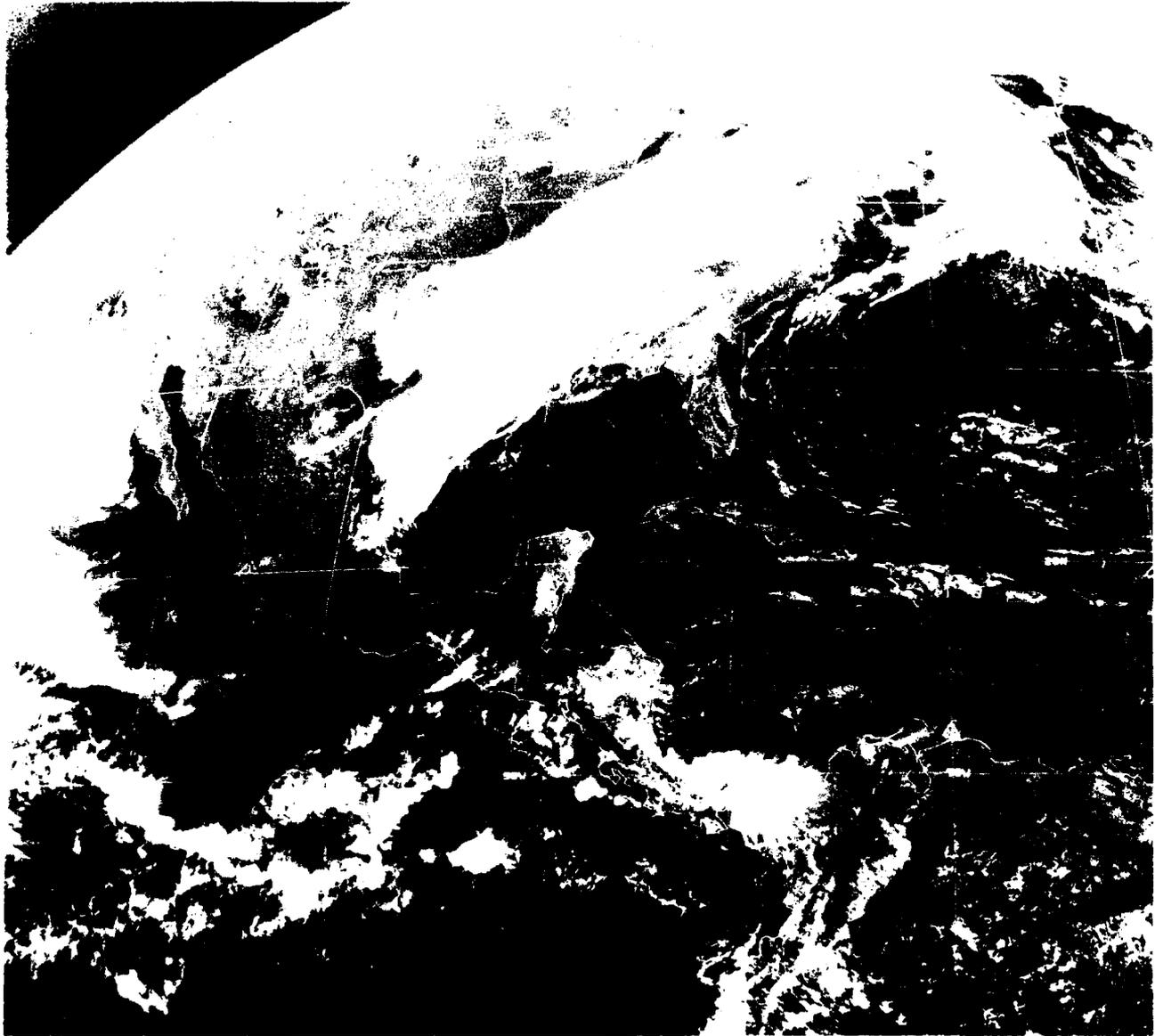
Figure 4-11(a): GOES (WB1 VIS) 4 May 1700G

46
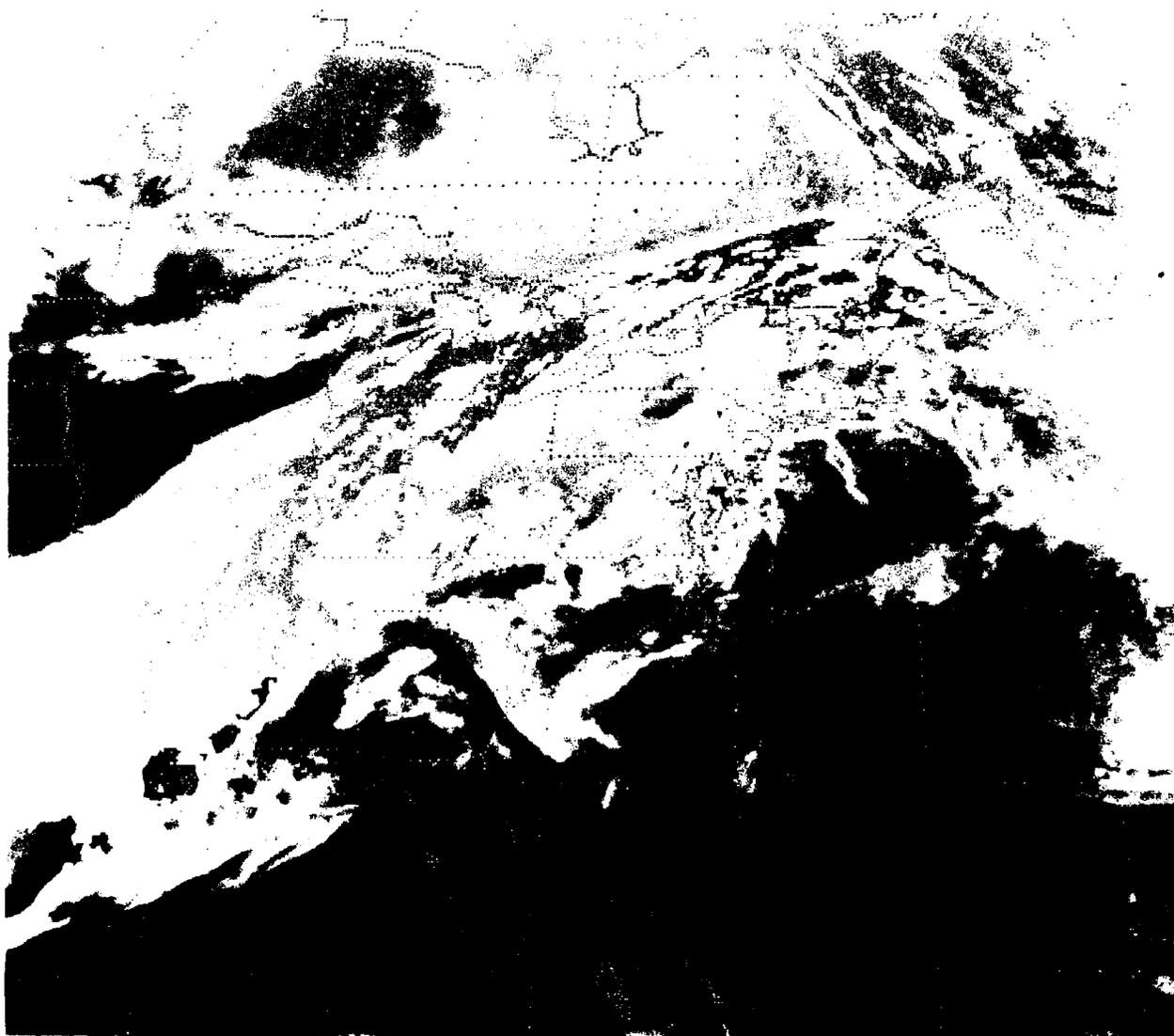
Figure 4-11(b):   GOES (DB5 IR) 4 May 1700G

47

the cloud shield. The GOES images display greater detail in the visible and considerable detail in the IR because of the enhancement curve used; for example, individual cells along the southern part of the cloud system are depicted (Fig. 4-11(b)).

Over the southeastern U.S. and Florida peninsula, the land-based cellular field is very distinct in the DMSP visible image (Fig. 4-10(a)), in contrast to the GOES visible image (Fig. 4-11(a)) where the individual cells cannot be distinguished. A band of cloud with a sharply defined edge extending off the coast north of Florida is deduced from the IR data to be high (cold) cloud; in the DMSP visible image, this cloud appears opaque, whereas in the GOES image the cloud is seen to be a band of thin cirrus.

4.2.3.3 NOAA (1951 GMT) to DMSP (1651 GMT)

The DMSP images shown in Figures 4-10(a) and 4-10(b) can be compared with NOAA AVHRR images some three hours later (Figs. 4-12(a) and 4-12(b)). Although the NOAA viewing angle is poor because of edge distortion, it is possible to compare the overall cellular field and other clouds over Florida and the Southeast. Of particular interest is the observation that the cellular cloud is more distinct in the DMSP visible image than in the NOAA visible image, whereas in the IR images, the opposite is true. These differences are due, at least in part, to the resolution differences in the DMSP data (fine resolution visible but smoothed IR). The NOAA images also verify that the cloud band to the northeast of Florida (still easily-identified despite the time interval) is indeed thin cirrus.

4.2.4 6 May 1979 (GOES to DMSP)

4.2.4.1 GOES (1200 GMT) to DMSP (1149 GMT)

The availability of data from three DMSP satellites on 6 May provides the opportunity to view the eastern U.S. three times over a four-hour period. Two of these observations are discussed below; the third observation is discussed in Section 4.3. The first of these observations is shown in Figure 4-13(a); the corresponding GOES image is shown in Figure 4-13(b). This DMSP visible image is similar to that shown in Figure 4-9(a), with the low sun angle resulting in pronounced cloud shadowing and a strong sun glint pattern. The GOES image has very low contrast, with clouds near the terminator (in the

48
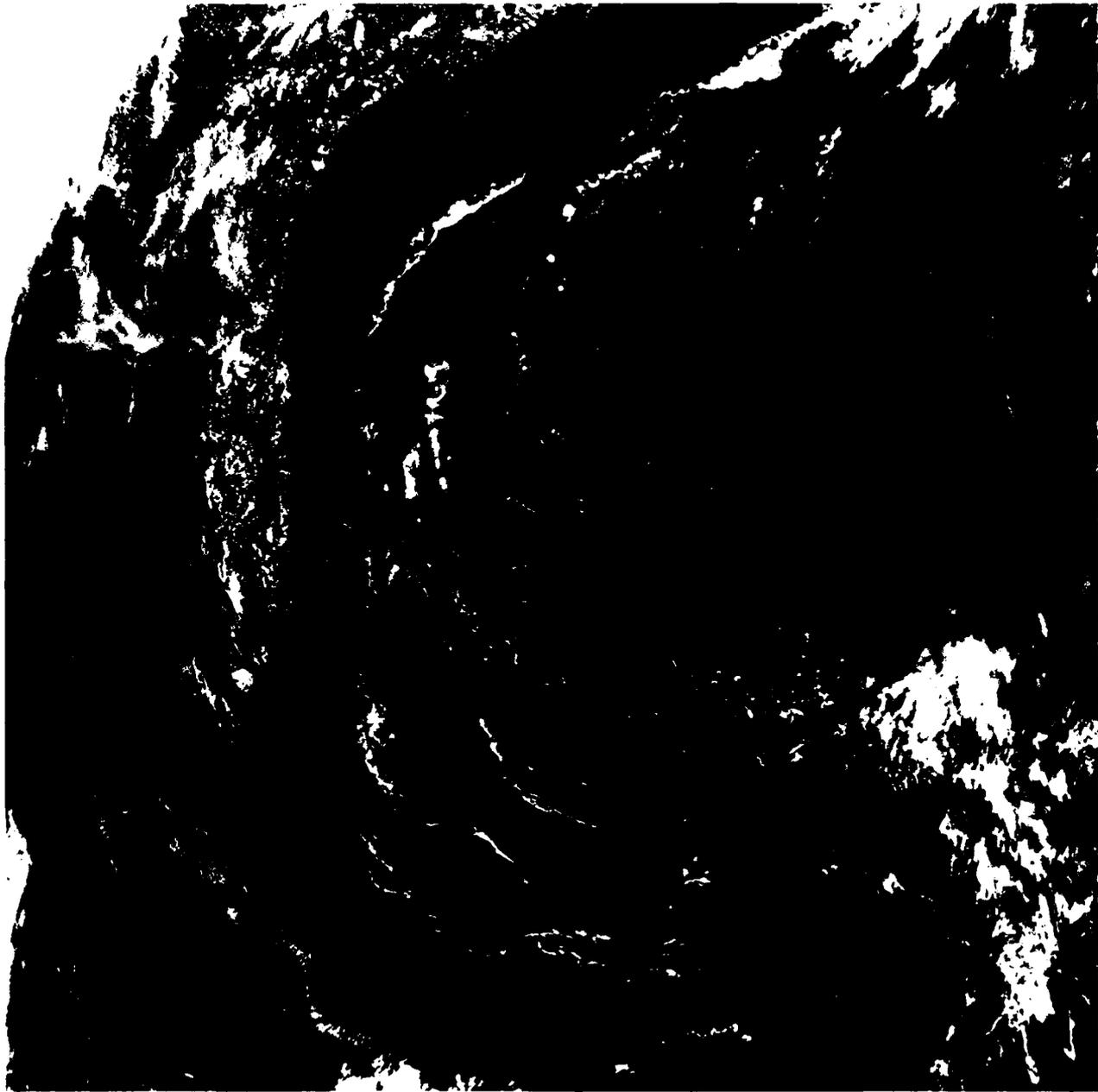
Figure 4-12(a):   NOAA AVHRR (VIS) 1951G (Florida area)

Figure 4-12(b): NOAA AVHRR (IR) 1951G (Florida area)

Figure 4-13(a):   DMSP (LF) 6 May 1149G

51

Figure 4-13(b): GOES (WB1 VIS) 6 May 1200G

central U.S.) difficult to detect. As in the earlier DMSP low sun angle image, terrain features along the east coast and tropical cloudiness over the ocean appear to be enhanced by the shadowing and sun glint. However, some cloud features, such as the frontal band extending off the East Coast, are almost obscured due to the lack of contrast between the high reflectance of the cloud and the sun glint. This cloud band is well defined in the GOES image.

4.2.4.2 GOES (1400 GMT) to DMSP (1348 GMT)

The same general area is viewed two hours later by DMSP (Fig. 4-14(a)) and GOES (Fig. 4-14(b)). At this time ,there is only a slight indication of sun glint in the DMSP image and much better contrast in the GOES image. Essentially the same cloud features can be seen as in the earlier observations. The frontal band that was obscured by sunglint earlier is now well defined. However, cumulus bands over the ocean south of Florida that were well defined in the earlier DMSP image because of the low sun angle are now less distinct. Similarly, there is less structure discernible in the clouds over the Caribbean to the west of Florida because of reduced shadowing.

4.3 Image Intercomparison of Cloud Features in Areas with Landsat Coverage

Landsat MSS imagery was acquired for some portion of the eastern United States on each of the four days of the May 1979 data set discussed above. The Landsat coverage is, of course, very limited as compared to DMSP and GOES because of the narrow width of the Landsat swath. Image intercomparisons for three of the days are presented in the following sections. On one day (3 May), it was possible only to compare Landsat to GOES because the DMSP image did not cover the same area; on 2 May, the greater time difference between the Landsat and DMSP observations did not permit a useful comparison.

4.3.1 6 May - Landsat Imagery

The data on 6 May provided the best opportunity to make use of the Landsat imagery because of the small time difference between the corresponding observations on that day. The only limitation to this data set is that the DMSP image available at nearly the same time as the Landsat pass is the smoothed resolution data.

53

Figure 4-14(a): DMSP (LF) 6 May 1348G
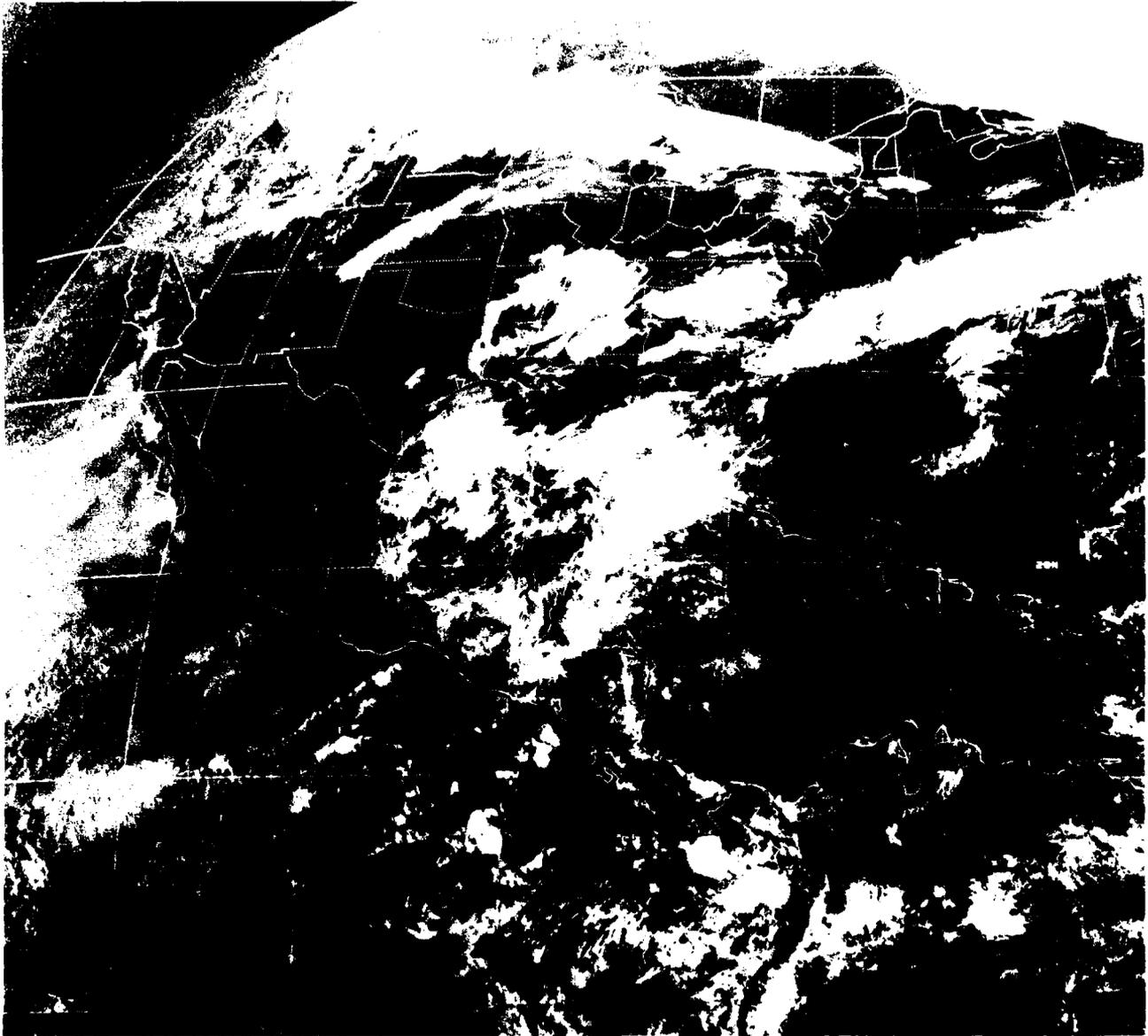
Figure 4-14(b): GOES (WB1 VIS) 6 May 1400G

A portion of the DMSP (LS) image at 1614 GMT, covering the northern U.S., is shown in Figure 4-15. Enlargements of the GOES visible and IR images at 1600 GMT, covering the north central U.S., are shown in Figures 4-16(a) and 4-16(b). These images are about two hours later than the images discussed in Section 4.2.4.2, and many of the cloud features seen in the earlier observations can be recognized. The addition of the GOES IR data at this time helps to verify the cloud types deduced from the earlier visible data; for example, the clouds over the south central U.S. that appear rather bright in the visible images are confirmed to be low-level stratus, whereas the cloud band across southern Lake Michigan is a band of high cirrus.

Landsat data were collected on this day (also at 1614 GMT) on a pass just west of Lake Michigan. The area covered by three Landsat scenes on this pass is outlined on the DMSP and GOES images (Figs. 4-15, 4-16(a), and 4-16(b)). The three Landsat MSS scenes (Band 5) are shown in Figures 4-17(a) through 4-17(c). The northernmost of the three scenes covers the southern boundary of the broad east-west cloud area over the Great Lakes; the middle scene is at the edge of the cirrus band just south of the Great Lakes; the southernmost scene is within the cirrus band.

4.3.1.1 Supporting Meteorological Observations

The surface weather chart at 1500 GMT on 6 May (Figure 4-18) indicates a stationary front lying east-west across the northern U.S. By 1800 GMT, the front in the Lake Michigan area is analyzed as a warm front. Stations in the area of Lake Superior report precipitation. Several cloud types are reported from stations north of the front; several stations south of the front are reporting cirrus.

Upper air charts at 1200 GMT indicate a southerly flow over the central U.S. at lower levels (850 mb) with dry air to the south and moisture over the northern Great Lakes. At the 500 mb level (Fig. 4-19), a trough is centered on the west coast with a broad area of west to southwesterly flow across the central U.S. The strongest winds at the 500 mb level appear to be in a band crossing the Great Lakes. An upper air sounding from a station in Minnesota located within the frontal cloud band shows considerable moisture at all levels up to nearly the 300 mb level.

56
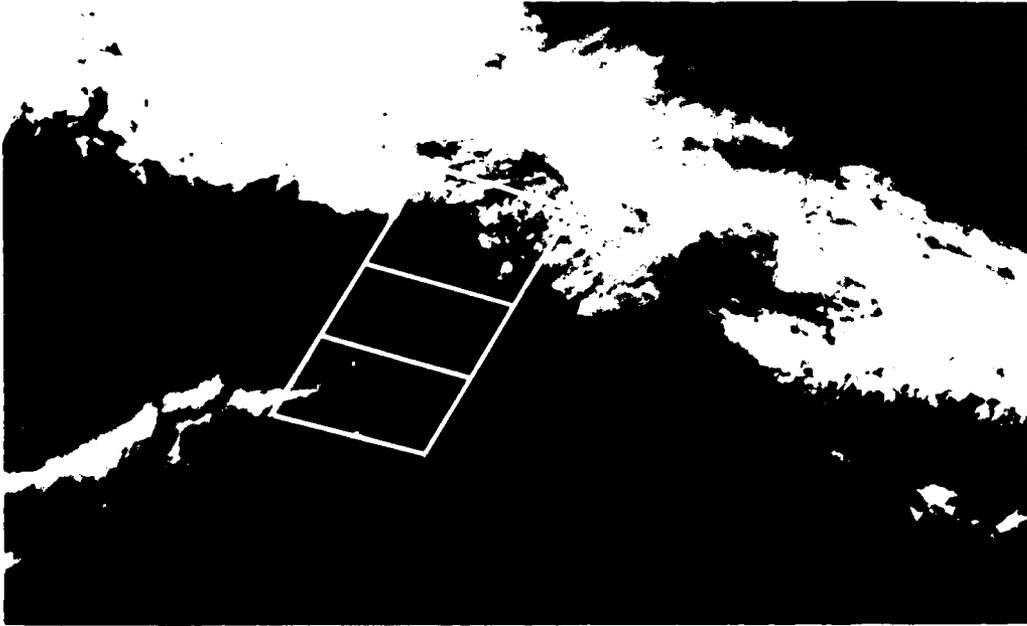
Figure 4-15: DMSP (LF) 6 May 1614G - Portion enlargement
(see Fig. 4-2(a))
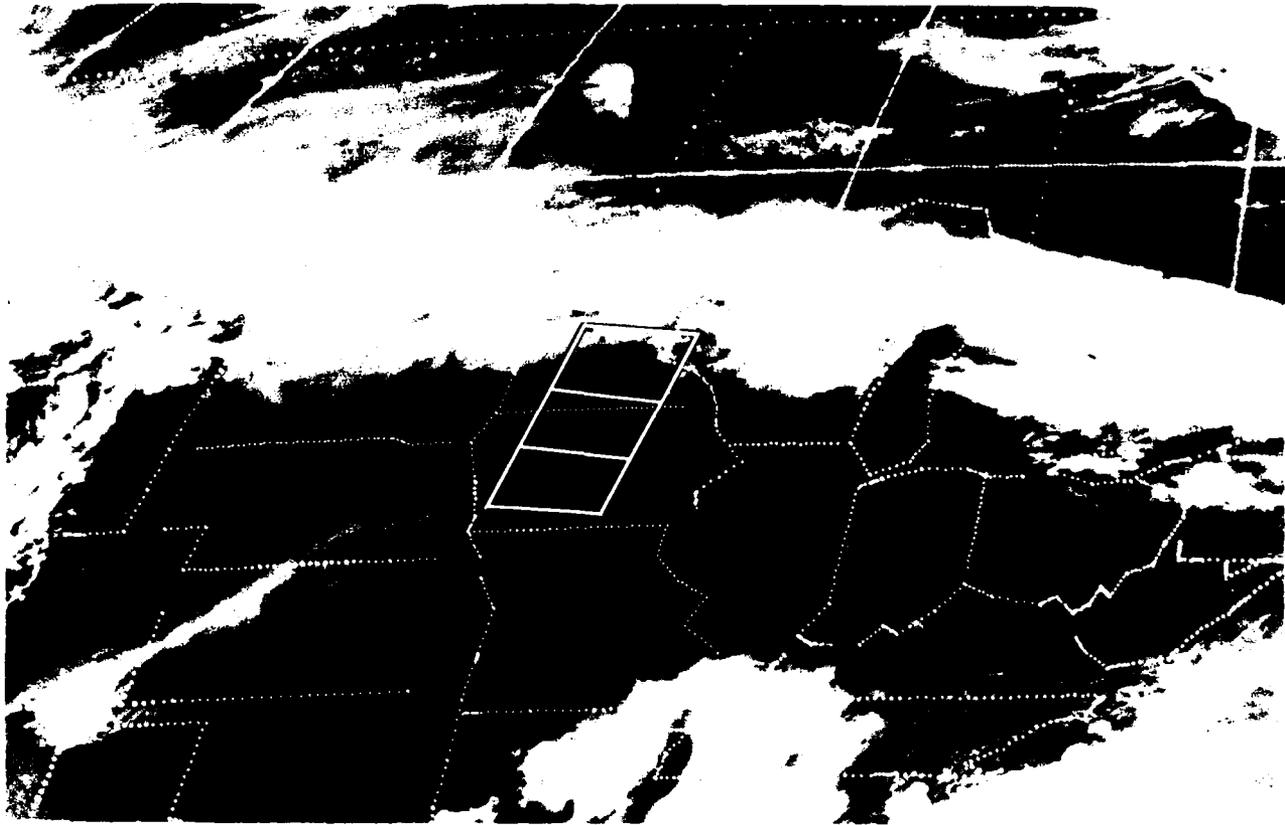
Figure 4-16(a): GOES (VIS) 6 May 1600G - Enlargement

58
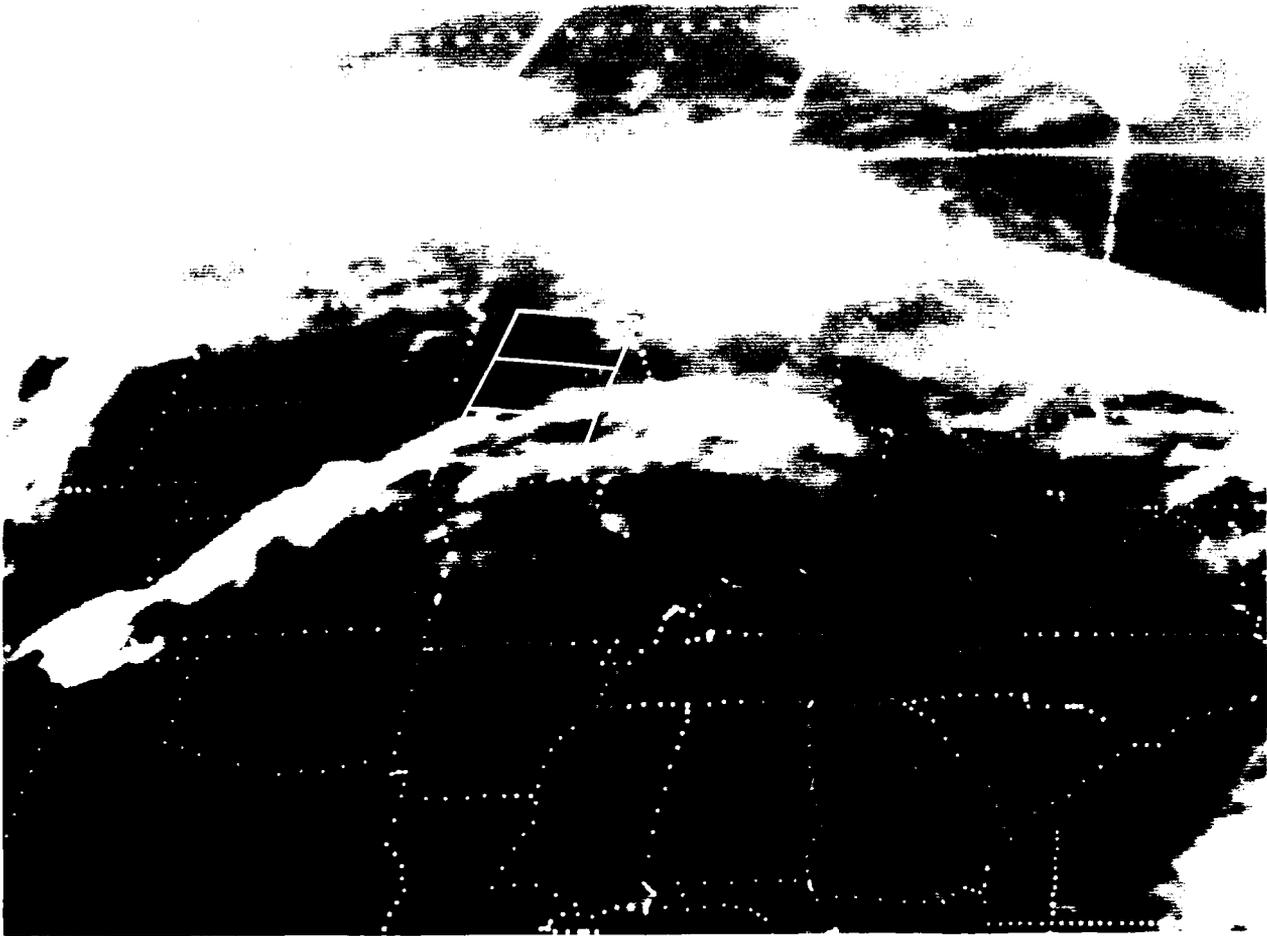
Figure 4-16(b):   GOES (IR) 6 May 1600G - Enlargement
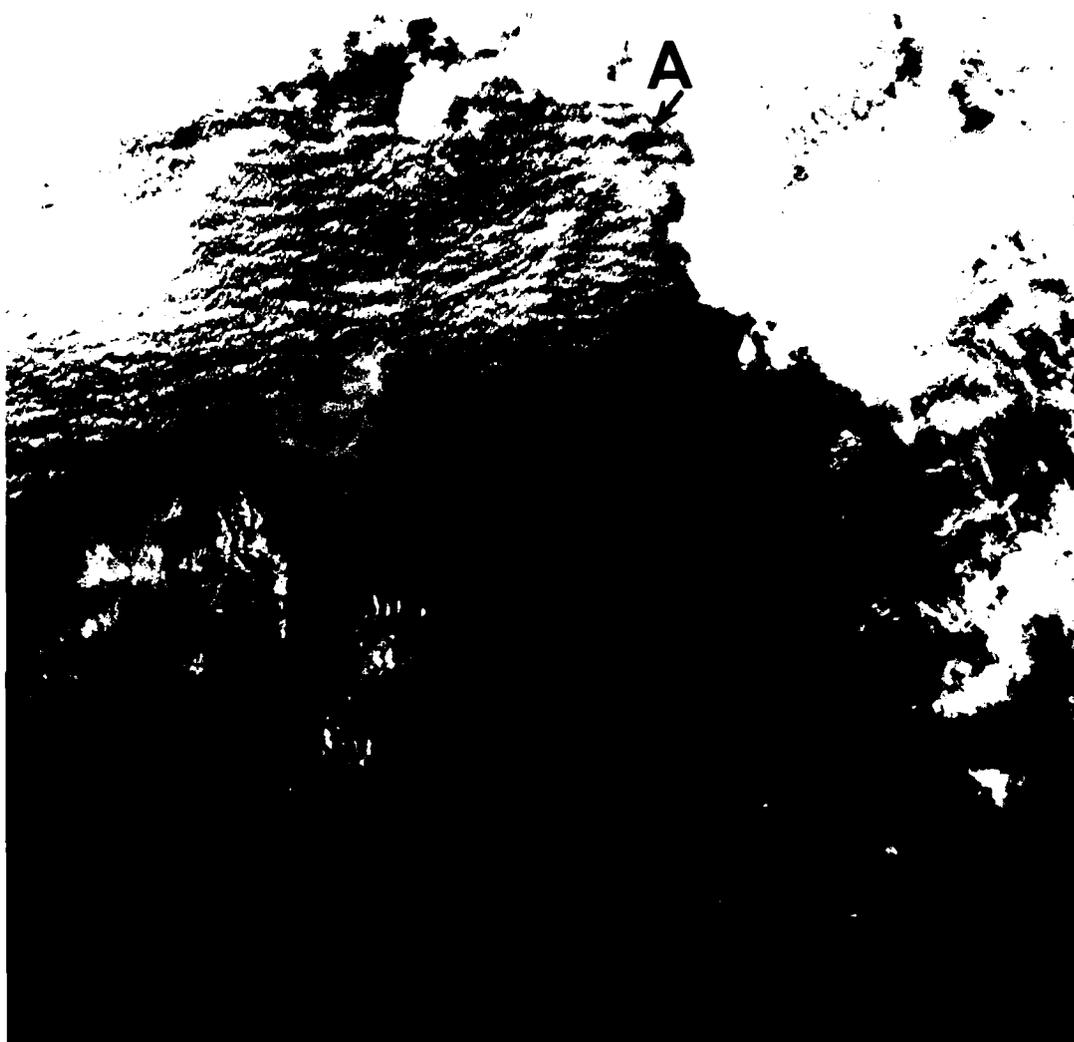
Figure 4-17(a):   Landsat MSS Band 5 (6 May) 1614G – Scene (a)
(Reproduced by permission of EOSAT)
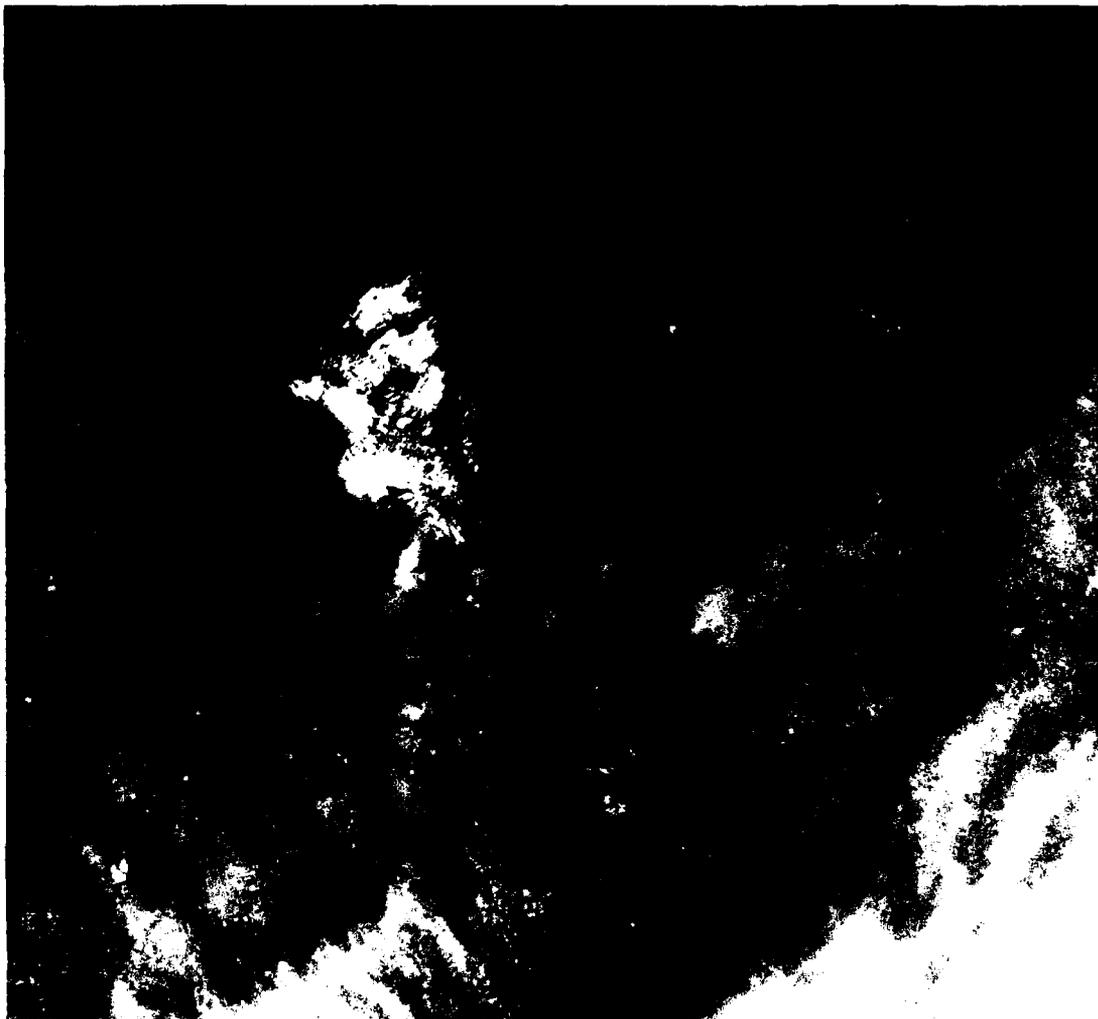
Figure 4-17(b):   Landsat MSS Band 5 (6 May) 1614G - Scene (b)
(Reproduced by permission of EOSAT)
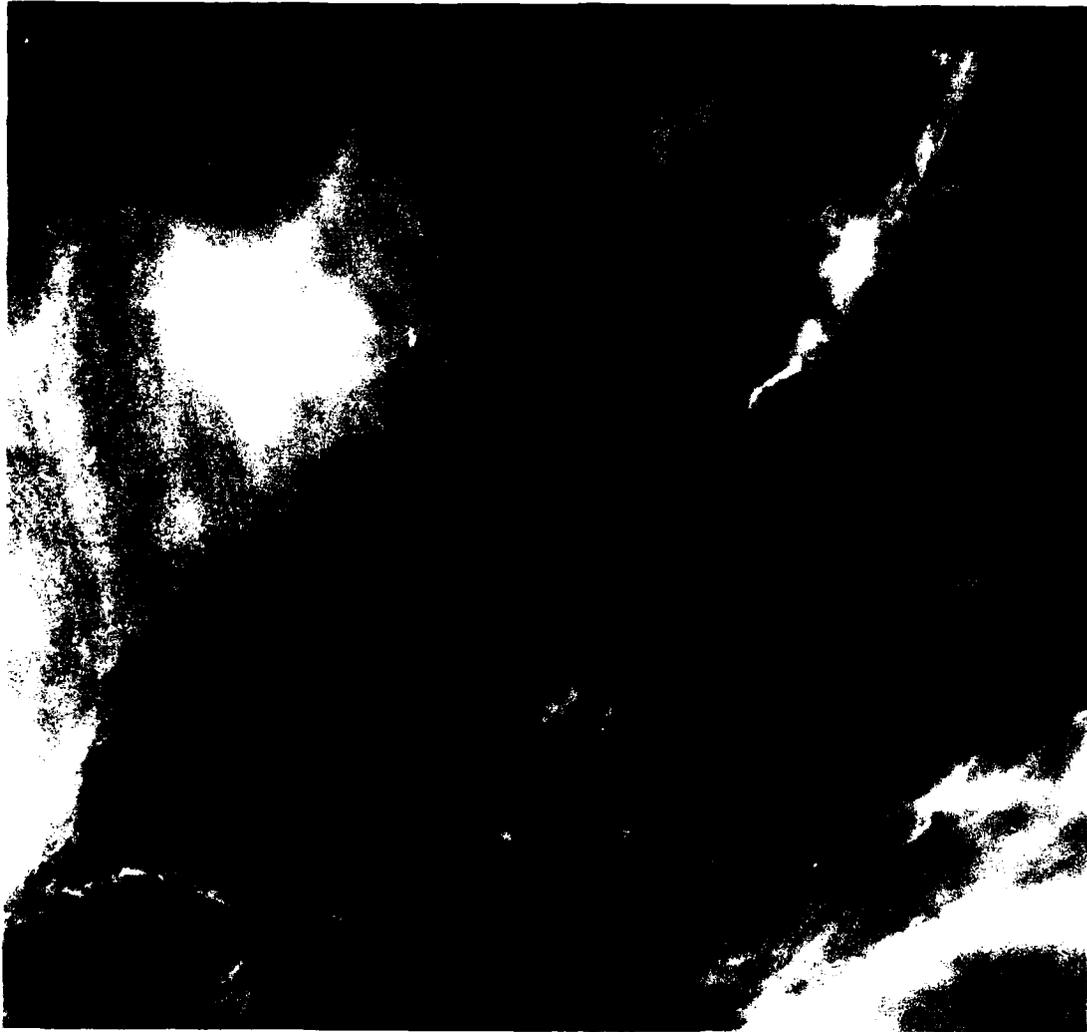
Figure 4-17(c):   Landsat MSS Band 5 (6 May) 1614G — Scene (c)
(Reproduced by permission of EOSAT)

62
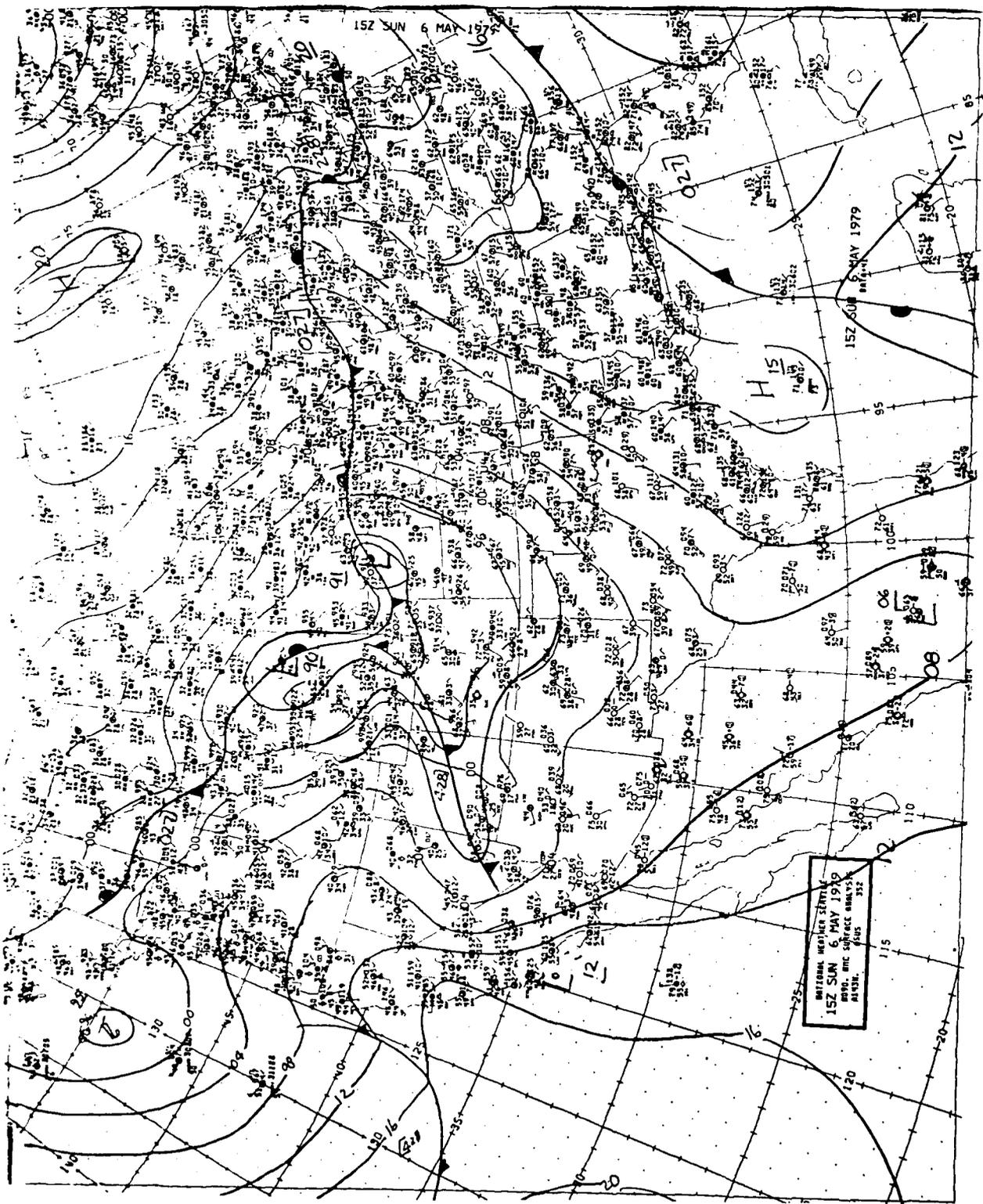
Figure 4-18: Surface chart 6 May 1500G
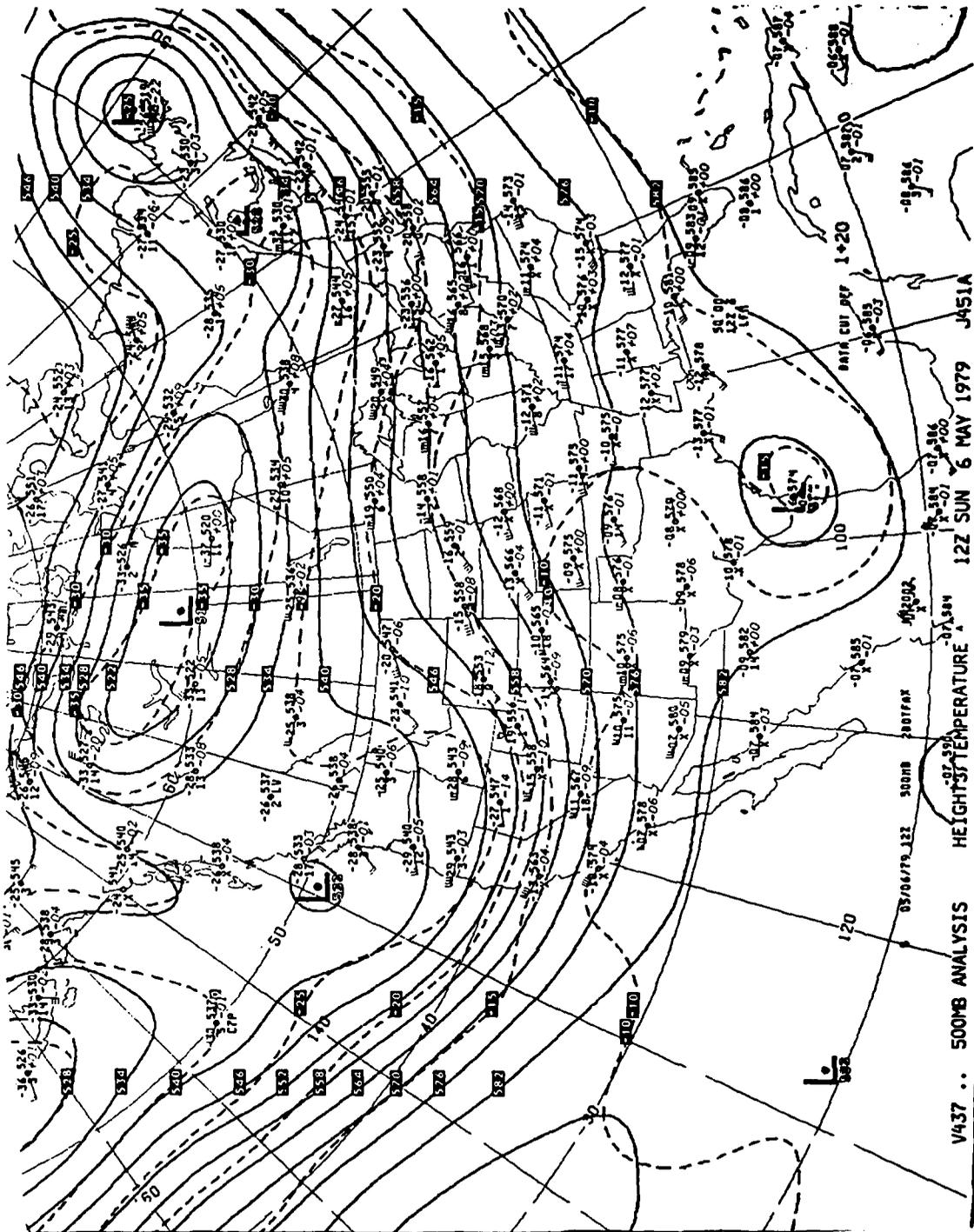
Figure 4-19:   500 mb Chart 6 May 1200G

At approximatley the time of the satellite observations, two reporting stations in Minnesota within the cloud covered area (St. Cloud and Minneapolis) report ten-tenths stratus. Minneapolis, located at Point A in the Landsat scene (Fig. 4-17(a)), reports five-tenths stratocumulus (Sc), one-tenth alto-cumulus (Ac), and three-tenths cirrus (Ci). Before the time of the Landsat pass, Minneapolis had been reporting ten-tenths Sc, and a couple of hours after the pass, reported a sky cover of one-tenth Ac and eight-tenths Ci, with three-tenths opaque. These observations appear to fit closely with the cloud types deduced from the Landsat image (Fig. 4-17(a)). Assuming a cloud motion toward the east or northeast, Minneapolis was first under the solid cloud seen in the northeast portion of the image, then under the area of less solid cloud that appears to be Sc or Ac, and finally under an area of Ci, which is likely the area of thin cloud seen in the west central part of the Landsat image.

4.3.1.2 Comparison of Cloud Features in Landsat, DMSP, and GOES Images

The overall cloud features can be identified in the DMSP and Landsat images, but because of the greatly differing resolutions, some of the cloud elements seen in Landsat are difficult to detect in DMSP. The area of Sc/Ac in Fig. 4-17(a) cannot be seen, for example, in the DMSP image. Al-though the cirrus band to the south that is very well defined in the Landsat images (Figs. 4-17(b) and (c)) can also be seen in the DMSP image, it is of interest to note that the small, very bright cloud (apparently lower cloud under the edge of the cirrus) in the middle Landsat scene (Fig. 4-17(b)) can-not be detected at all in the DMSP image. Undoubtedly, considerably more cloud detail would be evident if the DMSP image were the fine resolution.

In this instance, greater cloud detail can be seen in the enlarged GOES image (Fig. 4-16(a) than in the DMSP image. The area of Sc/Ac just to the south of the solid cloud can be detected in GOES, and there is even an indica-tion in GOES of the cloud area (Ac and Ci) seen in the west central portion of the Landsat image (Fig. 4-17(a)) just to the south of the Sc/Ac area. More-over, the cirrus band is more evident in GOES than in DMSP and, of course, is well defined in the IR data. The bright cloud in the middle Landsat scene, mentioned above, can be detected in the GOES visible image, although the cloud does not appear nearly as bright as in the Landsat images.

4.3.1.3 Spectral Variations in Landsat Imagery

The Landsat images shown in Figure 4-17 are all Band 5 (0.6-
0.7 μm). For the northernmost of these scenes, images for all four MSS bands
were acquired; these additional bands are shown in Figures 4-20(a) through
20(c). In the Band 4 image, much of the cloud is saturated, but the areas of
Sc/Ac and Ci show up quite well. In Bands 6 and 7, terrain features become
more visible, with opaque water bodies in sharp contrast to the highly reflec-
ting vegetation. The thinner clouds became more difficult to detect and
appear much more transparent than in Bands 4 or 5. In fact, an analyst would
likely estimate a greater percentage of Sc/Ac cloud cover from Band 4 than
from Band 7. The spectral variations in this scene are discussed further in
Section 5.

4.3.2 4 May 1979 - Landsat Imagery

On 4 May, a Landsat pass covered the area just to the west of Lake
Michigan about an hour before the DMSP image shown in Figure 4-10(a). The
specific area covered by four Landsat scenes acquired for use in this study is
outlined in an enlargement of a portion of the DMSP fine-resolution image
(1651 GMT) shown in Figure 4-21(a). The Band 5 image for the northernmost
Landsat scene (1600 GMT) is shown in Figure 4-21(b). The Bands 4 and 7 images
for the southernmost of the four Landsat scenes are shown in Figures 4-22(a)
and 4-22(b).

The Landsat path extends from a cloud area just west of Lake Michigan
southward across a clear slot to an extensive cloud area covering a large
portion of the central U.S. The DMSP IR image (Fig. 4-10(b)) indicates that
the extensive cloud system consists of high cloud in the area of the Landsat
pass (this cloud system is associated with a strong frontal system with sever-
al waves along it); the clouds near Lake Michigan, however, are indicated to
be primarily lower clouds with only a few patches of high cloud. The corre-
sponding GOES images at this time are shown in Figures 4-11(a) and 4-11(b).

Visible terrain features (rivers) in Landsat (Fig. 4-21(b)) and DMSP
provide excellent reference points for comparison of cloud features in the
corresponding images. Using the rivers as reference points, the cloud
movement in the time between the Landsat and the DMSP observations can be
determined. Because of the cloud movement, identification of exact cloud

66
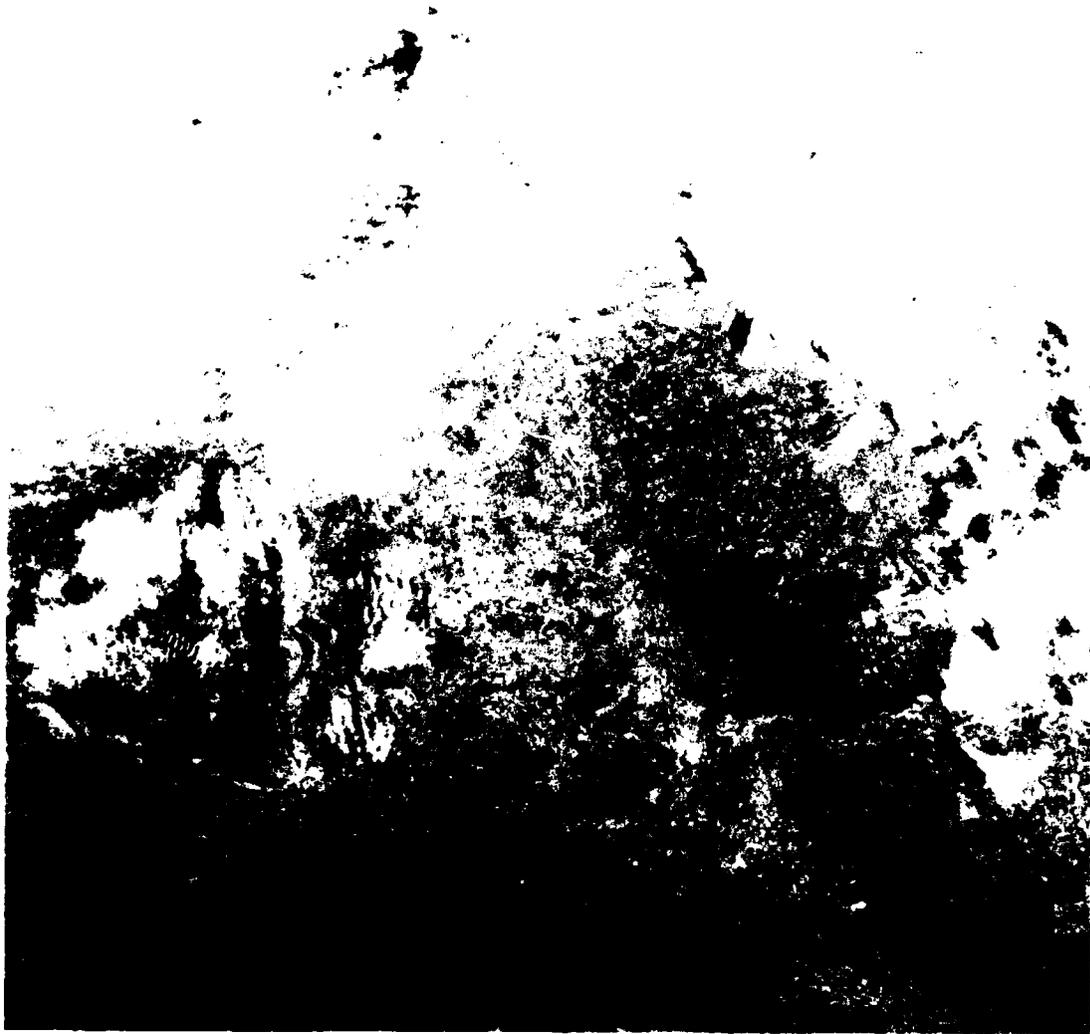
Figure 4-20(a):   Landsat MSS Band 4 (6 May) 1614G - Scene (a)
(Reproduced by permission of EOSAT)

67
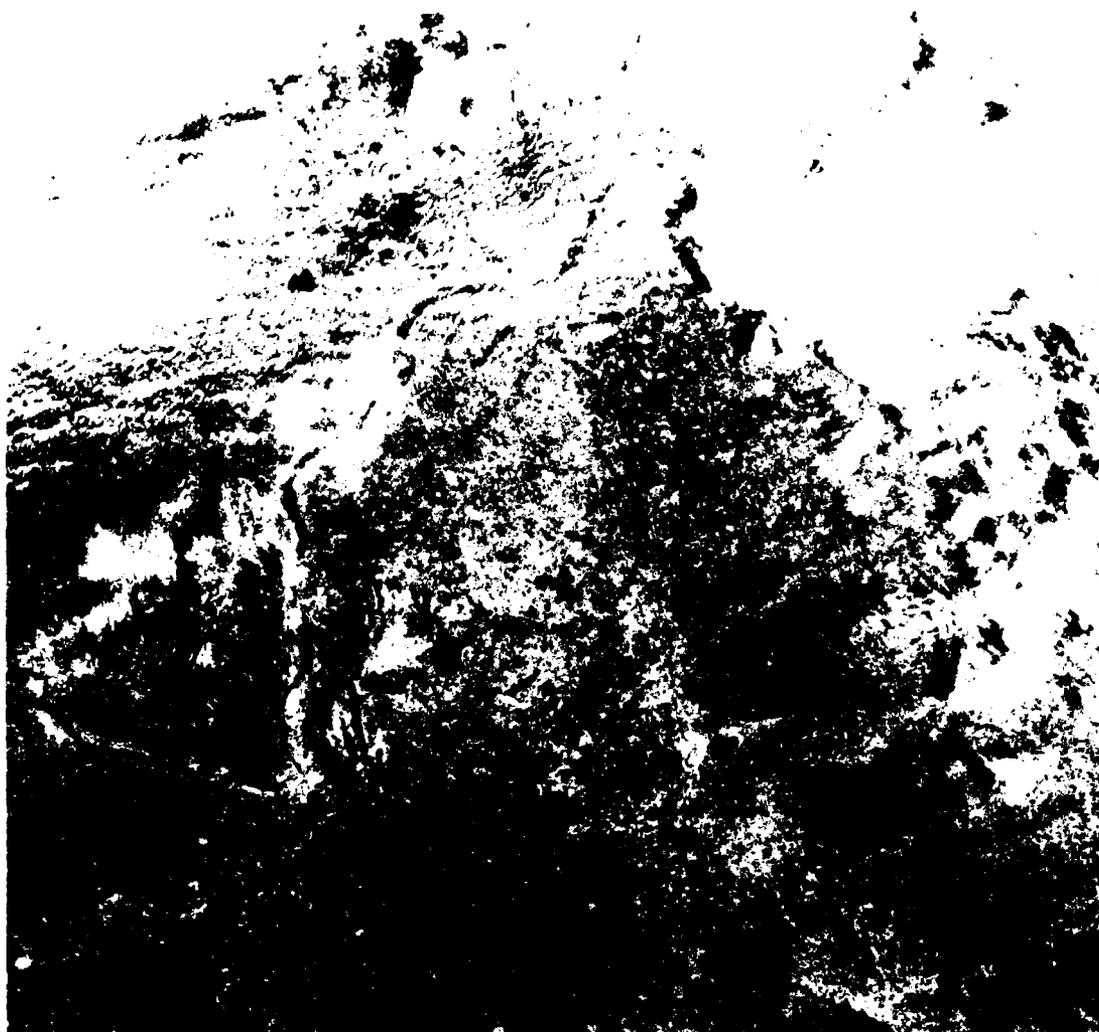
Figure 4-20(b): Landsat MSS Band 6 (6 May) 1614G – Scene (a)
(Reproduced by permission of EOSAT)

68
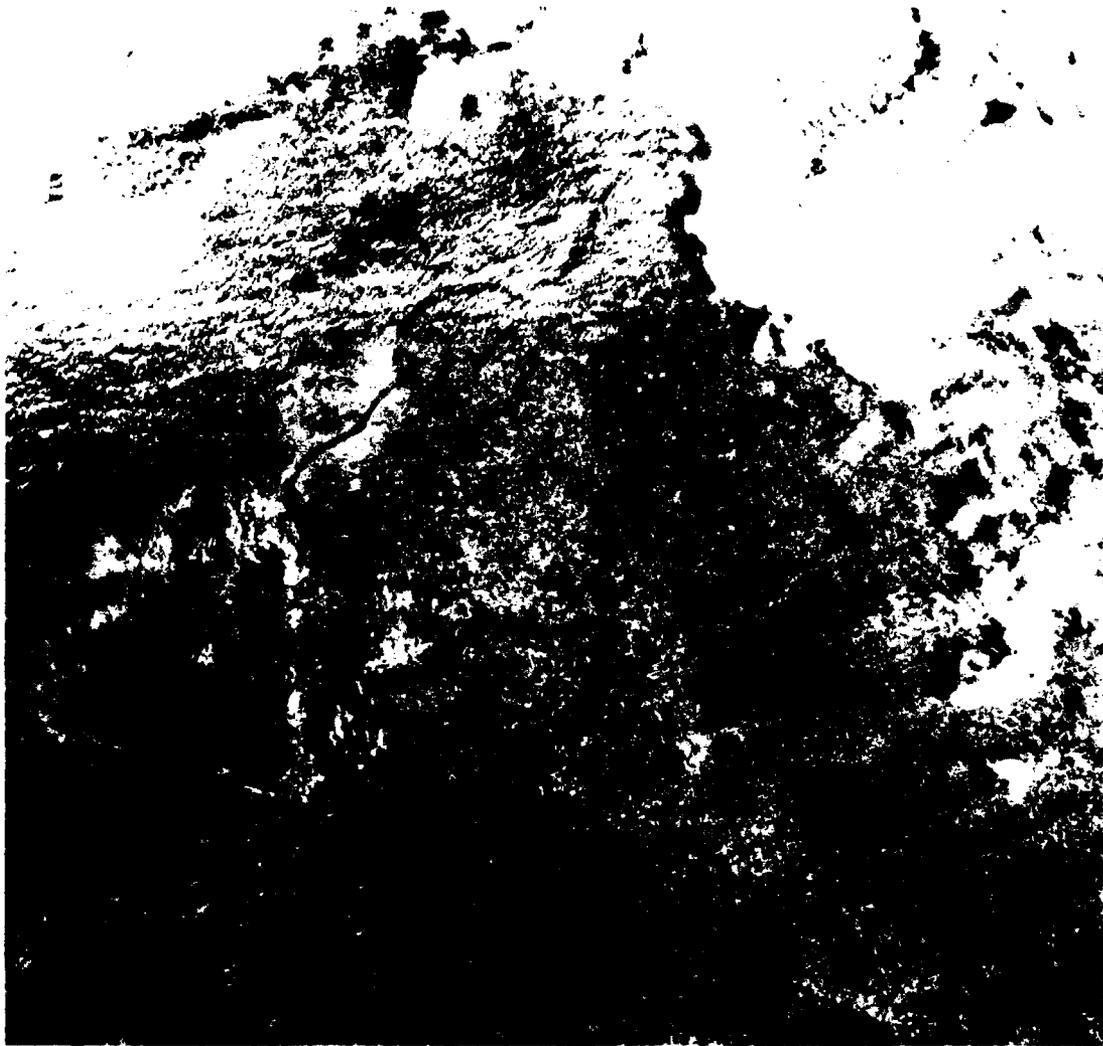
Figure 4-20(c): Landsat MSS Band 7 (6 May) 1614G – Scene (a)
(Reproduced by permission of EOSAT)

Figure 4-21(a): DMSP (LF) 4 May 1651G - Enlarged portion
(See Figure 4-10(a))

70
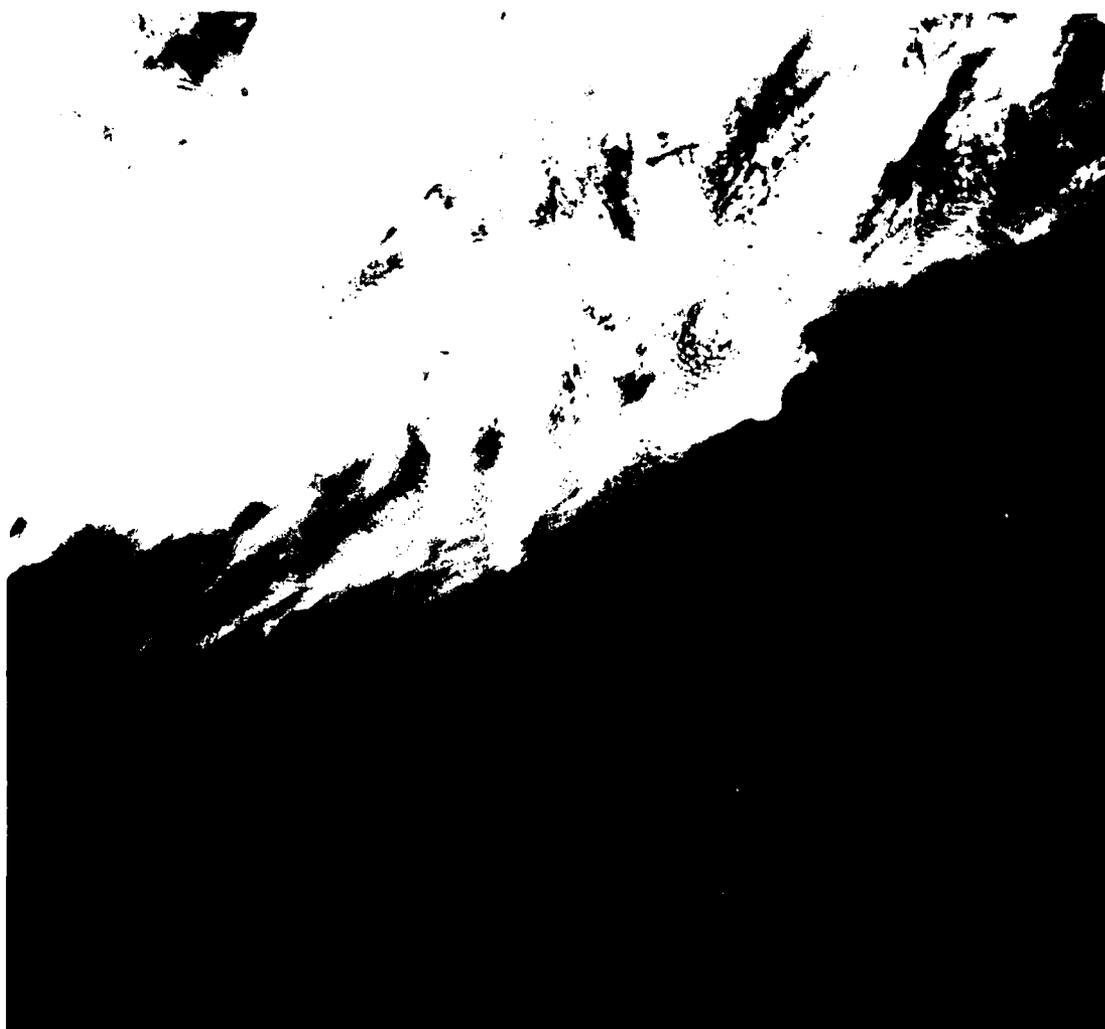
Figure 4-21(b): Landsat MSS Band 6 (4 May) 1600G - Scene (a)
(Reproduced by permission of EOSAT)

71

Figure 4-22(a):   Landsat MSS Band 4 (4 May) 1600G – Scene (d)
(Reproduced by permission of EOSAT)

Figure 4-22(b):   Landsat MSS Band 7 (4 May) 1600G – Scene (d)
(Reproduced by permission of EOSAT)

73

elements is difficult, but the general structure of the cloud edge is evident in both images. The detail in the DMSP image is significantly greater than the smoothed resolution image discussed in the previous section; in fact, except for some areas of thin cirriform cloud, much of the structure of the cloud edge seen in Landsat can also be detected in DMSP. In this case, the detail in the DMSP image is considerably greater than that in the GOES image.

The Landsat scene covering the edge of the extensive cloud system to the south becomes quickly saturated at all spectral bands (Figs. 4-22(a) and 4-22(b)). The "fuzziness" of the cloud edge, somewhat evident in DMSP and GOES, is seen in Landsat to be cirrus cloud overlying the lower cloud layers. A comparison of these two figures indicates the cirrus to be much more opaque in Band 4; terrain features that are not visible at all in that band can be seen through the cirrus in the Band 7 image.

4.3.3 3 May 1979 - Landsat Imagery

A Landsat image covers southwest Florida on 3 May at almost the exact time of the GOES image shown in Figure 4-4(b). The DMSP image at that time (Fig. 4-4(a)) does not extend far enough east to cover Florida, so it is possible in this instance only to compare Landsat to GOES. An enlargement of the GOES visible image (1500 GMT) showing the area covered by Landsat is shown in Fig. 4-23(a); the Landsat Band 5 image (1516 GMT) is shown in Fig. 4-23(b).

At the time of these observations, Florida is completely covered by small cumulus cloudiness. The structure of the cumulus field is very evident in the Landsat image, including cells aligned in bands and the differing sizes of the cumulus cells. Areas of suppressed cloudiness over the western end of the Lake Okeechobee and over two smaller water bodies to the north of the lake are evident. In the GOES image, the detailed structure of the cumulus field cannot be seen. However, even at the reduced GOES resolution, the two bays along the Florida west coast can be detected as can the inland areas of suppressed cloudiness (even the two smaller areas north of Lake Okeechobee). Also, there is an indication of the northwest-southeast orientation of the cumulus streets so clearly evident in the Landsat image and of the slightly brighter cloud in areas that are seen in the Landsat image to be areas of larger cumulus cells, such as just south of the small area of suppressed cloud north of Lake Okeechobee. The overall reflectance of the cumulus field over Florida in the GOES image is considerably less than that of the cloud areas to the north.

74
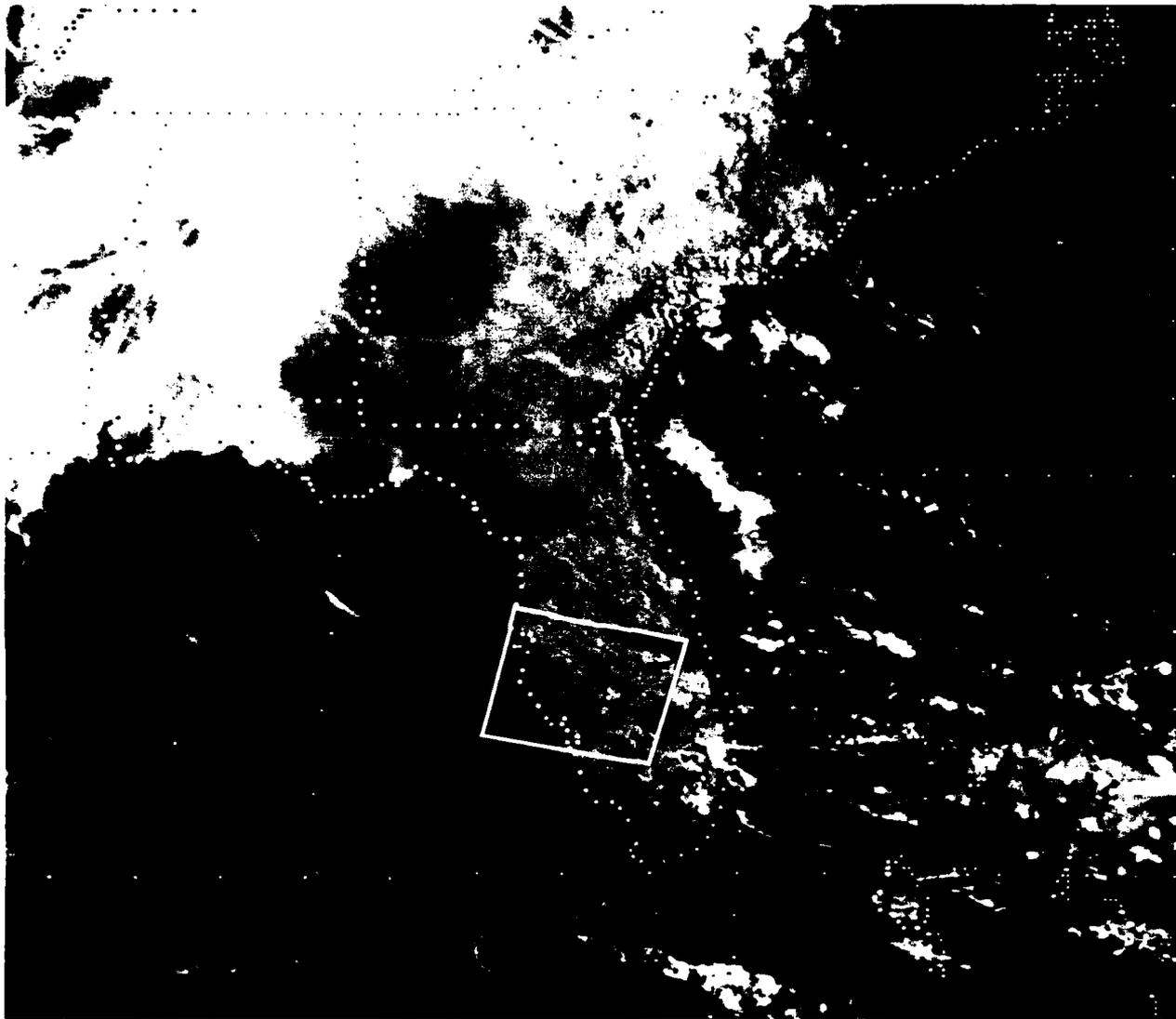
Figure 4-23(a): GOES VIS 3 May 1500G – Enlargement (Florida)
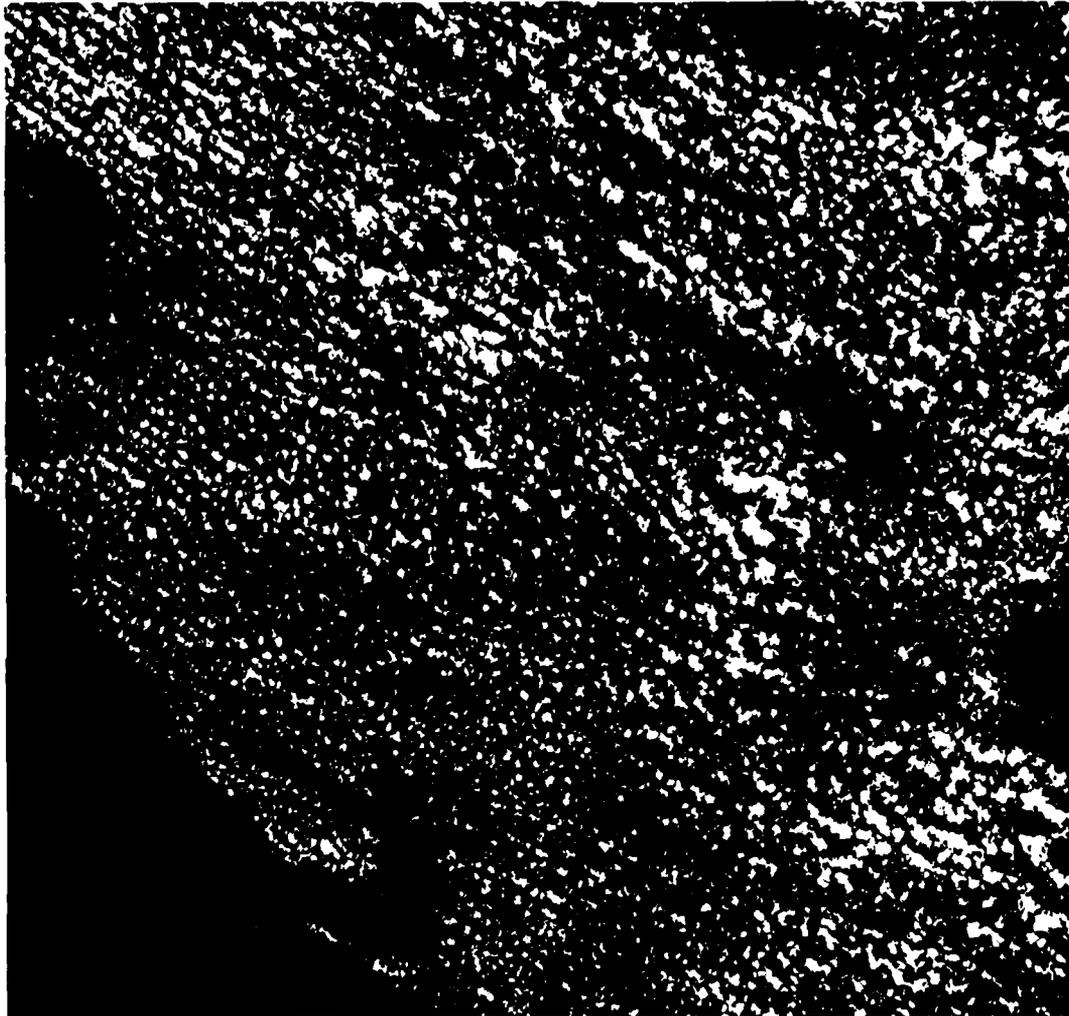
Figure 4-23(b): Landsat MSS Band 5 - 3 May 1516G (Florida)
(Reproduced by permission of EOSAT)

76

4.4 Summary of Results of Imagery Intercomparison

The imagery intercomparisons presented above are qualitative in nature because of the many factors, discussed earlier in this section, that influence the processing and display of photographic products. Nevertheless, satellite imagery in the formats shown in this section are typically used in analysis and forecasting. The image intercomparisons can provide guidelines for the analyst to assist in the correct interpretation of imagery from different satellite sensors. Some of the results of the analysis of imagery are summarized below (these results pertain to visible imagery except where noted as being infrared).

4.4.1 GOES to DMSP

- Many DMSP images are processed with high picture contrast. The high contrast results in saturation of some cloud features, especially extensive cloud areas, thus reducing detail in those areas. GOES images are processed at lower contrast, so even extensive, highly reflective cloud areas are not saturated.

- Terrain features can be seen in much greater detail in DMSP than in GOES images. The higher resolution of the DMSP fine-resolution data, the higher contrast of the images, and the broader spectral bandwidth of the DMSP OLS (extending into the near-IR) are all factors that may enhance terrain features. Except for coastlines and major inland water bodies, terrain features are not readily visible in the GOES images.

- Cloud shadows at low sun angles in DMSP images greatly enhance clouds with vertical development and high clouds over lower layers. Cloud shadowing is less pronounced in GOES images.

- At low sun angles, sunglint patterns may also be significant in DMSP images. Sunglint may obscure some clouds over the ocean because of reduced contrast between cloud and water but may also enhance some types of clouds such as tropical cumulus over water. Reversal in reflectance of water-land occurs in sunglint areas. Because of the viewing geometry, sunglint is not a problem in GOES images.

- Depiction of thin cirrus cloud may vary considerably depending on the processing of the image. Cloud that appears as thin cirrus in GOES may appear opaque in a high contrast DMSP image; in other

77

images, thin cirrus that is difficult to detect in GOES can be seen in DMSP.

- DMSP fine resolution imagery provides considerably more detail of cloud edge features than GOES. Cumulus fields also have considerably more definition in DMSP than in GOES; in the lower resolution GOES images (such as the WBl) cumulus fields generally appear as overall gray areas. In some instances, however, GOES may depict more cloud detail than DMSP smoothed resolution data.

- DMSP IR images tend to be saturated over large cloud masses; the enhancement curve used for the GOES IR data appears to display greater detail in those cloud areas.

4.4.2 NOAA to DMSP

- NOAA AVHRR and DMSP were difficult to intercompare, because the data set did not provide concurrent observations. The NOAA images are displayed at a larger scale than DMSP but have edge distortion, which is removed in the DMSP images.

- The NOAA resolution is better than the DMSP smoothed resolution data. In one comparision where the corresponding observations were only three hours apart, the definition of a field of cumulus cells was better in the NOAA IR image than in the DMSP smoothed-resolution IR image; conversely, the definition in the DMSP fine-resolution visible image was better than in the NOAA visible image.

- The depiction of thin cirrus is usually better in NOAA visible imagery than in the high contrast DMSP imagery.

- Because of similar orbital characteristics, the overall cloud depiction is quite similar in NOAA and DMSP imagery.

- Terrain features are better depicted in DMSP fine resolution imagery than in NOAA imagery probably due, at least in part, to the broader band pass of the OLS visible sensor.

4.4.3 Landsat to DMSP

- Individual cloud elements may be difficult to identify in corresponding Landsat and DMSP images because of the different resolutions and changes in clouds that occur over even relatively short time periods.

- The cloud types and amounts deduced from Landsat imagery agree well with cloud types and amounts reported by ground observers. Thus, Landsat can be used as a source of "ground truth" for evaluating meteorological satellite imagery.

- Although major cloud features can be identified in both types of imagery, the detail of the cloud edges seen in Landsat cannot be seen in DMSP smoothed resolution imagery; the fine-resolution imagery compares much better with Landsat, especially when terrain features are visible for use as reference points.

- Because of a gain setting for viewing the ground rather than clouds, Landsat images saturate quickly over large cloud masses.

- Thin cirrus cloud that may be difficult to detect in DMSP can be readily detected in Landsat. Moreover, at the Landsat resolution, a considerable amount of information on the structure wihin the cirrus cloud is apparent.

- Considerable variation in cloud depiction is observed over the four Landsat MSS spectral bands. Thin cloud is much better depicted at the shorter wavelengths (Bands 4 and 5), but cloud saturation is a greater problem; at the longer wavelengths (Bands 6 and 7), penetration through thin cloud is substantially greater than at the shorter wavelengths.

- In one set of concurrent observations, a small cloud feature that appears very bright in Landsat cannot be detected at all in the smooth resolution DMSP; it may be simply that the smooth resolution DMSP data are too coarse to resolve the feature.

4.4.4 Landsat to GOES

- It is difficult to compare the North American (WB1) GOES image with Landsat because of the great differences in scale and resolution. A meaningful comparison can be carried out, however, using enlargements of the areas of interest in the GOES images.

- In one data set examined, features seen in Landsat could be identified better in the corresponding GOES image than in the DMSP smooth resolution image. An area of cirrus was better defined in GOES and a small cloud feature that could not be detected at all in DMSP could be seen in GOES.

- Some of the overall structure of a cumulus field over Florida could be detected in an enlarged GOES image, although the individual cells seen clearly in the concurrent Landsat image were not resolved by GOES.

- The percentage of cloud amount within the area of a Landsat scene estimated from Landsat and from GOES or DMSP imagery could vary considerably depending on cloud type. The analyst might arrive at similar cloud percentages if the scene contains a well-defined cloud edge; however, with a broken field, a "fuzzy" cloud edge, or thin cirrus cloud, the estimated cloud percentage could be quite different between Landsat and either DMSP or GOES.

5. DIGITAL DATA TECHNIQUE DEVELOPMENT

5.1 Preprocessing of Digital Data Sets

As discussed in Section 3.5, digital data sets were acquired for the 6 May 1979 case for both the Landsat MSS and GOES VISSR. These sensors concurrently viewed essentially the same geographic areas providing an excellent opportunity to explore quantitatively some of the hypotheses developed during the qualitative analysis of the imagery data. Because the digital data were acquired late in the study period, it was not possible to convert the required software to read the GOES tape from IBM to CDC formats, nor was it possible to process all three Landsat scenes. Therefore, the digital data analysis focused on the Landsat MSS data for one scene. Since the MSS data provide the highest spatial and spectral resolution, the approach taken in this initial study was to synthesize other sensor imagery data sets (e.g., the OLS and VISSR) from the available MSS data set. Analysis of the Landsat imagery for this scene is discussed in Section 4.3.1, and the images for the four MSS spectral bands are shown in Figures 4-17(a) and 4-20(a) through 4-20(c).

The first step in the processing of the Landsat MSS digital data was to read and unpack the acquired Landsat tapes using software developed for the AFGL Cyber 750 computer system. Programs developed at AFGL (J. Willand, personal communication) were utilized to process the 6250 BPI Landsat data tapes and create permanent files of digital data counts for each MSS band. Due to the high spatial resolution of the MSS data, it was not possible to treat an

entire MSS scene. To expedite the analysis, two subscenes were identified. These subscenes, designated Scenes A and B, respectively, are illustrated in Figure 5-1. For each scene, there are four digital data files, each corresponding to a MSS band, of dimensions 600 pixels by 400 scan lines. The value of each pixel is a digital count with range from zero (black) to 127_8 (white). Each file was transferred via the HASP protocol to AER's Harris H800 computer for further analysis and converted to a binary file to facilitate efficient I/O operations. Table 5.1 summarizes the file designations for each digital data file.

Table 5.1

Landsat MSS Digital Data Files

Scene	MSS band	Cyber ASCI File	AER ASCII File	AER Binary File
A	4	A4	A4L	A4B
	5	A5	A5L	A5B
	6	A6	A6L	A6B
	7	A7	A7L	A7B
B	4	B4	B4L	B4B
	5	B5	B5L	B5B
	6	B6	B6L	B6B
	7	B7	B7L	B7B

5.2 McIDAS Imagery Renditions of Selected Digital Cases

In order to provide hard copies of each band of the selected subscenes, laserfax images were generated using the AFGL McIDAS system. The rationale for this undertaking was both to investigate approaches to provide imagery simulations for each sensor data set generated for comparison to the actual sensor imagery and to gain experience manipulating the McIDAS system. Since the McIDAS does not interface directly with the AFGL Cyber, it is necessary to generate an 800 BPI McIDAS compatible tape from each permanent file for each subscene band. For the purpose of the laserfax, the dynamic range of the MSS is reduced to one of 16 gray shades. The McIDAS renditions corresponding to Scene A, Bands 1-4, are illustrated in Figures 5-2(a) through 5-2(d) and those for Scene B are shown in Figures 5-3(a) through 5-3(d).
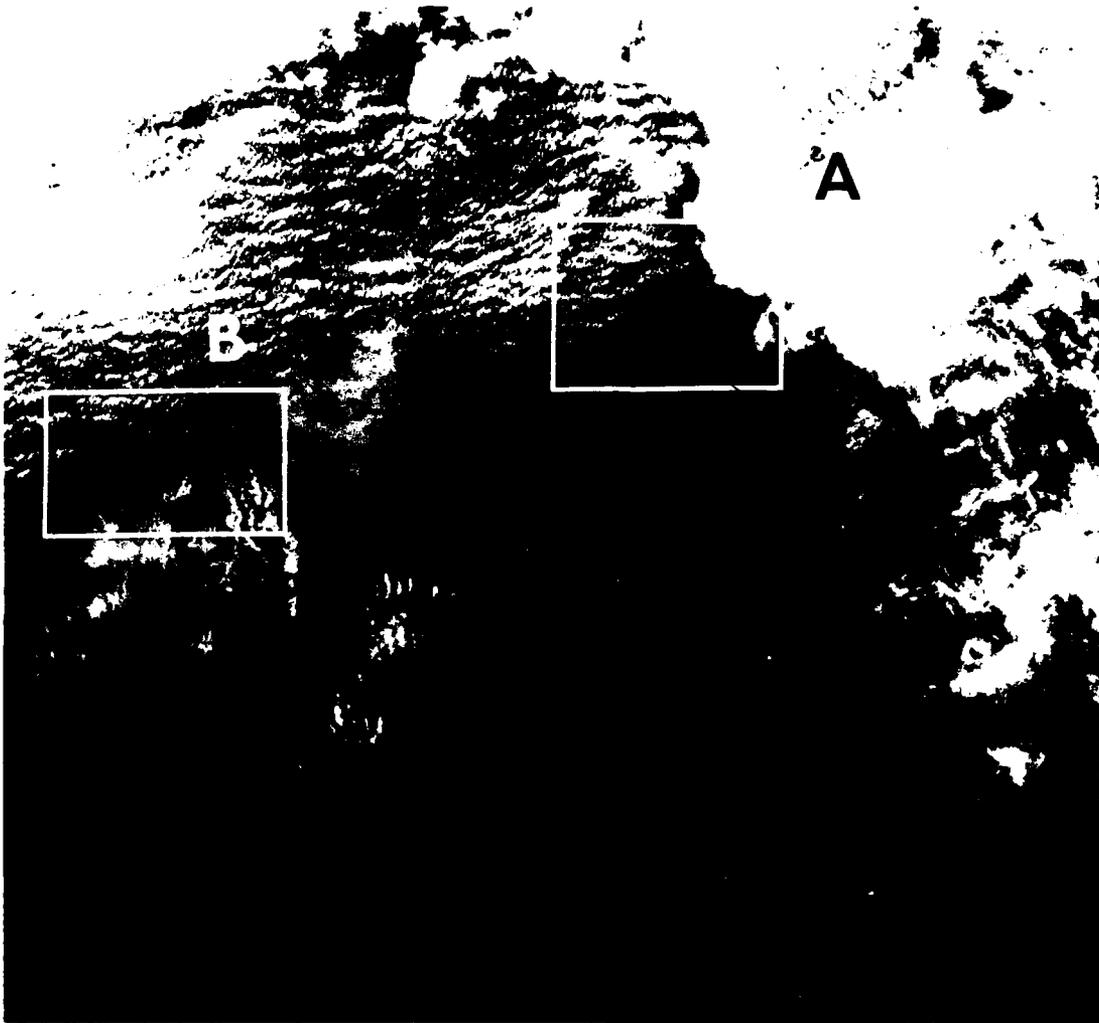
Figure 5-1: Landsat subscenes A and B for digital data analysis. (Reproduced by permission of EOSAT)
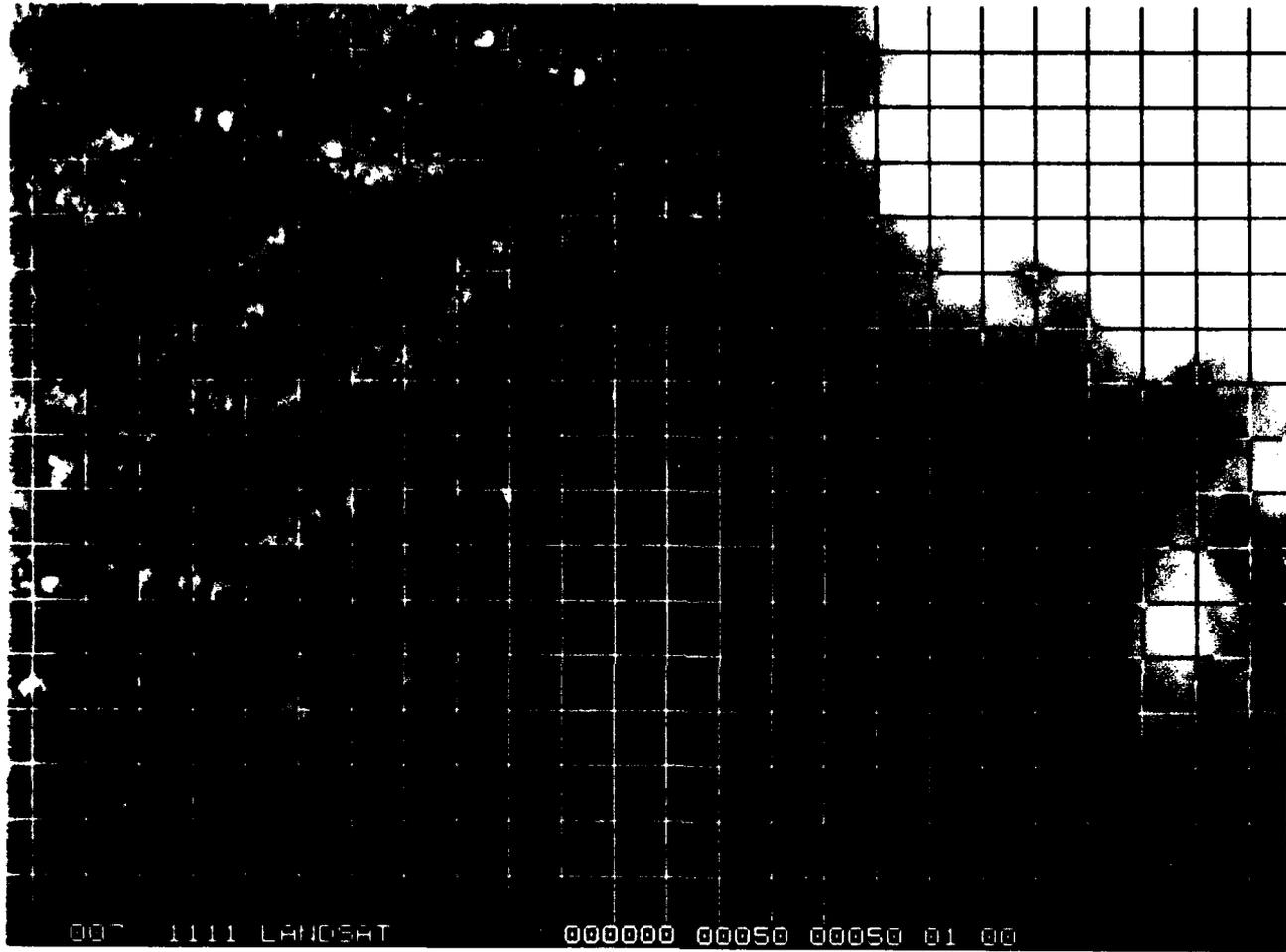
Figure 5-2(a): McIDAS rendition of Landsat subscene A (Band 4)

Figure 5-2(b): McIDAS rendition of Landsat subscene A (Band 5)

84
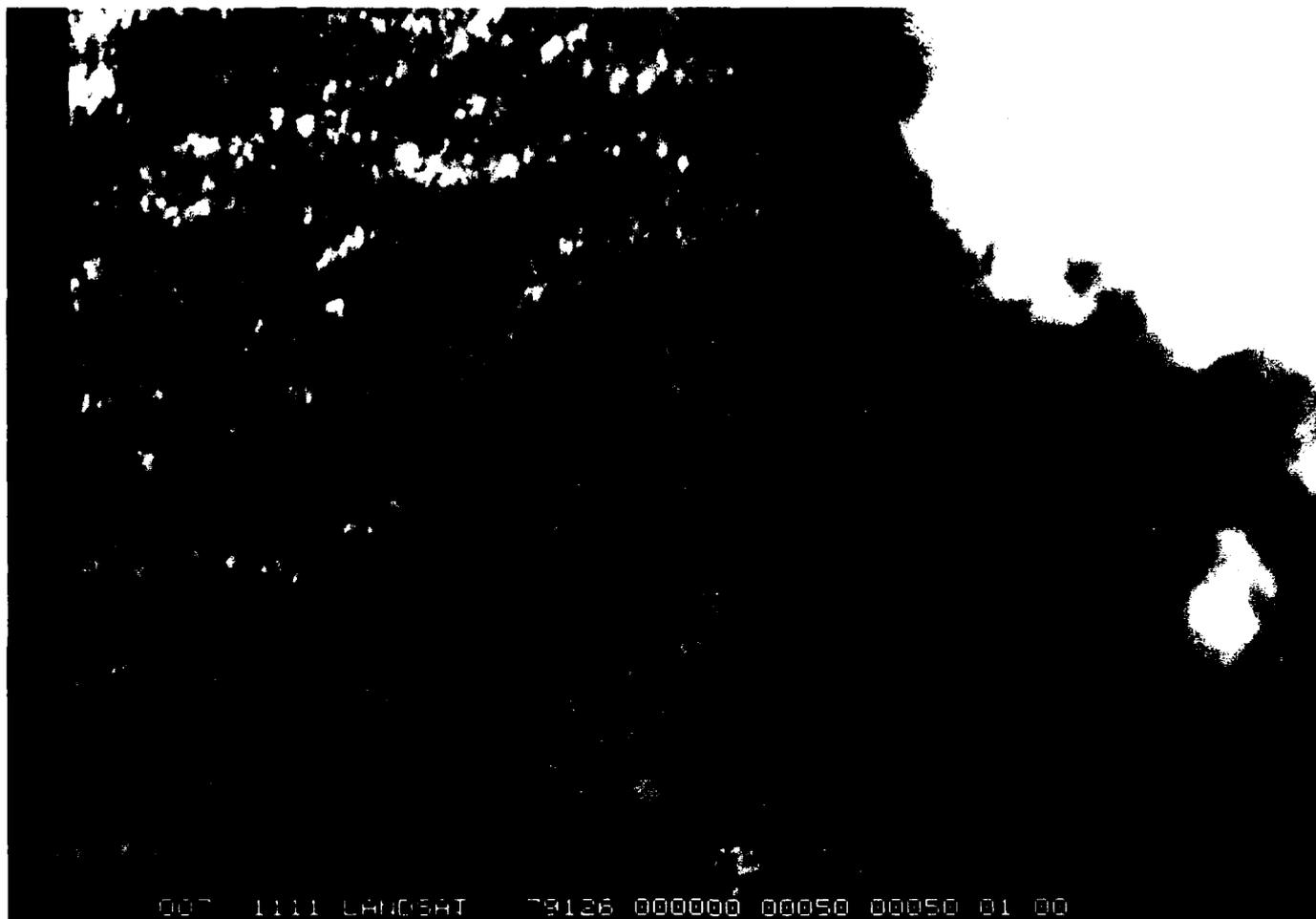
Figure 5-2(c): McIDAS rendition of Landsat subscene A (Band 6)

Figure 5-2(d): McIDAS rendition of Landsat subscene A (Band 7)

007   1111 LANDSAT   79126 000000 00050 00050 01 00
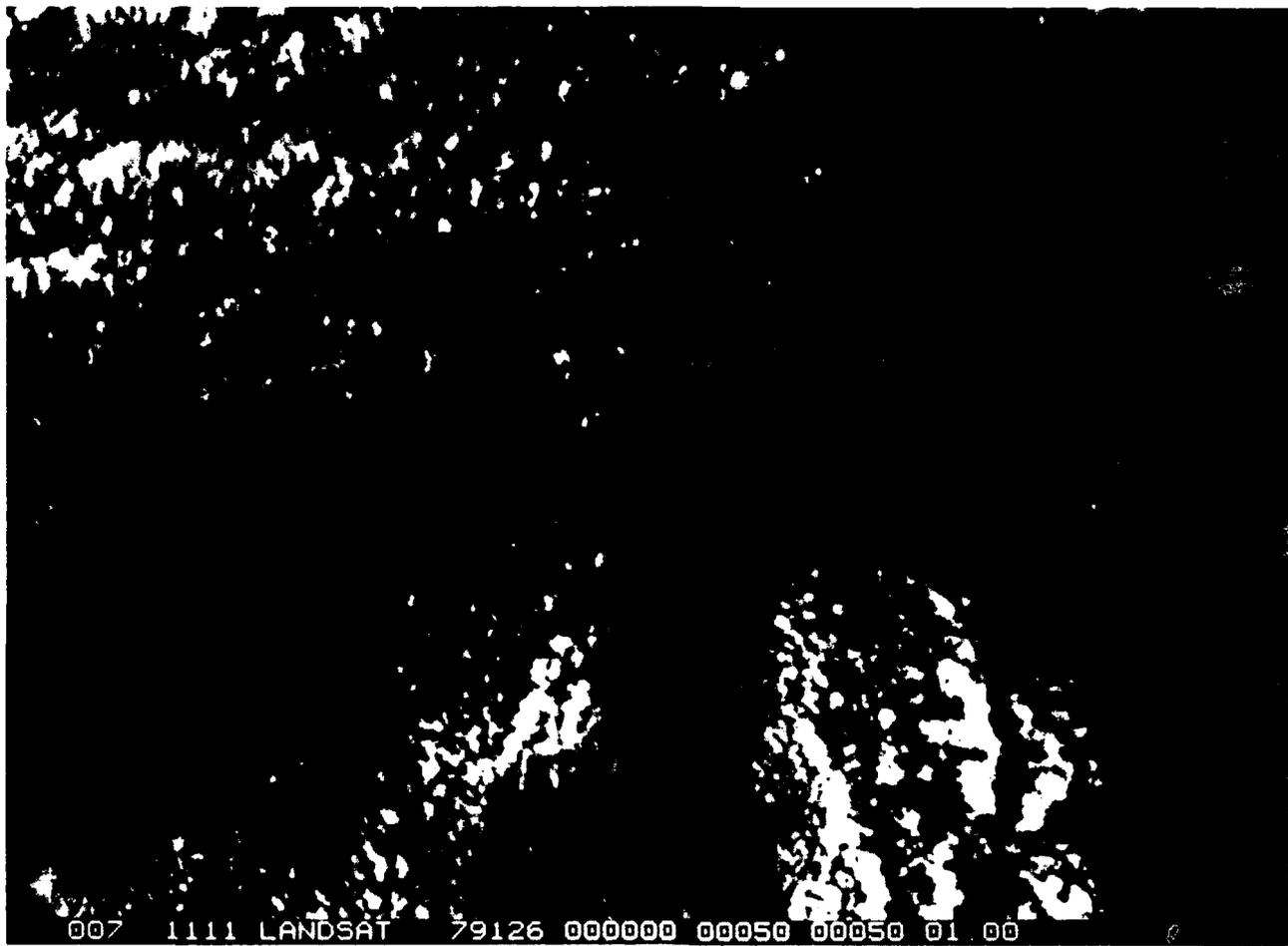
Figure 5-3(a):   McIDAS rendition of Landsat subscene B (Band 4)

Figure 5-3(b): McIDAS rendition of Landsat subscene B (Band 5)
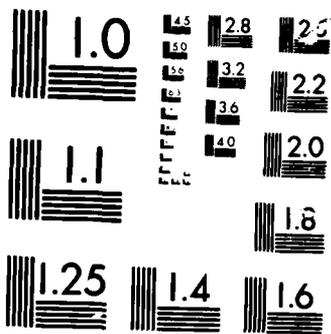
MICROCOPY CHART

Figure 5-3(c): McIDAS rendition of Landsat subscene B (Band 6)

89

Figure 5-3(d): McIDAS rendition of Landsat subscene B (Band 7)

These McIDAS renditions provide a reasonable representation of the original imagery. For example, the corresponding McIDAS renditions of subscenes A and B for each band (Figures 5-2 and 5-3) can be compared with the images shown in Figures 4-20(a), 4-17, 4-20(b), and 4-20(c) for MSS bands 4 through 7, respectively. Qualitative similarities such as the increasing visibility of terrain features and corresponding difficulty in detecting thinner clouds with increasing spectral band (i.e., wavelength), as noted in Section 4.3.1.3, are evident.

However, it was noted that the contrast of the resulting hardcopy images can vary considerably. The uncertainty of resulting laserfax hardcopy contrast is apparently due to such factors as paper changes and undocumented mechanical adjustments to the equipment (J. Willand, personal communication). Since our ultimate goal is to manipulate one type of digital imagery to simulate another and these transformations often involve dynamic range and sensitivity variations to image elements such as cloud edges, thin cloud, and terrain features, the contrast problem appeared to introduce an unacceptable uncertainty.

Additionally, it was decided that the procedure for obtaining McIDAS hardcopies of digital data described above was simply too inconvenient for interactive developmental analysis. Specifically, the necessity of generating McIDAS compatible formatted tapes as an intermediate step for each imagery data set simply takes too much time. For these reasons, an alternative method to generate digital data hardcopies was developed. This approach is described in the following section.

5.3 Half-tone Renditions of Selected Digital Cases

A more convenient and effective method to produce hardcopies of digital images employed the Versatec printer plotter at AER and software developed to generate half-tone images. For each pixel within the digital data field constituting the image, a physical area element (typically 0.04 inches) is allocated within the plot boundary. The number of dots per inch assigned to this area element on the hardcopy plot is then determined by the digital count or radiance value assigned to the associated pixel. A dynamic range is specified for the pixel values and this range is binned by specifying a range increment. By varying the size of the area element, dynamic range, and bin

increment, the contrast rendition of the desired sensor is simulated. The accuracy of this rendition is limited for a given choice of parameters by the intrinsic resolution of the plotter, which is 200 points per linear inch. The physical dimensions of the resulting plot of a 600 pixel by 400 scan line sub-scene digital image is thus 24 by 16 inches. This image is output in three equal segments 8 by 16 inches.

Figures 5-4 and 5-5 illustrate half-tone renditions of MSS band 4, Land-sat subscenes A and B, respectively. Note that the banding which makes it possible to discern the three segments contituting the complete subscene image is a vestige of the reproduction process used, not the half-tone generation software. Intensities are continuous across these artificial boundaries in the original Versatec half-tone plots. The line that bisects the upper and lower half of the reconstricted image is merely a paper fold and is not part of the digital data. Note, also, that these were produced as negative images, i.e., the highest digital count values are black and the lowest are white. This rendition of the digital data seemed easiest to understand. The software can also provide positive renditions.

5.4 Digital Imagery Transformations

With both digital data in hand and the means to produce reasonable hard-copies of digital imagery, it is possible to investigate techniques to simu-late numerically the data of one sensor system from that of another. General discussions of digital image processing have been provided by Hord (1982) and Schowengerdt (1983). Of the four most important sensor characteristic differ-ences discussed in Section 2 (i.e., scan geometry, wavelength response, spa-tial resolution, and dynamic range), the qualitative analysis of the imagery data described in detail in Section 4 suggests that many salient differences in the depiction of cloud features among the various sensors can be attributed to resolution and response factors. It was decided to focus on these factors in this initial Phase I study with the goal of demonstrating the feasibility of numerically simulating the relevant sensor behavior noted in the discussion in Section 4. As noted previously, the Landsat MSS data set, which provides the highest spatial and spectral resolution, was used as the basis for these simulations.

92
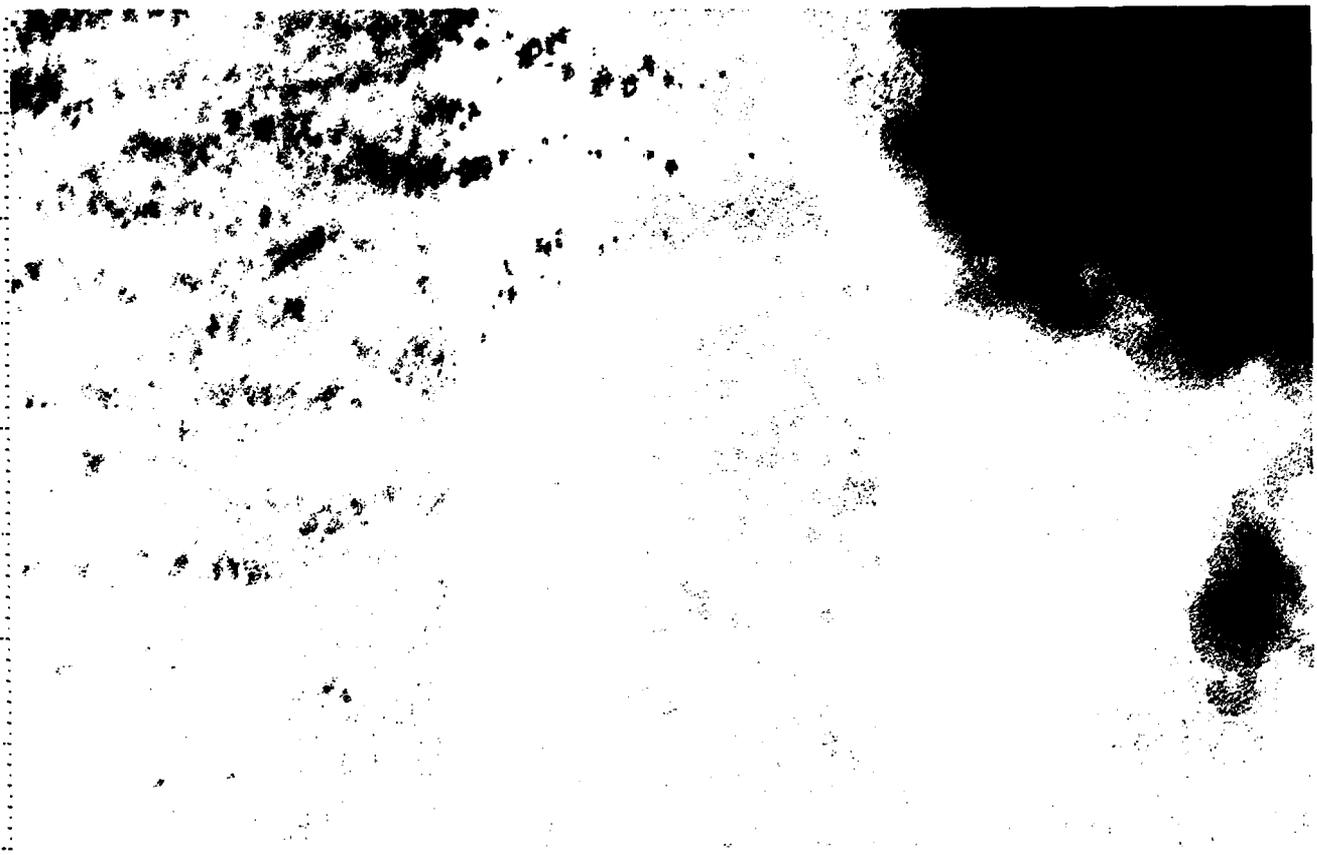
Figure 5-4: Half-tone rendition of Landsat subscene A (Band 4)

93

Figure 5-5: Half-tone rendition of Landsat subscene B (Band 4)

5.4.1 Spatial Resolution

As discussed in Section 4.4, the depiction of certain small scale cloud elements clearly visible in Landsat data can be missed altogether in smoothed DMSP and GOES data. To simulate this behavior, a simple spatial averaging program was developed. This algorithm reads the Landsat MSS data from the specified AER binary file (see Table 5.1), averages the data for a box size determined by specifying the number of pixels and scan lines in the original data to be averaged, and outputs the average image for plotting. Averaging commences at the upper left corner of the digital image. Scanlines and pixels that are not included in the averaging process (due to an insufficient number of pixels to constitute a complete box of the desired resolution) retain their original digital count values. These can sometimes be found along the right edge and bottom of some images. A simplified version of the averaging program is provided in Appendix A.

Synthetic VISSR and DMSP smooth (LS) resolution images of 0.8 and 2.5 km, respectively, were simulated from the Landsat MSS band 4 data for subscene A depicted in Figure 5-4. For this comparison, the differing spectral response of the sensors (and other factors) were ignored. Results are shown in Figures 5-6 (VISSR) and 5-7 (DMSP LS), respectively. These may be compared to the actual images from these sensors presented in Section 4, Figures 4-16(a) (GOES) and 4-15 (DMSP), respectively. The scattered small-scale cloud evident in the upper right-hand corner of the original Landsat digital imagery (Figure 5-4), is quite difficult to discern in the smooth DMSP data (Figure 5-7), although it is visible in the GOES data (Figure 5-6). The same apparently resolution-dependent behavior can be noted in the original imagery (although this may not be possible with the reproduction quality in this report copy).

Similar spatial averaging calculations were performed for subscene B using the original Landsat MSS band 4 digital data set previously illustrated in Figure 5-5. The Landsat imagery for this subscene (Figure 5-1) shows an area of broken small-scale clouds and possible some upper-level cirrus. These features are recognizable in the corresponding digital rendition. The effects of spatial averaging are illustrated in Figures 5-8 and 5-9, which correspond to the VISSR (0.8 km resolution) and DMSP smooth (LS) resolutions (2.8 km), respectively. While considerable detail is lost when viewed by the GOES VISSR instrument due to its larger field of view, the occurence of the broken cloud

Figure 5-6: Simulated VISSR image 0.8 km resolution for subscene A

96

Figure 5-7: Simulated DMSP OLS smooth (LS) resolution (2.6 km) image for
subscene A

Figure 5-8: Simulated VISSR image (0.8 km resolution) for subscene B
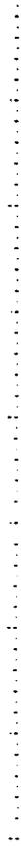
Figure 5-9: Simulated DMSP OLS smooth (LS) resolution (2.6 km) image for subscene B

areas, particularly that in the lower right hand corner of the image, is noticeable (Figure 5-8). There is much greater difficulty analyzing what is happening in the smooth resolution DMSP OLS image (Figure 5-9) where there is little to suggest that small-scale clouds exist within the subscene. Again, the numerical simulations of the effect of spatial resolution confirm what is seen in the actual imagery from these sensors presented in Section 4.

5.4.2 Spectral Resolution

As discussed in Section 2, each of the sensors examined in this study has inherently different spectral responses. The imagery intercomparison summarized in Section 4.4 noted, for example, that the broader spectral bandwidth of the DMSP OLS sensor was one factor contributing to the apparent enhancement of terrain features and water/land boundaries when observed from DMSP as compared to the GOES VISSR or NOAA AVHRR. The effect of wavelength on the observation of terrain versus atmospheric features can be noted by examining the series of McIDAS renditions of the Landsat MSS band digital data sets corresponding to subsceness A and B, previously shown (Figures 5-2(a) - (d) and 5-3(a) - (d), respectively). In each set, the (a) and (b) figures (shortest wavelengths) show cloud and very little surface information while the corresponding (c) and (d) figures (longest wavelengths) show less atmospheric information (particularly from optically-thin cloud) and considerable surface detail.

For the purpose of this initial study, it was decided to focus on the two sensors with the most distinct spectral response characteristics: the OLS nad the Landsat MSS. The relative spectral response of these imagers is illustrated in Figure 2-1. Note that although the MSS and OLS span similar ranges in wavelengths, the MSS has roughly four times the spectral resolution. This is achieved by breaking the wavelength range spanned by the OLS into four distinct channels. The GOES sensor uses one visible channel, which is qualitatively similar to MSS 4 and 5, while the AVHRR uses two channels in this region roughly covering MSS channels 5 and part of 6, and the rest of 6 and all of 7, respectively (see Table 2-2).

Spectral resolution was treated numerically in a manner similar to that employed for spatial resolution. The low spectral resolution DMSP sensor was simulated from an appropriate linear combination of the high spectral resolution Landsat MSS channels. The appropriate transformation can be written as:

$$R(i',j',OLS) = \int_{\Delta\lambda} R(i,j,k)\phi(A)d\lambda \bigg/ \int_{\Delta\lambda} \phi(\lambda)d\lambda$$

where R(OLS) is the simulated DMSP radiance at the i',j'th array element loca-
tion of the image; the spectral response functions, $\phi(A)$, are given in Figure
2-1 for the kth MSS band. This integral can be reduced to a simple sum given
by:

$$R(i',j',OLS) = \sum_k R(i,j,k)\phi(k) \bigg/ \sum_k \phi(k)$$

or, since each response function is normalized to unity:

$$R(OLS) = 0.1R(MSS4) + 0.2R(MSS5) + 0.25R(MSS6) + 0.45R(MSS7).$$

Since, as has been discussed in the previous section, these sensors also
differ in spatial resolution, the transformation from the (i,j) array location
in the Landsat image to the (i',j') location in the DMSP image implies that
the necessary spatial averaging process described in Section 5.4.1 has already
been performed for each MSS channel. Thus, the procedure is first to spatial-
ly average all of the MSS band images to the desired DMSP resolution and then
spectrally average them to obtain the desired combination of MSS channels to
simulate the broad DMSP OLS sensor bandpass. A simplified version of the
spectral averaging algorithm is provided in Appendix B.

The procedure described above was used to simulate DMSP OLS fine (LF) and
smooth (LS) imagery for both subscenes A and B. Fine and smooth results for
subscene A are shown in Figures 5-10 and 5-11, respectively; fine and smooth
results for subscene B are shown in Figures 5-12 and 5-13, respectively.
These spectrally-averaged smooth data renditions can be compared to those pre-
viously shown based on the spatial averaging of MSS channel 4 alone (Figures
5-7 and 5-9 for subscenes A and B, respectively). There is considerably more
detail in the spectrally-averaged simulated images due to the enhanced reflec-
tance of terrain in the near infrared spectrum. Again, the visibility of ter-
rain features in the DMSP imagery has been noted in the imagery intercomparison.

Although fine resolution DMSP imagery was not available for these partic-
ular subscenes, simulations of the data were undertaken. These results (Fig-

ures 5-10 and 5-12) suggest that although small scale cloud should be discernible (the spatial resolution of the DMSP LF data is similar to that of the GOES sensor), some confusion may be introduced by the enhanced depiction of terrain features. For this reason, independent visible and near infrared channels would be useful.

5.4.3 Scene/Sensor Geometry

The effects of differing scene/sensor geometries is quite obvious in the imagery analysis results discussed in Section 4. For example, both Figures 4-9(a) and 4-13(a) illustrate DMSP LF data (4 May, 1229G and 6 May, 1149G, respectively) in which a low scene solar angle results in both pronounced cloud shadowing and a strong sun glint pattern. The sun angle effect often increases scene contrast so that features which are not visible in correponding high sun angle sensors (such as GOES) are highlighted. However, other features in the vicinity of the sunglint are often obscured. Examination of the operational platform characteristics given in Table 2-1 indicate that similar orbital characteristics are shared by the three low earth orbit satellite platforms. Much of the difference in scene illumination is attributable to the approximate time of the equator crossing (or the time of the ascending node, AN).

The first step required in performing geometric trnasformations between sensors is a model to simulate scene geometry. To fulfill this requiement, we have adapted a DMSP scan line generation program (SLGP) developed previously (Isaacs, 1982) to provide calculations of the solar zenith angle, sensor zenith angle, the azimuth angle difference as a function of pixel within a DMSP scene. This program enables one to map solar zenith angle and scattering geometry throughout the image field of view. Additionally, the location of potential sunglint areas can be defined by identifying the primary specular point (PSP). The approach is easily modified to treat other polar orbiters.

A brief description of the calculation is provided in Appendix C. The major assumption of the model is that the spacecraft orbit is nominally circular resulting in a satellite subtrack which is a great circle. As discussed in Tsui and Fett (1980), who used the same approach in locating the PSP, the magnitude of the errors introduced by adopting this assumption should be acceptable for practical purposes. The calculation can be divided into three fundamental steps: (1) location of the satellite subtrack position as a

function of time, (2) specification of the sensor scan line pixels according to the scanning geometry of the sensor, and (3) calculation for each pixel of the spherical coordinates determining the local sun and sensor positions.

The input data required includes: (a) the longitude of the ascending node of the desired satellite pass, (b) the GMT time of the ascending node, and (c) the desired day of the year. The latter is used to calculate the solar declination angle using an approximation. Based on this data, the resulting outputs include, for each pixel: (1) the latitude and longitude of the subsatellite point corresponding to the current scan line, (2) the latitude and longitude of the pixel, (3) the local zenith angle of the sensor, (4) the local solar zenith angle, and (5) the azimuth angle between sun and sensor positions. The last three parameters are related to the pixel scattering angle.

The scene/sensor geometry defined by the SLGP can be applied in a number of ways. For example, simply knowing the variation of the solar zenith angle within a sensor field of view can be used to interpret pronounced cloud shadowing effects for polar orbiters and to determine cloud altitudes from ground shadows. Another application related to the sunglint effects noted with respect to Figures 4-9(a) and 4-13(a) is illustrated here. Using the output of the SLGP to define the scene/sensor geometry and a model of the wind-roughened sea, the reflection of solar radiation from the ocean's surface for a morning DMSP OLS observation was calculated. The results in Figure 5-14 illustrate the simulation for the portion of the image to the right side of the satellite subtrack (i.e., looking east). The ordinate is relative scan position with position 1 at the satellite subtrack and position 11 at the easternmost edge of the scan. The abscissa is given in GMT time. Alternative labels in latitude nad longitude are possible. The contours are normalized intensities, with a maximum at the position of the PSP. This pattern assumes a uniform wind speed throughout the image but simulates typical patterns quite well.

An interesting exercise with this model of the scene geometry would be to simulate the appearance of a specified cloud top field with given vertical structure as observed by each sensor. Time did not permit us to pursue other uses of SLGP within the initial Phase I effort.

103
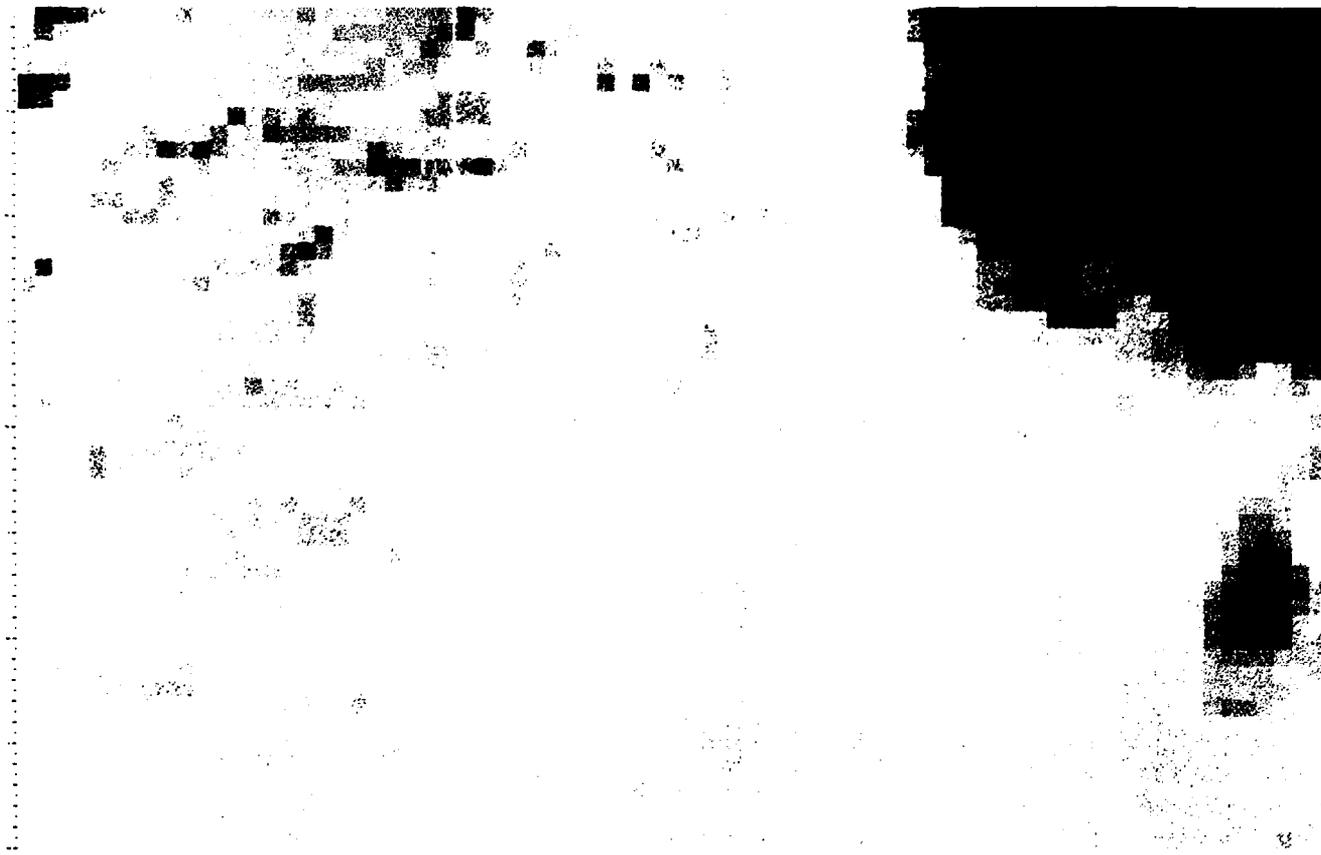
Figure 5-10: Simulated spectrally-averaged DMSP OLS fine (LF) resolution
(0.6 km) for subscene A
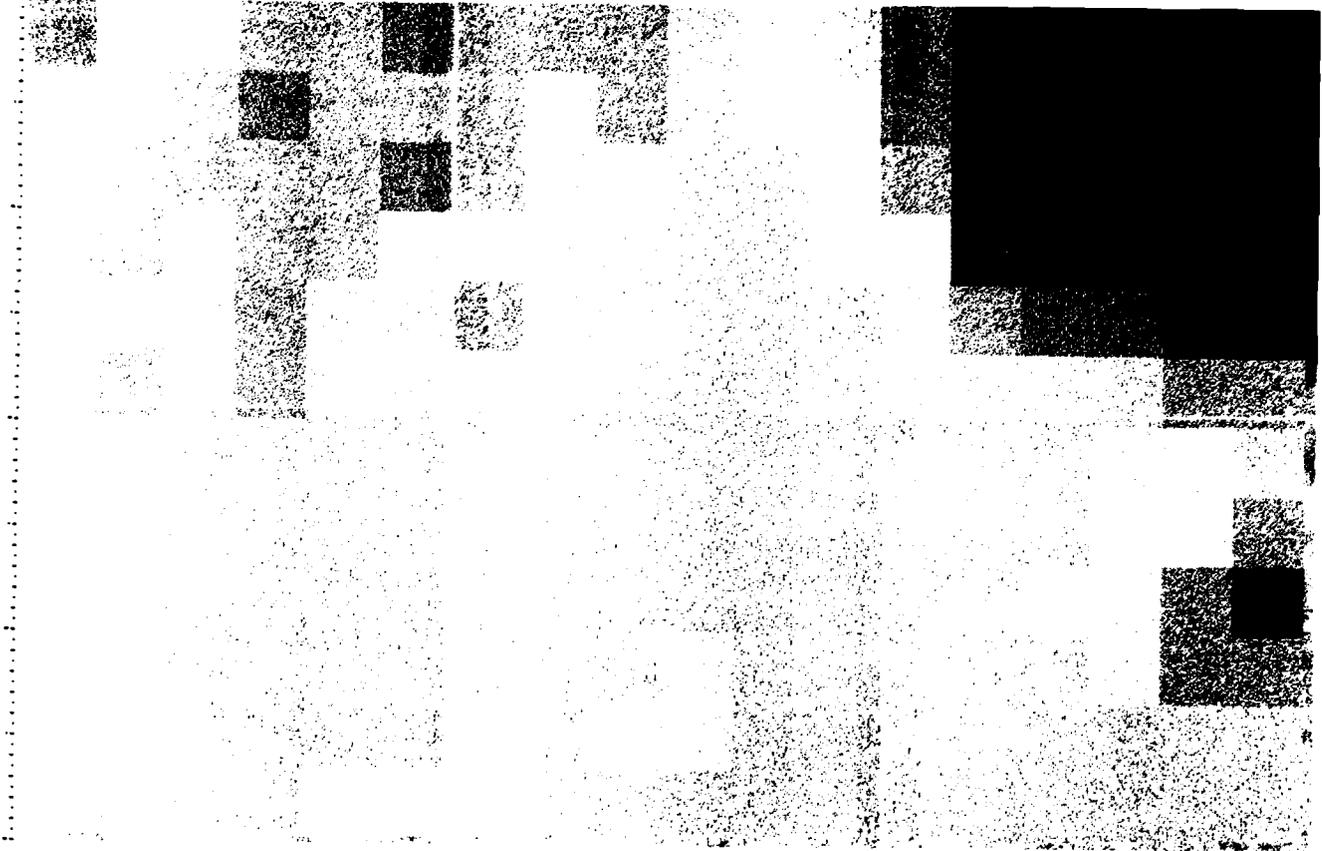
Figure 5-11: Simulated spectrally-averaged DMSP OLS smooth (LS) resolution
(2.6 km) for subscene A

105
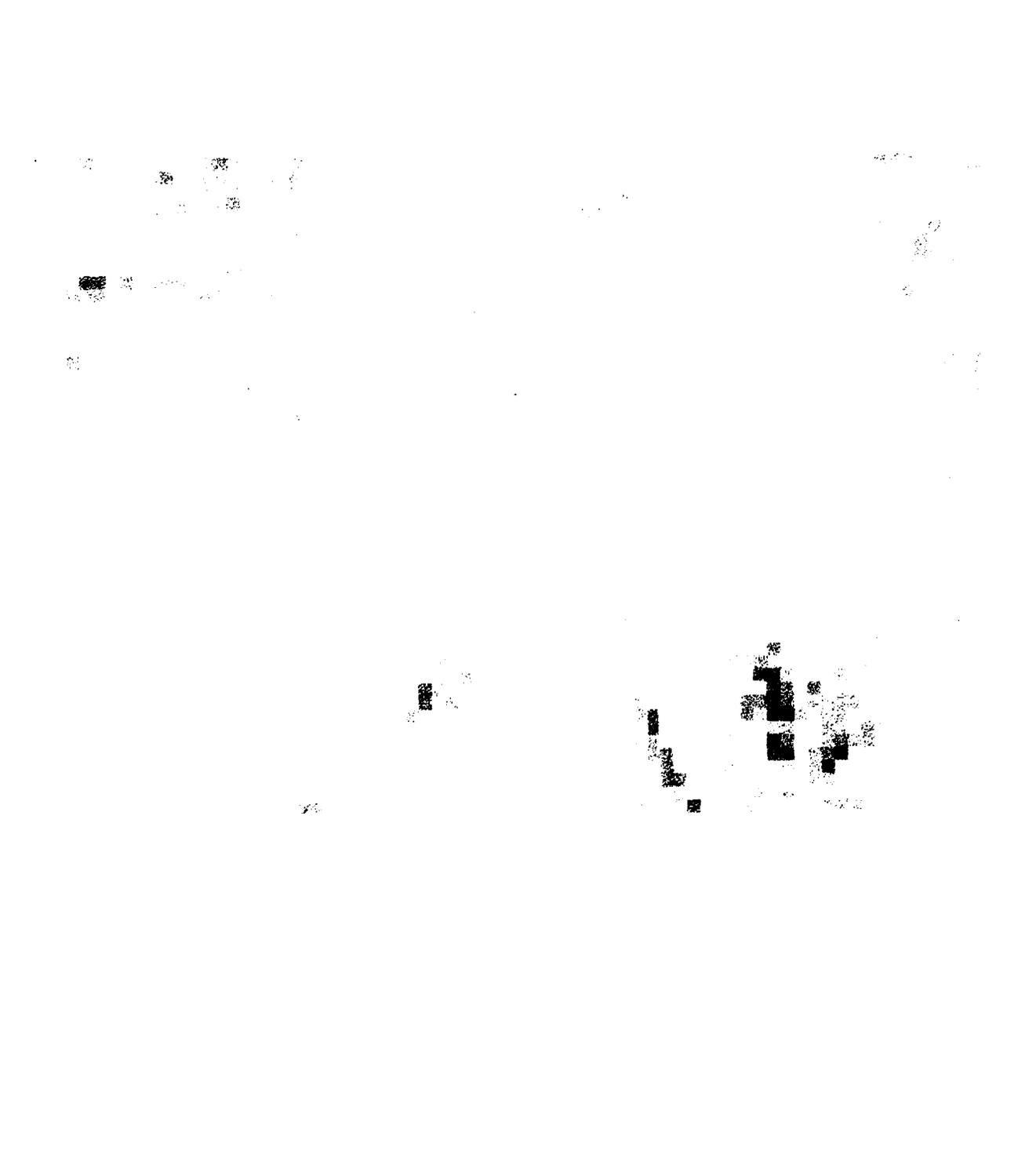
Figure 5-12: Simulated spectrally-averaged DMSP OLS fine (LF) resolution (0.6 km) for subscene B

106
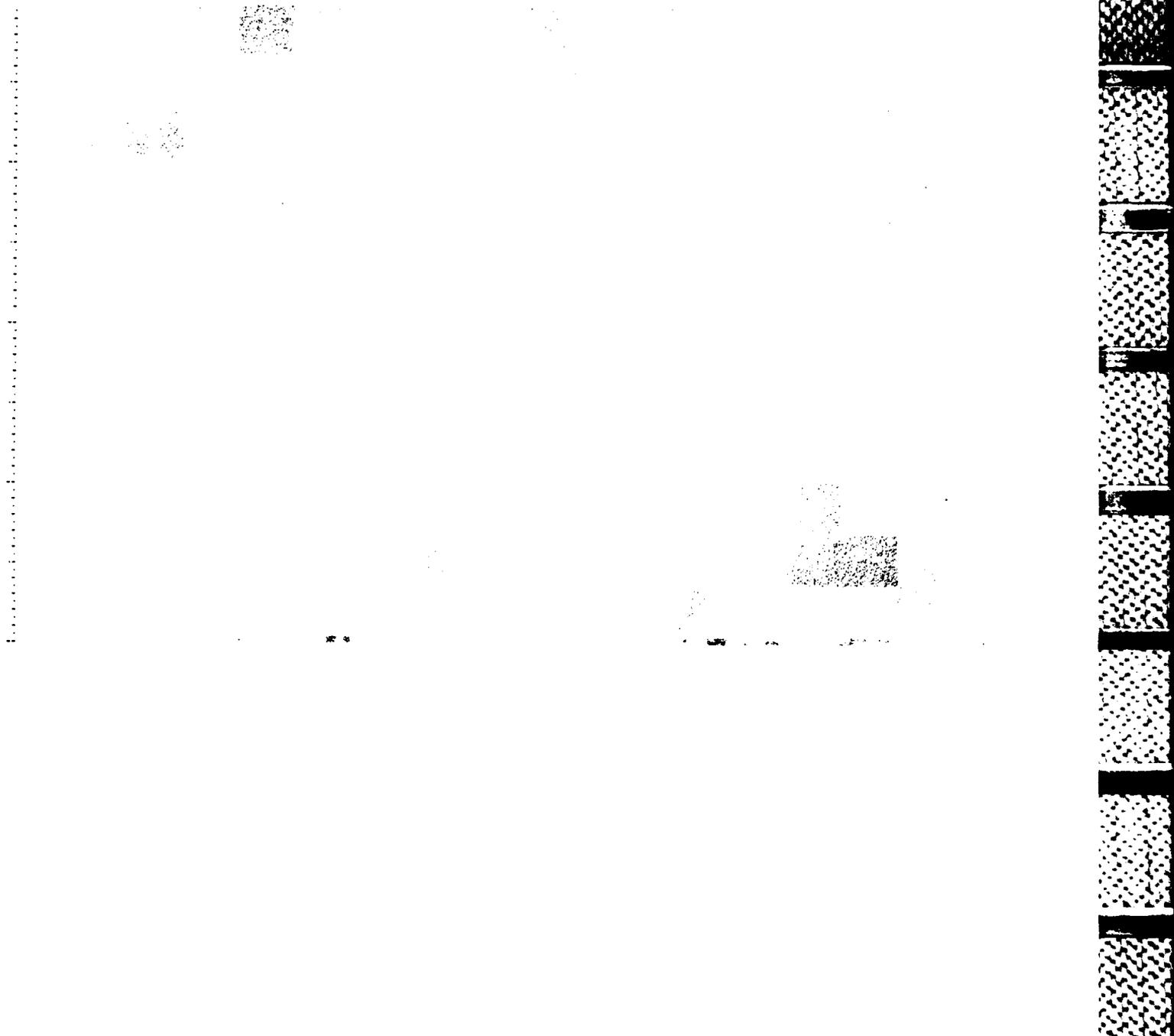
Figure 5-13:   Simulated spectrally-averaged DMSP OLS smooth (LS) resolution
(2.6 km) for subscene B
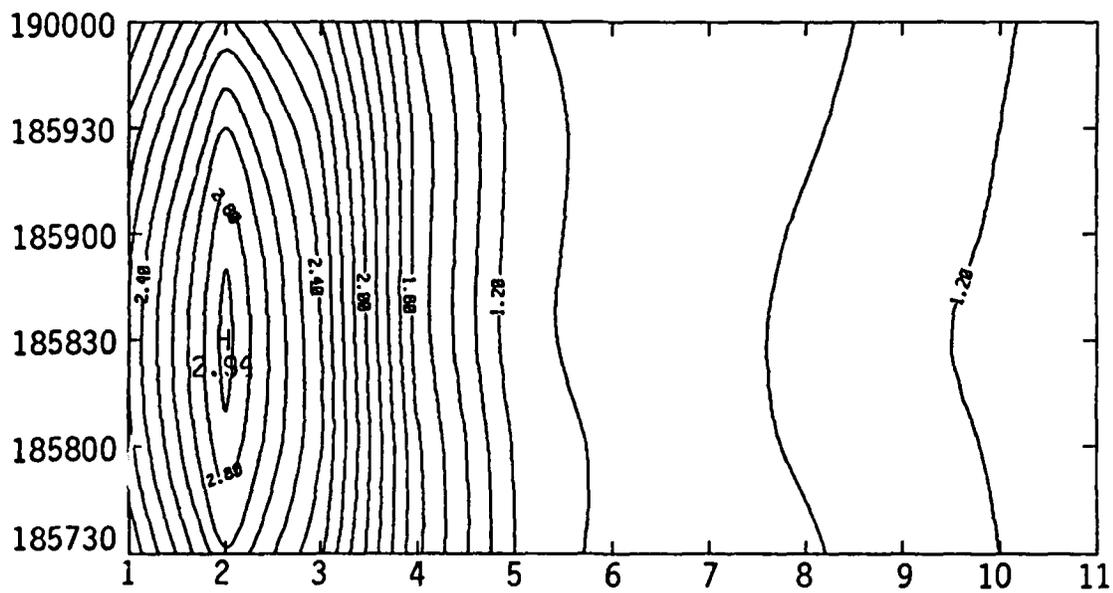
Figure 5-14. Simulated DMSP intensities for a morning satellite observing sunglint (wind speed = 5 m/s).

6. CONCLUSIONS AND RECOMMENDATIONS

This report has summarized the results of our Phase I effort to develop
methods to aid in the interpretation of cloud from essentially different imag-
ing sensors based on experience gained from the analysis of actual image data
sets. The sensors of interest are the DMSP OLS, the NOAA AVHRR, the GOES
VISSR, and the Landsat MSS. The objectives of this initial effort were: (a)
to provide a thorough description of the salient instrumental characteristics
of each satellite sensor system (Section 2), (b) to select and acquire an ap-
propriate sample of concurrent imagery from each sensor system (Section 3),
(c) to compare directly the imagery data sample sets and analyze cloud and
other features observed in each (Section 4), and (d) to develop machine pro-
cessing techniques to intercompare data from various sensors based on the re-
sults of the image analysis and to provide a plan for further algorithm devel-
opment (Section 5).

As noted in Section 3, the collection of a concurrent data set from all
pertinent satellites is not a trivial task. In fact, the difficulty in accom-
plishing this task is demonstrated by the recognition that few such data sets
are in existence. Thus, the unique imagery data sets assembled under this
Phase I effort, consisting of approximately 50 individual images covering the
eastern United States in early May 1979 (see Table 3-1) is an accomplishment
in itself. This data set offers the capability to examine distinctive cloud
features as concurrently as possible from the four satellite systems (it is
even possible to comapre some features in DMSP and NOAA AVHRR imagery despite
the inherent time difference between these observations).

In addition to the imagery, we have acquired representative samples of
digital data for both Landsat and GOES. NOAA AVHRR digital data were not ac-
quired under the Phase I effort due to the lack of other concurrent sensor
data in the sample, and there is no archive of digital data for DMSP. As dis-
cussed in Section 5, Landsat tapes were read and methods were developed to
display conveniently the digital data. Use of the AFGL McIDAS system was in-
vestigated, but it was judged too inconvenient to use as an interactive device
for these types of imagery transformation studies. Therefore, an alternative
technique for producing half-tone hardcopies from the digital data sets was
employed. Although not exploited during this initial effort, the half-tone
algorithm described in Section 5.3 can easily be used to explore the effect of

sensor dynamic range and digitization on the rendition of the digital data. Time constraints did not permit analysis of more than one Landsat digital scene nor of the GOES digital data set.

A major part of the Phase I effort was devoted to the analysis of imagery, the results of which are summarized in Section 4.4. As pointed out in that section, imagery intercomparisons are qualitative in nature because of the many factors that influence the processing and display of photographic products. Nevertheless, imagery in the formats shown are typically used in analysis and forecasting, and the results of the analysis, with the many examples presented in this report, can provide guidelines for the analyst to assist in the correct interpretation of imagery from the different satellite sensors.

The results of the imagery analysis indicate that sensor resolution and spectral response are both important considerations for correct image interpretation. Because of the broader bandwidth of the OLS, for example, terrain features are much more prominant in DMSP than in GOES; with regard to resolution, the DMSP fine resolution (F) data show significantly more detail than either the GOES or NOAA AVHRR data. Other orbital characteristics can be important, especially with regard to sunglint and shadowing, which can obscure some cloud features but greatly enhance others. The photographic contrast with which the images are processed (DMSP images tending to be high contrast) can be critical for correct interpretation of certain cloud features, such as thin cirrus.

Landsat imagery provides an excellent source of "ground truth" cloud information for comparing the other types of satellite imagery (keeping in mind the infrequency of Landsat repeat coverage and the fact that Landsat images saturate quickly over large cloud masses). The appearance of cloud and terrain features in the four MSS spectral band images can be useful for interpreting the broader band images from the other sensors. It also appears that further study of Landsat imagery could be very helpful in developing improved methods to interpret thin cirrus cloud, which remains a problem in satellite image analysis.

Of particular significance with respect to this study was work accomplished with the digital data set to demonstrate the feasibility of transforming data acquired from one sensor (Landsat) to the gross characteristics of

110

another (GOES and DMSP). Although the methodology employed was crude, it was demonstrated that features noted in the imagery-based analysis of cloud could be attributed to specific sensor characteristics (such as spatial and spectral resolution), whose effects could be simulated numerically by simple models. With respect to scene/sensor geometry, we have adapted a useful algorithm to provide relevant pixel dependent sun and sensor angles applicable to the simulation of cloud shadowing, sensor perspective, and sunglint effects.

As the above discussion indicates, this has been a successful initial effort. The feasibility of machine-based digital data intercomparison and transformation has been demonstrated for simple cases. However, much remains to be done to refine these techniques and apply them to practical and operational problems. Ultimately, such tools could be applied operationally to provide a digital data formatter that would interface between available sensor data sets and automated cloud analysis algorithms (e.g., RTNEPH), which are highly tuned for a specific sensor system (DMSP). Figure 6-1 provides a schematic of a hypothetical digital data formatter encompassing submodels to treat the specific sensor characteristics discussed above. Our initial effort has treated each of these aspects at least to first order.

The digital data set already on hand from the Phase I effort has direct application to further studies to refine techniques and develop the concept of a digital data formatter. Digital tapes for three Landsat scenes and one GOES scene were acquired, but due to time constraints, it was possible to work with only the one Landsat scene. It is recommended, therefore, that this excellent data set be applied both to further technique development and to further study of specific issues. Among the specific issues to be addressed, for example, is the effect of sensor characteristics on the detection and characterization of cirrus cloud. The Landsat and GOES digital data sets view an area that includes a band of high cirrus cloudiness extending across southern Lake Michigan. A considerable amount of information on the structure of this cirrus band is evident in the four channels of the corresponding Landsat MSS imagery; moreover, for comparison, there are nearby terrain features and a layer of low level cloud. This is an excellent case to investigate the effects of spatial and spectral resolution on the detection of Cirrus.

Additionally, it is strongly recommended that further studies include the acquisition of a DMSP digital data set. Because no DMSP digital archive
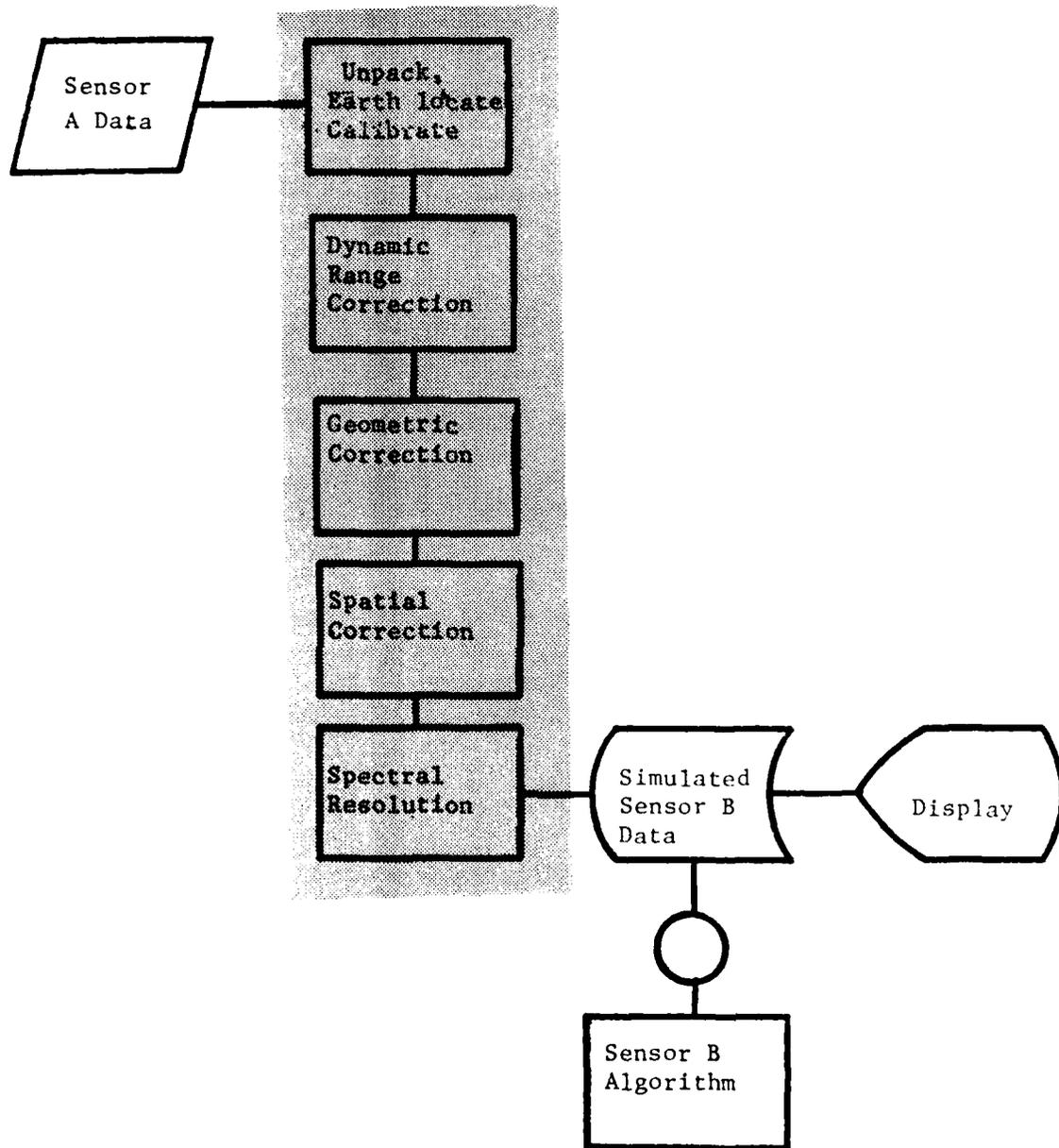
Figure 6-1. Schematic of digital data formatter (DDF) for simulation of Sensor B data from A data input (shaded area).

exists, it would be necessary to arrange for a digital tape to be saved. However, through a coordinated effort with the Air Force, NASA, and EOSAT (the corporation now operating the Landsat system under the Landsat Commercialization Act), it should be possible to acquire DMSP digital data at a time when Landsat data (as nearly concurrent as possible) will also be read out. Then GOES, and perhaps NOAA AVHRR, can also be acquired, since these digital data are routinely archived. Such an effort would provide an invaluable data set for use in a Phase II study that would lead toward the eventual development of automated techniques to combine satellite data.

8. REFERENCES

Arking, A., and J. Childs, 1985: Retrieval of cloud cover parameters from multispectral satellite images. J. Climate Appl. Meteorol., 24, 322-333.

Barnes, J. C., R. G. Isaacs, C. J. Bowley, and A. J. Bussey, 1979a: Comparative Study of Anomalous Gray-Scale Patterns in DMSP and LANDSAT Imagery. Final Report under Contract N00228-77-G-3164 for Naval Environmental Prediction Research Facility, ERT, Inc. Concord, MA.

Barnes, J. C., C. J. Bowley, and H. K. Burke, 1979b: Evaluation of the Capabilities of Satellite Imagery for Monitoring Air Pollution Episodes, NASA CR-159197. Langley Research Center.

Barnes, J. C., C. J. Bowley, M. D. Smallwood, and J. H. Willand, 1981: The Application of Heat Capacity Mapping Mission (HCMM) Thermal Data to Snow Hydrology, Final Report Contract No. NAS5-24316, NASA/GSFC, ERT, Inc., Concord, MA, 99 pp.

Barnes, J. C., and M. D. Smallwood, 1982: TIROS-N Series Direct Readout Services Users Guide, NOAA/NESS, Washington.

Bowley, C. J., J. C. Barnes, and A. Rango, 1979: Satellite snow mapping and runoff prediction handbook. Final Report under Contract NAS5-24410 to NASA Goddard Space Flight Center, ERT, Inc., Concord, MA, 87 pp.

Brandli, H. W., 1976: Satellite Meteorology. AWS/TR-76-264, USAF AWS, Scott AFB, IL (NTIS No. AD-A067090), 203 pp.

Bunting, J. T., R. S. Hawkins, and R. P. d'Entremont, 1983: R and D Nephanalysis at the Air Force Geophysical Laboratory. Fifth Conference on Atmospheric Radiation, Baltimore, MD, American Meteorological Society. ADA134137

Cornillon, P. C., 1982: A guide to environmental satellite data. Univ. of R.I. Marine Technical Reprint 79, Narragansett, RI 02882.

Dismachek, D. C., A. L. Booth, and J. A. Leese, 1980: National Environmentla Satelltie Service Catalog of Products, Third Edition, NOAA Tech. Memo, NESS 109, Washington, DC.

Engle, J. L., and O. Weinstein, 1983: The thematic mapper -- an overview, IEEE Trans. Geosc. Remote Sensing, GE-21, pp. 258-265.

ESA, 1983: Comparative Study of Image Data Produced by Satellites with Different Characteristics, Final Report, Societé d'Etudés Techniques et d'Entreprises Generales, Leplessis-Robinson (France), 82 p.

Feteris, P. J. A. S. Lisa, C. J. Bowley, M. G. Fowler, and J. C. Barnes, 1976: Investigation of Mesoscale Cloud Features Viewed by LANDSAT. Final Report under Contract NAS5-20804 for NASA/GSFC, ERT, Inc., Concord, MA, 76 pp.

Fett, R. W., and W. F. Mitchell, 1977: Navy tactical applications guide: vol. 1, Technique and applications of image analysis (DMSP). NEPRF Applications Report 77-03, Tactical Applications Department, Naval Environmental Prediction Research Facility, Monterey, CA.

Fett, R. W., and R. G. Isaacs, 1979: Concerning causes of "anomalous gray shades" in DMSP visible imagery. J. Appl. Meteorol., 18, 1340.

Haig, Thomas O., 1982: The role of meteorological satellites in tactical battlefield weather support. AFGL-TR-82-0124. ADA116936

Hord, R. M., 1982: Digital Image Processing of Remotely Sensed Data. Academic Press, 256 pp.

Hughes, N. A., and A. Henderson-Sellers, 1985: Global 3D-Nephanalysis of total cloud amount: Climatology for 1979. J. Climate Appl. Meteorol., 24, 669-686.

Isaacs, R. G. 1980: Investigation of the effect of low level maritime haze on DMSP VHR and LF imagery. NAVENVPRED/RSCHFAC CR-80-06, Naval Environmental Prediction Research Facility, Monterey, CA.

Isaacs, R.G., 1982: Remote sensing of surface propagation parameters: Application of imagery simulation model results. AER Document No. P70, prepared for Office of Naval Research, Arlington, VA 22217.

Isaacs, R. G., and D. T. Chang, 1975: Experimental evaluation of atmospheric effects on radiometric measurements using the EREP of Skylab. Final Report, Contract NAS9-013343. ERT, Inc., Concord, MA.

Kaehn, A. J., Jr., 1982: Military applications evolution and future. The Conception, Growth, Accomplishments, and Future of Meteorological Satellites, NASA CP 2257, 41-47.

Kneizys, F.X., E.P. Shettle, W. O. Gallery, J. H. Chetwynd, Jr., L.W. Abreau, J.E.A. Selby, R.W. Fenn and R.A. McClatchey 1980: Atmospheric transmittance/radiance: Computer code LOWTRAN5. AFGL-TR-80-0067. Air Force Geophysics Laboratory, Hanscom AFB, MA 01731. ADA088215

NASA, 1982: LANDSAT Data Users Notes (No 23), U. S. Geological Survey. EROS Data Center, Sioux Falls, SD.

NOAA, 1981: NOAA polar orbiter data (TIROS-N and NOAA-6) users' guide. NOAA-EDIS-NCC-SDSD. Washington, DC.

Nichols, D. A., 1975: Block 5D compilation, Defense Meteorological Satellite Program, Los Angeles AFS, CA 90009.

Norwood, V. T., L. R. Fermelia, and G. A. Tadler, 1972: Multispectral Scanner System for ERTS: Four-Band Scanner System. Final Report, Fol. I. Report No. HS324-5214. Hughes Aircraft Co., El Segundo, CA.

Rivers, J. W., Jr., and C. P. Arnold, Jr., 1982: Defense meteorological satellite program (DMSP). Meteorological Satellites -- Past, Present, and Future. NASA CP 2227, 31-34.

Santa Barbara Research Center, 1978: System description (revision b): visible infrared spin scan radiometer. Report to NASA under contract no. NAS5-20769 from SBRC, Santa Barbara, CA.

Schiffer, R. A., and W. B. Rossow, 1983: The International Satellite Cloud Climatology Project (ISCCP): The first project of the World Climate Research Programme. BAMS, 64, No. 7, 779-784.

Schiffer, R. A., and W. B. Rossow, 1985: ISCCP global radiance data set: A new resource for climate research. BAMS, 66, No. 12, 1498-1505.

Schowengerdt, R. A., 1983: Techniques for Image Processing and Classification in Remote Sensing. Academic Press, 149 pp.

Schwalb, A., 1978: The TIROS-N/NOAA A-G Satellite Series. NOAA TM NESS 95, Dept. of Commerce, Washington, D.C.

Shenk, W. E. and V. V. Salomonson, 1972: A simulation study exploring the effects of sensor spatial resolution on estimates of cloud cover from satellites. J. Appl. Meteorol., 11, 214-220.

Silverman, B. A., and E. D. Sprague, 1970: Airborne measurement of in-cloud visibility. Second National Conference on Weather Modification, Santa Barbara, CA, 6-9 April, 271-276.

Snow, J. W., J. T. Bunting, R. P. D'Entremont, D. D. Grantham, and K. R. Hardy, 1985: Space shuttle cloud photographs assist in correcting meteorological satellite data. EOS, June 11 issue, 478-490, AGU. ADA162059

Spangler, M. J., 1974: The DMSP primary data sensor. Proceedings of the Sixth Conference on Aerospace and Aeronautical Meterology, El Paso, TX. 150-157.

APPENDIX A

SPATIAL AVERAGING PROGRAM

```
      PROGRAM SPATAV
C
C**********************************************************************
C
C         AER Satellite Data Imagery Spatial Averaging Program
C              R.G. Isaacs, R.D. Worsham, AER,Inc.,1985
C
C**********************************************************************
C
      INTEGER A,AVGA,NEWA
      SPECIAL COMMON PIC
C
      COMMON/PIC/ILINE,A(400,600),NEWA(400,600)
      DIMENSION AVGA(400,600),IPLOT(600)
      EQUIVALENCE (A(1,1),AVGA(1,1))
C
      DATA JBIN,KTAPE/25,26/
C
      DATA IPIX,ISCAN/600,400/
C
C
      WRITE(3,*) 'Imagery Averaging Program:'
      WRITE(6,*) 'Imagery Averaging Program:'
C
      NCOUNT=IPIX*ISCAN
      WRITE(6,*)'Original image is ',IPIX,' pixels by ',ISCAN,' scanline
     1s.'
      WRITE(6,*)'Total number of points in image is : ',NCOUNT
C
      WRITE(3,*) 'INPUT AVERAGE BOX SIZE'
C
      READ(3,*) NAV
C
      WRITE(6,*)'Desired box size average is ',NAV,' x ',NAV,' pixels.'
      NPIX=INT(IPIX/NAV)
      NSCAN=INT(ISCAN/NAV)
      JCOUNT=NPIX*NSCAN*NAV*NAV
      WRITE(6,*)'The averaged array is ',NPIX,' pixels by ',NSCAN,' scan
     1lines for a total of ',JCOUNT,' points averaged. '
C
C     Read in original image array.
C
      WRITE(3,*) 'Read Image Array'
C
      DO 10 I=1,ISCAN
C
      READ(JBIN) ILINE,(A(I,J),J=1,IPIX)
C
 10   CONTINUE
C
C     Begin pixel averaging process
C
      WRITE(3,*) 'Begin averaging'
C
      ICOUNT=0
      DO 20 KK=1,NSCAN
      DO 22 JJ=1,NPIX
      SUM=0.0
      DO 30 I=(KK-1)*NAV+1,KK*NAV
      DO 32 J=(JJ-1)*NAV+1,JJ*NAV
      SUM=SUM+  A(I,J)
      ICOUNT=ICOUNT+1
 32   CONTINUE
 30   CONTINUE
```

```
       NEWA(JJ,KK)=SUM/(NAV*NAV)
22     CONTINUE
20     CONTINUE
       WRITE(6,*)'Total Number of Pixels Averaged= ',ICOUNT
       IF(ICOUNT.NE.JCOUNT) WRITE(3,*)'ERROR 1,Pixel # Mismatch'
C
C      Output Averaged Array
C
       WRITE(3,*) 'Output Averaged Array'
C
       NOUT=NSCAN*NPIX
       WRITE(6,*)'Number of output pixels= ',NOUT
       WRITE(6,*)'Averaged image is ',NPIX,' pixels by ',NSCAN,' scanline
      1s.'
       DO 50 KK=1 , NSCAN
       DO 52 JJ=1,  NPIX
       DO 60 I=(KK-1)*NAV+1,KK*NAV
       DO 62 J=(JJ-1)*NAV+1,JJ*NAV
       AVGA(I,J)=NEWA(JJ,KK)
       LCOUNT=LCOUNT+1
62     CONTINUE
60     CONTINUE
52     CONTINUE
50     CONTINUE
C
C      Averaged array in original dimensions
C
       DO 70 I=1,ISCAN
C
       WRITE(KTAPE) I, (AVGA(I,J),J=1,IPIX)
C
70     CONTINUE
C
       IF(LCOUNT.NE.JCOUNT) WRITE(6,*) 'Error 2: Pixel # Mismatch'
C
       STOP
       END
```

APPENDIX B

SPECTRAL AVERAGING PROGRAM

```
      PROGRAM SPECAV
C
C*******************************************************************************
C
C           AER Satellite Data Imagery Spectral Averaging Program
C                R.G. Isaacs, R.D. Worsham, AER,Inc.,1985
C
C*******************************************************************************
C
      INTEGER A4,A5,A6,A7,AOUT
      SPECIAL COMMON PIC
C
      COMMON/PIC/A4(600),A5(600),A6(600),A7(600),AOUT(600)
C
      DATA AF4,AF5,AF6,AF7/.10,.20,.25,.45/
C
      DATA JBIN4,JBIN5,JBIN6,JBIN7,KTAPE/25,26,27,28,29/
C
      DATA IPIX,ISCAN/600,400/
C
C     Read in original image array, average it and write back out.
C
      DO 10 I=1,ISCAN
C
      READ(JBIN4) ILINE4,A4
      READ(JBIN5) ILINE5,A5
      READ(JBIN6) ILINE6,A6
      READ(JBIN7) ILINE7,A7
C
      DO 5 J=1,IPIX
C
      R4=A4(J)
      R5=A5(J)
      R6=A6(J)
      R7=A7(J)
      ROUT=AF4*R4+AF5*R5+AF6*R6+AF7*R7
      AOUT(J)=INT(ROUT)
C
    5 CONTINUE
C
      WRITE(KTAPE) I,AOUT
   10 CONTINUE
C
      STOP
      END
```

APPENDIX C

SCANLINE GENERATION PROGRAM

This appendix provides the background for an application oriented analysis tool which directly models the sun/sensor geometry of specific polar-orbiting satellite platforms (such as DMSP). Given basic information regarding the orbital parameters of the satellite and the desired time of the observed scene (since the imagery is annotated in GMT time), one can both locate (i.e., latitude/longitude) specific surface elements (pixels) along the sensor scan line perpendicular to the satellite subpoint track and provide information regarding the solar and sensor positions relative to each fo the individual pixels. The relative solar and sensor positions can then be used for a variety of applications.

The problem is simplified considerably if the satellite subtrack is assumed to be a great circle. A nominal circular orbit is assumed. These calculatiosn are discussed in the following sections with reference to Figure C-1 which illustrates the satellite subtrack (AB) and sensor scan line (BE) geometry for a generic polar orbiting satellite with ascending node A. Indicated are the positions of the pole, C(P), equator (E), and prime meridian (M).

C.1 Satellite Subtrack Position

Assuming the satellite subtrack (SST) in Figure C-1 (arc AB) to be a great circle, the position in latitude (θ_s) and longitude (ϕ_s) of point B at time t_1 can be calculated given the time, t_0, and longitude, ϕ_0, of the ascending node (crossing of the equator, point A) provided an orbital period, p, and inclination of the orbit to the equatorial plane, ε, are assumed. For DMSP (see Table 2-1), a nominal circular orbit would have a period of 101.35 m (or 1.6982 h), an orbital inclination of 98.7° (making it sun synchronous), and an altitude of 833 km.

The length of side C (in degrees) will be:

$$C = 360(t_1 - t_0)/p. \tag{C-1}$$

The angle at A is determined by the orbital inclination or

$$A = \varepsilon - 90 = 8.7°. \tag{C-2}$$
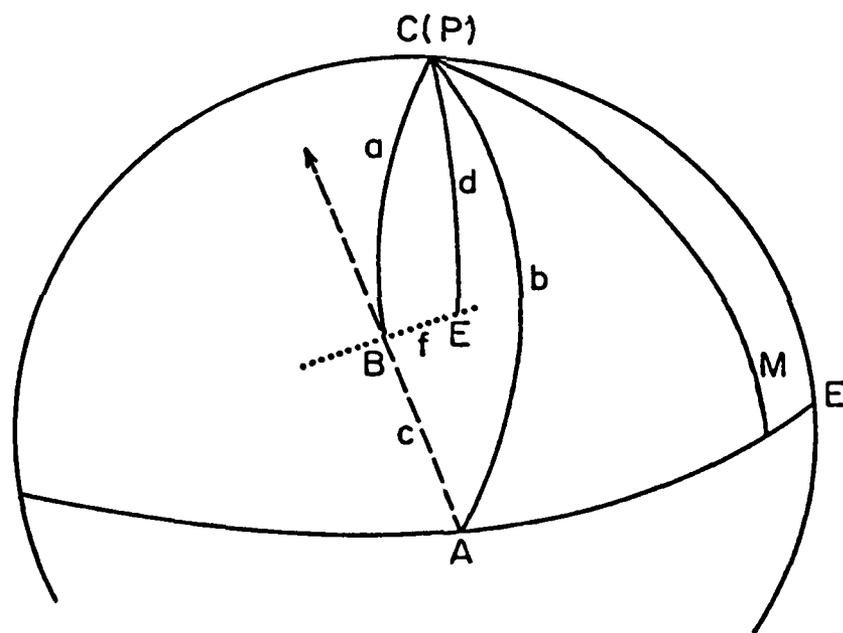
Figure C-1. Scan line generation geometry based on nominal satellite parameters.

The arc length (in degrees) from point A (on the equator) to the pole C(P) is side b, or:

$$b = 90°. \qquad (C-3)$$

The latitude of the subsatellite point at t_1 will be given by side a:

$$\theta_s = 90 - a \qquad (C-4)$$

while the longitude will depend on the angle at point C(P) or:

$$\phi_s = \phi_0 + C + (t_1 - t_0)15. \qquad (C-5)$$

(The final term above accounts for Earth's rotation at a rate of $15°h^{-1}$ during the time interval from t_0 to t_1.) Solution for the unknown quantities (a and C, above) is based on Napier's analogies for a spherical triangle.

$$a = 2 \tan^{-1} [h(b,c,B,C)] \qquad (C-6)$$

$$C = \tan^{-1} [f(b,c,A)] - \tan^{-1} [g(b,c,A)] \qquad (C-7)$$

where:

$$B = \tan^{-1} [f(b,c,A)] + \tan^{-1} [g(b,c,A)] \qquad (C-8)$$

and the functions f, g, and h are given by:

$$f(b,c,A) = \tan\tfrac{1}{2} (B + C) = \cos\tfrac{1}{2} (b - c) \sec\tfrac{1}{2} (b + c) \cot\tfrac{1}{2} A \qquad (C-9)$$

$$g(b,c,A) = \tan\tfrac{1}{2} (B - C) = \sin\tfrac{1}{2} (b - c) \csc\tfrac{1}{2} (b + c) \cot\tfrac{1}{2} A \qquad (C-10)$$

$$h(b,c,B,C) = \tan\tfrac{1}{2} a = \tan\tfrac{1}{2} (b - c) \sin\tfrac{1}{2} (B + C) \csc\tfrac{1}{2} (B - C) \qquad (C-11)$$

Upon substitution of the known quantities c (C-1), A (C-2), and b (C-3) into (C-8) through (C-11), the unknowns a (C-6) and C (C-7) can be evaluated. Equations (C-4) and (C-5) then yield the desired satellite subtrack point latitude and longitude, respectively.

C.2 Sensor Scan Line Position

Applying similar considerations, the location of specific surface elements along a sensor scan line can be evaluated. It is assumed that the location and time (θ_s, ϕ_s, t_s) of the subtrack point (B in Figure C-1) associated with the desired sensor scan line are known based on the procedure described in the previous section and that the scan line including point B (i.e., arc BE) is also a great circle perpendicular to the subpoint track. Considering spherical triangle BEC(P), the length of side A (deg) from (C-4)

C-3

is:

$$a = 90 - \theta_s. \tag{C-12}$$

The angle at B is determined by the orbital inclination and thus from the figure:

$$B = 81.3°. \tag{C-13}$$

The length of the scan line (in degrees, side f, is determined from the length of the scan from subpoint to horizon (1479 km) and Earth's radius, R_E (6370 km):

$$f = 360(1479)/2\pi(6370 = 13.303°. \tag{C-14}$$

The $\underline{i}$th surface element pixel is chosen such that the length of the arc from the subpoint B to the pixel is given by:

$$f_i \text{ (deg)} = \left((i-1)/n\right) 13.303 \tag{C-15}$$

for i = 1 to n + 1. Thus, the first pixel (i = 1) corresponds to the subtrack point (B), and the last pixel (n + 1) corresponds to the point on the easterly horizon (E). The latitude of the ith pixel along the scan line will be:

$$\theta_i(\text{deg}) = 90 - d_i \tag{C-16}$$

and the corresponding longitude will be

$$\phi_i(\text{deg}) = \phi_s - C_i. \tag{C-17}$$

Again, using Napier's analogies to solve:

$$d_i = 2\tan^{-1}[h(a,f_i,E,C_i)] \tag{C-18}$$

$$C_i = \tan^{-1}[f(a,f_i,B)] - \tan^{-1}[g(a,f_i,B)] \tag{C-19}$$

where:

$$E_i = \tan^{-1}[f(a,f_i,B)] + \tan^{-1}[g(a,f_i,B)] \tag{C-20}$$

and the functions f, g, and h are given by:

$$f(a,f_i,B) = \tan\tfrac{1}{2}(E_i + C_i)$$
$$= \cos\tfrac{1}{2}(a - f_i) \sec\tfrac{1}{2}(a + f_i) \cot\tfrac{1}{2}B \tag{C-21}$$

$$g(a,f_i,B) = \tan\tfrac{1}{2}(E_i - C_i$$
$$= \sin\tfrac{1}{2}(a - f_i) \csc\tfrac{1}{2}(a + f_i) \cot\tfrac{1}{2}B \tag{C-22}$$

$$h(a,f_i,E_i,C_i) = \tan\tfrac{1}{2}d$$

$$= \tan\frac{1}{2} (a - f_i) \sin\frac{1}{2} (E_i + C_i) \csc\frac{1}{2} (E_i - C_i) \qquad (C\text{-}23)$$

Substitution of (C-18) through (C-23) into (C-16) and (C-17) yields pixel latitude and longitude.

C.3   Pixel-related Sun/Sensor Geometry

Evaluation of pixel location (θ_i, ϕ_i) using the procedures outlined in the previous sections provides the necessary data to calculate the solar zenith angle, θ_o^i, sensor zenith angle, θ_o^i, and azimuth angle difference, $\Delta\phi_i$, relative to each pixel location.

The solar zenith angle at the ith pixel, θ_o^i, and its associated zenith angle cosine, $\mu_o^i = \cos\theta_o^i$ are given by:

$$\theta_o^i = \cos^{-1}\left[\mu_o^i\right] = 90 - \sin^{-1}[\sin\theta_i \sin\delta + \cos\theta_i \cos\delta \cos\eta_i] \qquad (C\text{-}24)$$

where δ is the solar declination angle and η_i is the hour angle (deg) given approximately by the difference between the pixel longitude (ϕ_i) and the longitude (ϕ_{SSP}) of the subsolar point (SSP), i.e.:[†]

$$\eta_i = \phi_i - \phi_{SSP}. \qquad (C\text{-}25)$$

The solar declination angle, δ, is a functio nfo the date (zero at the equinoxes and $\pm 23°27'$ at the solstices) and may be obtained from a solar ephemeris. It is given approximately by the equation:

$$\delta(d) = \sin^{-1}\left\{.3978 \sin[.9863(d-80)]\right\} \qquad (C\text{-}26)$$

where d is the day of the year (i.e., January 1 is 001 and December 31 is 365.

The solar azimuth angle, α_i (the azimuth of the sun measured clockwise from north) at pixel location (θ_i, ϕ_i) is given by:

$$\alpha_i = \begin{array}{ll} \cos^{-1}(1-2q_5) & \text{for } \eta_i > 0 \text{ (morning)} \\ 360 - \cos^{-1}(1-2q_5) & \eta_i < 0 \text{ (afternoon)} \end{array} \qquad (C\text{-}27)$$

[†]For morning satellites, η_i will generally be positive; that is the scan line pixels will be at earlier solar times than the SSP.

where:

$$q_5 = \frac{\sin(q_4 - q_2)\ \sin(q_4 - q_1)}{\sin q_2\ \sin q_1}$$

$$q_4 = (q_1 + q_2 + q_3)/2$$

and: $q_1 = 90 - \theta_i$

$\qquad q_2 = \theta_o$

$\qquad q_3 = 90 - \delta.$

Since the sensor azimuth lookign eastward is fixed at 261.3°, the azimuth angle difference is:

$$\Delta\phi_i = 261.3 - \alpha_i. \qquad\qquad (5\text{-}28)$$

The satellite zenith angle at the ith pixel, θ_R^i, and its associated zenith angle cosine, $\mu^i = \cos\theta_R^i$ are given by:

$$\theta_R^i = \cos^{-1} \mu^i = \tan^{-1}\left[\frac{(i-1)}{n}\ 1479/833\right] \qquad\qquad (C\text{-}29)$$

for $i = 1, 2, 3 \ldots (n + 1)$ pixels and ssuming a sensor altitude for 833 km for a nominal circular orbit.

APPENDIX D

SATELLITE DATA ARCHIVES

DMSP

The archive for DMSP imagery is operated by the Cooperative Institute for Research in Environmental Sciences (CIRES), University of Colorado. There is no existing DMSP digital archive.

> National Snow and Ice Data Center/DMSP
> CIRES, Campus Box 449
> University of Colorado at Boulder
> Boulder, Colorado 80309
>
> Telephone: (303) 492-5171 (FTS 320-5311)

NOAA and GOES

NOAA AVHRR and GOES imagery and digital data are archived at the World Weather Building, Washington, DC.

> NOAA/NESDIS/NCDC
> Satellite Data Services Division
> Room 100, World Weather Building
> Washington, DC 20233
>
> Telephone: (301) 763-8111

Landsat

Landsat imagery and digital data products are now available from the Earth Observation Satellite Company (EOSAT) in accordance with the Landsat Commercialization Act of 1984.

> Earth Observation Satellite Company
> C/o EROS Data Center
> Sioux Falls, SD 57198
>
> Telephone: 1-800-367-2801

END

DTIC

7 - 86